# Mimicry drives convergence in structural and light transmission features of transparent wings in Lepidoptera

Charline Pinna[1$], Maëlle Vilbert[2], Stephan Borensztajn[3], Willy Daney de Marcillac[4], Florence Piron-Prunier[1], Aaron F. Pomerantz[5,6], Nipam Patel[5], Serge Berthier[4], Christine Andraud[2], Doris Gomez[7*], Marianne Elias[1*]

Affiliations:
[1] ISYEB, 45 rue Buffon, CP50, Paris, CNRS, MNHN, Sorbonne Université, EPHE, France
[2] CRC, 36 rue Geoffroy-Saint-Hilaire, CP21, Paris, MNHN, France
[3] IPGP, 1 rue Jussieu, Paris, Université de Paris, CNRS, France
[4] INSP, 4 place Jussieu, boîte courrier 840, Paris, Sorbonne Université, CNRS, France
[5] Marine Biological Laboratory, Woods Hole, Massachusetts, USA
[6] Department Integrative Biology, University of California Berkeley, USA
[7] CEFE, 1919 route de Mende, Montpellier, CNRS, Univ Montpellier, EPHE, IRD, France

*Equal contribution

$ corresponding author: charline.pinna1@edu.mnhn.fr

## Abstract

Müllerian mimicry is a positive interspecific interaction, whereby co-occurring defended prey species share a common aposematic signal. In Lepidoptera, aposematic species typically harbour conspicuous opaque wing colour patterns with convergent optical properties among co-mimetic species. Surprisingly, some aposematic mimetic species have partially transparent wings, raising the questions of whether optical properties of transparent patches are also convergent, and of how transparency is achieved. Here we conducted a comparative study of wing optics, micro and nanostructures in neotropical mimetic clearwing Lepidoptera, using spectrophotometry and microscopy imaging. We show that transparency, as perceived by predators, is convergent among co-mimics. Underlying micro- and nanostructures are also convergent despite a large structural diversity. We reveal that while transparency is primarily produced by microstructure modifications, nanostructures largely influence light transmission, maybe enabling additional fine-tuning in transmission properties. This study shows that transparency might not only enable camouflage but can also be part of aposematic signals.

## Introduction

Lepidoptera (butterflies and moths) are characterized by large wings typically covered by scales, as testified by the name of the order (after the ancient greek *lepís* - scale and *pterón* – wing). Scales can contain pigments or generate interference colours, thereby producing colour patterns across the entire wing. Wing colour patterns are involved in thermoregulation (Dufour et al., 2018; Heidrich et al., 2018), sexual selection (Kemp, 2007) and anti-predator defences, such as crypsis (Cook et al., 2012; Endler, 1984; Webster et al., 2009), masquerade (Skelhorn et al., 2010; Stoddard, 2012), disruptive coloration, and deflection of predator attacks (Vallin et al., 2011). Another type of anti-predator defence in Lepidoptera involving wing colour pattern is aposematism, where the presence of secondary defences is advertised by the means of bright and contrasted colour patterns. Because of the positive frequency-dependent selection incurred on aposematic signals (Greenwood et al. 1989, Chouteau et al. 2016), aposematic species often engage in Müllerian mimetic interactions, whereby species exposed to the same suite of predators converge on the same colour pattern and form mimicry 'rings' (Müller, 1879). Co-mimetic species (species that share a common aposematic colour pattern) are often distantly related, implying that the same colour pattern has evolved independently multiple times. Among such co-mimetic lepidopteran species, several studies using visual modelling have shown that analogous colour patches (i. e., those occupying a similar position in the wing and harbouring similar colour) cannot be discriminated by birds, believed to be the main predators (Bybee et al., 2012; Llaurens et al., 2014; Su et al., 2015; Thurman & Seymoure, 2016). Therefore, mimicry selects for convergent (when a trait in different species evolves towards the same value) or advergent (when a trait of a given species evolves towards the trait value in another species) colourations, as perceived by predators.

Surprisingly, although most aposematic Lepidoptera species harbour brightly coloured patterns, some unpalatable, aposematic species exhibit transparent wing patches (McClure et al., 2019). In those species, wing colour pattern typically consists of a mosaic of brightly coloured and transparent patches. Notably, in tropical America, many mimicry rings comprise such transparent species (Beccaloni, 1997; Elias et al., 2008; Willmott et al., 2017). Mimicry among species harbouring transparent patches raises the question of selection for convergence in optical properties, as perceived by predators, in those transparent patches.

A related question is whether transparency in co-mimetic species is achieved by the means of similar structural changes in wings and scales. Previous studies on a handful of species (most of which are not aposematic) have revealed several, non-mutually exclusive means to achieve transparency, through scale modification or scale shedding, with the effect of reducing the total coverage of the chitin membrane by scales. Scales can fall upon adult emergence (Yoshida et al., 1996); they can have a reduced size (Dushkina et al., 2017; Perez Goodwyn et al., 2009) and even resemble bristle (Binetti et al., 2009; Hernández-Chavarría et al., 2004; Perez Goodwyn et al., 2009; Siddique et al., 2015); they can be either flat on the membrane (Perez Goodwyn et al., 2009) or erected (Dushkina et al., 2017; Perez Goodwyn et al., 2009), which also reduces effective membrane coverage by scales. Reducing scale density could also make wings transparent to some extent (Perez Goodwyn et al., 2009). Although this has not been reported in transparent Lepidoptera, transparent scales, such as those covering coloured scales in the opaque butterfly *Graphium sarpedon* (Stavenga et al., 2010), could also be a means to achieve transparency. In addition to scale modifications, the presence of nanostructures on the surface of the wing membrane may enhance transparency through the reduction of light reflection, by generating a gradient of refractive index between the chitin-made membrane and the air (Binetti et al., 2009; Siddique et al., 2015; Yoshida et al., 1997). Yet, so far, no study has compared the microstructures (scales) and nanostructures present in transparent patches across co-mimetic species. Furthermore, the diversity of structures described above may lead to a large range of transparency efficiencies. Exploring the link between structural features and optical properties can shed light on whether and how different structures might achieve similar degrees of transparency in the context of mimicry.

Here, we investigate the transmission properties of transparent patches among co-mimetic butterflies and moths and the structural bases of transparency on 62 Neotropical transparent species, which belong to seven different lepidopteran families and represent 10 distinct mimicry rings. We characterise wing micro- and nanostructures with digital microscopy and scanning electron microscopy (SEM) imaging and measure transmission properties of transparent patches using spectrophotometry in the range of wavelengths 300-700 nm. We implement comparative analyses that account for phylogenetic relatedness, to (1) examine the putative convergence or advergence (hereafter, convergence, for the sake of simplicity) among co-mimetic species in visual appearance

of transparent patches as seen by bird predators, (2) identify and examine the putative convergence of structures involved in transparency in the different co-mimetic species and finally (3) explore the links between structural features and transmission properties of transparent patches.

## Results

### Convergence among co-mimics in visual appearance of transparent patches as seen by bird predators

To assess whether transparent patches of co-mimetic species were under selection for convergence due to mimicry, we tested whether these transparent patches were more similar, as perceived by predators, among co-mimetic species than expected (1) at random, and (2) given the phylogeny. The first test, which assesses whether predators have a similar perception of analogous transparent patches in co-mimetic species, informs on the selection on transparent patches incurred by predators. The second test, which accounts for the phylogenetic relationship between species, informs on the underlying process leading to similarity, and specifically on whether any case of similarity among co-mimics detected in the first test is due to shared ancestry or to evolutionary convergence. We used spectrophotometry to measure specular transmittance of the transparent patches, which is a quantitative measurement of transparency. As birds are supposed to be the main predators of butterflies (Brower, 1984), we applied bird perceptual vision modelling on the resulting spectra to calculate the chromatic and achromatic contrasts (respectively dS and dL) for each pair of species from our dataset. If transparent patches among co-mimetic species are more similar than expected at random or given the phylogeny, contrasts between pairs of co-mimetic species are expected to be smaller than predicted at random and given the phylogeny, respectively. We only compared analogous spots (i.e. occupying a similar position on the forewing) between species. The results presented in Figure 1 show that for three spots out of five and across all mimicry rings the difference in achromatic contrast (dL) between co-mimetic species is significantly smaller than expected both at random and given the phylogenetic distance between species (figure 1B), irrespective of the illuminating light or the visual system considered (see Supplementary table 1a and b for results under the full range of

conditions). Differences in chromatic contrasts (dS) between co-mimetic species are significantly smaller than expected at random and given the phylogenetic distance between species only for the most proximal spot on the forewing (figure 1B). These results mean that, on average, predators see transparent patches among co-mimetic species as more similar than among species that belong to different mimicry rings. The fact that these tests remain significant with the phylogenetic correction indicates that such similarity in transparent patches is due to convergent evolution. When looking more precisely at similarity between co-mimetic species for each individual mimicry ring (figure 1C), we show that in eight out of ten mimicry rings achromatic contrasts (dL) between co-mimetic species are smaller than expected at random for at least one spot on the forewing (Supplementary table 2a). After accounting for the phylogeny, this figure drops down to four out of ten mimicry rings (Supplementary table 2a). Regarding chromatic contrasts (dS), six mimicry rings out of ten comprise co-mimetic species exhibiting smaller chromatic contrast than expected at random and three out of them comprise co-mimetic species with smaller chromatic contrast than expected given the phylogeny (figure 1C, Supplementary table 2b). These results suggest that in most cases, the similarity in transparent patches between co-mimetic species is due to convergent evolution but we cannot rule out that for some mimicry rings (notably 'theudelinda', 'hewitsoni', 'panthyale') similarity could be due to shared ancestry. Achromatic aspects (achromatic contrast dL) appear more significant than chromatic aspects (chromatic contrast dS) (Figure 1, Supplementary table 1), suggesting that selection may act more on broadband transmittance (which is related to the degree of transparency) than on colour.

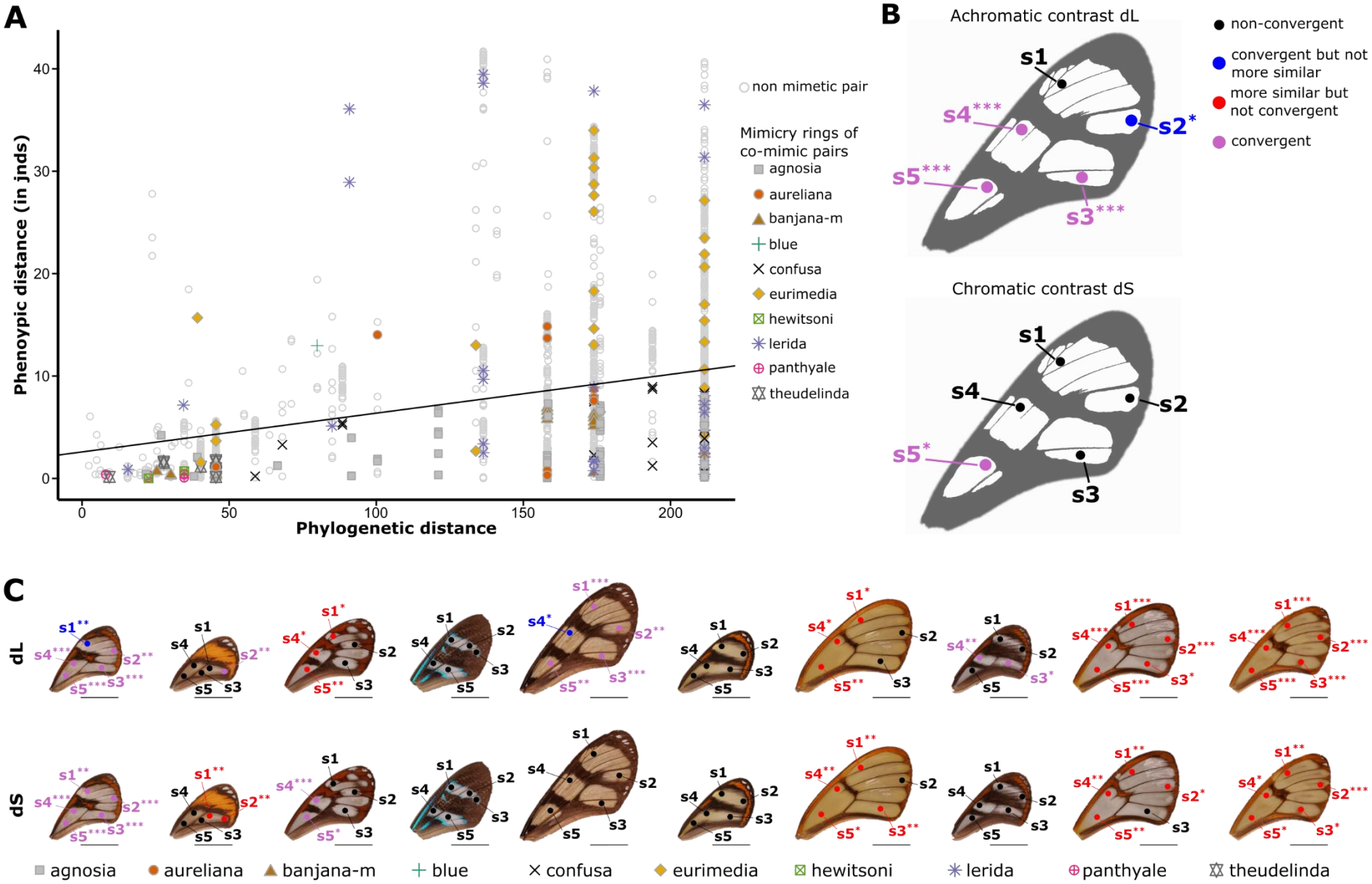
A
Phenoypic distance (in jnds)
Phylogenetic distance
non mimetic pair
Mimicry rings of co-mimic pairs
agnosia
aureliana
banjana-m
blue
confusa
eurimedia
hewitsoni
lerida
panthyale
theudelinda
B
Achromatic contrast dL
non-convergent
convergent but not more similar
more similar but not convergent
convergent
Chromatic contrast dS
C
dL
dS

158

**Figure 1. Test of convergence of transmission properties between co-mimetic species.**

**A. Relation between phenotypic distances (either chromatic or achromatic contrast, expressed in just noticeable differences (jnds), and phylogenetic distances.** Each point represents a pair of species that can be co-mimetic (in this case, the mimicry ring they belong to is represented with a specific symbol, as indicated in the legend) or not (in this case, the point in represented as an open grey circle). The black line represents the predicted value of the linear model linking phenotypic distances with phylogenetic distances. When a point is under the line, the two species represented by that point are more similar that what is expected according to the phylogeny., suggesting that the similarity between these two species is due to convergent evolution. We represent here on this graph the value of achromatic contrast for the 5$^{th}$ spot on the forewing viewed in large gap illuminant by a UVS-type bird but the graphs are similar for all significant tests presented in the Supplementary Table 1.

**B. Graphical representations of the results of the test of convergence for each spot measured on the forewing, for achromatic (top figure) and chromatic (bottom figure) contrasts, across all mimicry rings.** Each spot measured is localised on the forewing and the results of the test over all mimicry rings are represented by the colour of the spot. Black spots stand for spots that are neither more similar than expected at random nor convergent between co-mimetic species. Blue spots stand for spots that are no more similar than expected at random but which are convergent because they are more similar that what might be expected according to their phylogenetic distance. Red spots stand for spots that are more similar than expected at random but not convergent. Purple spots stand for spots that are both more similar than expected at random and convergent. Tests' p-values are represented with the following symbols: '***' $p < 0.001$, '**' $p < 0.01$, '*' $p < 0.05$. The same results were obtained irrespective of the bird visual system (either VS or UVS) or the illuminating light (either forest shade or large gap) considered (see Supplementary table 1 for details).

**C. Graphical representation of the results of the test of convergent for each spot measured on the forewing, for achromatic (dL, upper row) and chromatic (dS, lower row) contrasts, for each mimicry ring.** The results of the test are represented by the colour of the spot, as indicated above. Tests' p-values are represented with star symbols as indicated above. The same results were obtained irrespective of the bird visual system (either VS or UVS) or the illuminating light (either forest shade or large gap) considered (see Supplementary table 2 for details).

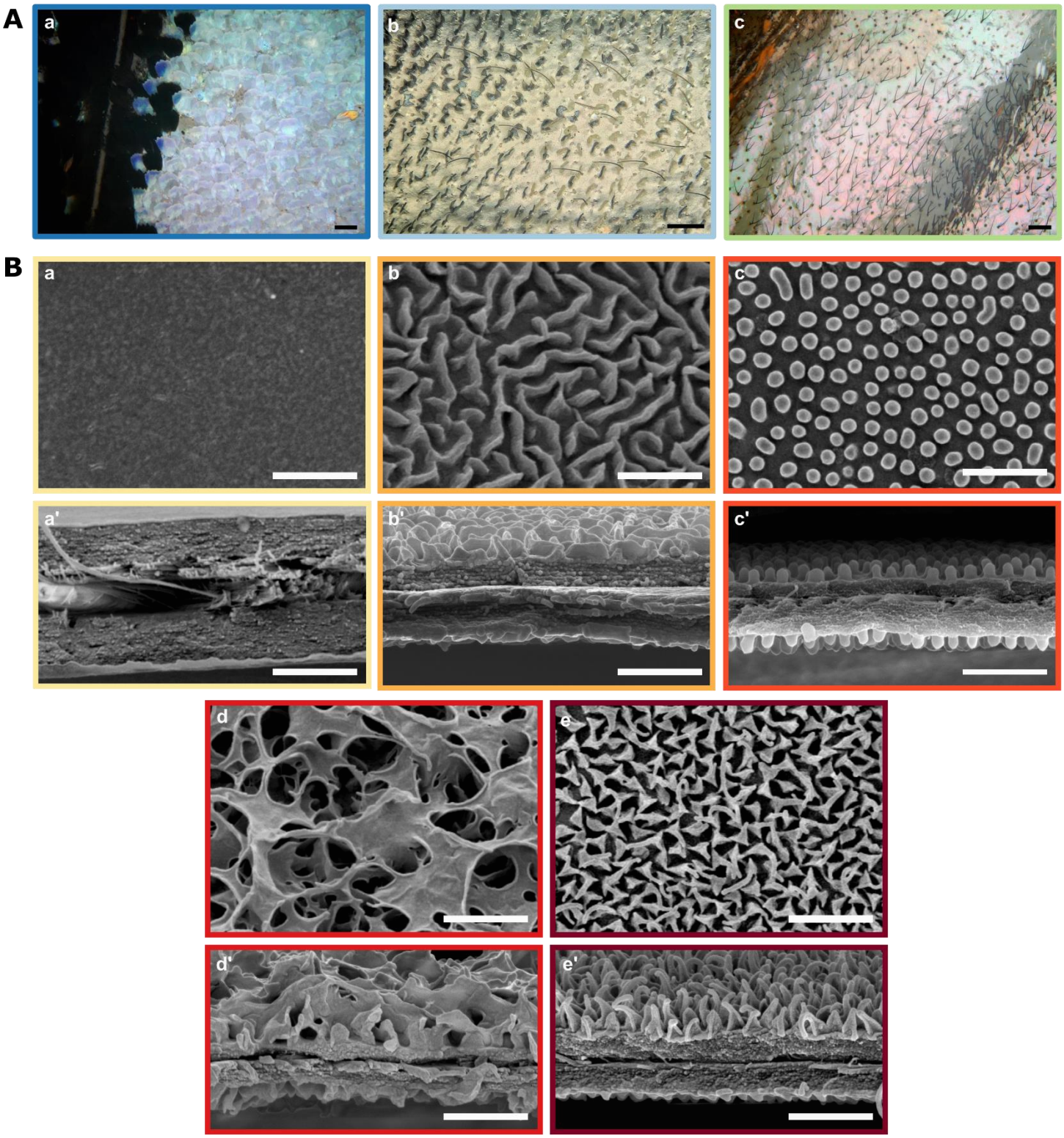


**Figure 2. Diversity of micro- and nanostructures involved in transparency.**

**A. Diversity of microstructures.** a. transparent lamellar scales of *Hypocrita strigifera,* b. erected lamellar scales of *Methona curvifascia* and c. piliform scales of *Hypomenitis ortygia*. Scale bars represent 100 µm.

**B. Diversity of nanostructures.** a, b, c, d and e represent top views and a', b', c', d' and e' represent cross section of wing membrane. Scale bars represent 1 µm. a, a'. absence of nanostructure in *Methona curvifascia*; b, b'. maze nanostructures of *Megoleria orestilla*; c, c'. nipple nanostructures of *Ithomiola floralis*; d, d'. sponge-like nanostructures of *Oleria onega*; e, e'. pillar nanostructures of *Hypomenitis enigma*. Each coloured frame corresponds to a scale type or nanostructure type, as defined in figure 3.

## Diversity and convergence among co-mimics of structures involved in transparency

Convergence in transmission among co-mimetic species raises the question of the nature and similarity of clearwing microstructures (scales) and nanostructures among co-mimetic species. We therefore explored the diversity of micro- and nanostructures present in the transparent patches in our 62 species. We used digital photonic microscopy and SEM imaging to characterise the structures present in the transparent patches (type, insertion, colour, length, width, and density of scales; type and density of nanostructures; wing membrane thickness).

We found a diversity of microstructural features in transparent patches (Figure 2A). Scales could be coloured (76% of species) or transparent (24%); they could be flat on the membrane (16%) or erected (84%). Scales could be lamellar (i. e., a two-dimension structure, 55% of species), or piliform (45%). In our dataset, piliform scales (mainly bifid) appeared to be almost exclusively found in the Ithomiini tribe, although one erebid species also harboured monofid piliform scales (figure 3).

We also revealed an unexpected diversity of the nanostructures that cover wing membrane (Figure 2B). In our sample, we found five types of nanostructures: absent (10% of species), maze (3%), nipple arrays (55%), pillars (21%), and sponge-like (11%).

Phylogenetic signal tests show that both micro- and nanostructure features are highly conserved in the phylogeny (Figure 3, Supplementary Table 4), suggesting the existence of constraints in the developmental pathways underlying micro- and nanostructures. However, the value of δ, the metrics used to quantify phylogenetic signal of traits with discrete states (Borges et al., 2019), is higher for scale type than for nanostructures. This means that the phylogenetic signal is stronger for scale type than for nanostructures. Moreover, in the nymphalid tribe Ithomiini, which is highly represented in our dataset, microstructures seem to be more conserved (all species but the basal species *M. curvifascia* have piliform scales in transparent patches) than nanostructures (all five types of nanostructures, mixed in the Ithomiini clade, Figure 3).

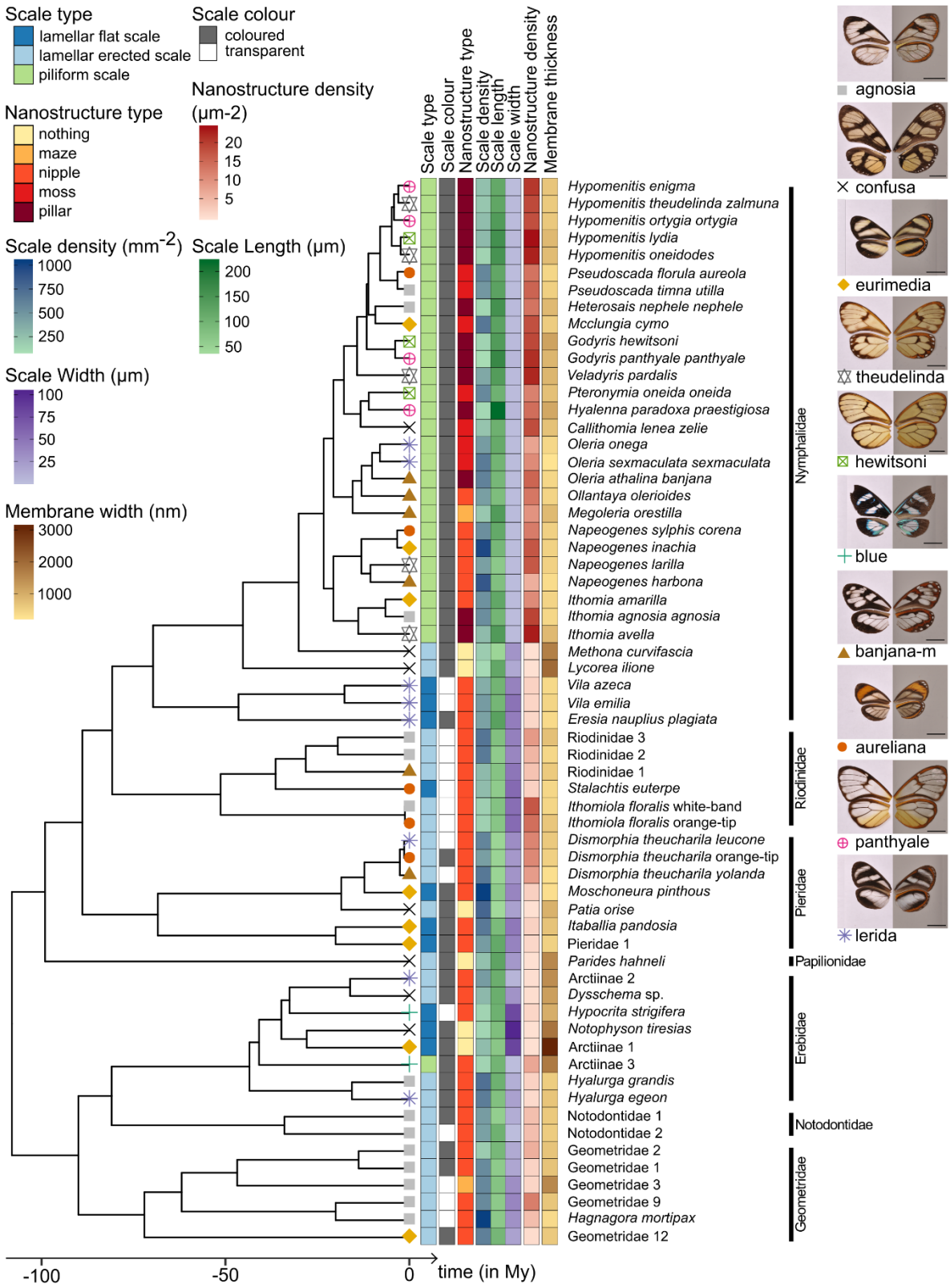


**Figure 3. Phylogeny of the 62 species considered in this study and distribution of traits along the phylogeny.** Mimicry rings are represented by a symbol and a specimen is given as an example for each mimicry ring. Dorsal side of wings has been photographed on a white background (left column) and ventral side on a gray background to highlight the transparent patches (right column). The x axis represents time in million years (My).

222 We then investigated the convergence of structures among co-mimetic species by
223 testing whether co-mimetic species shared structures more often than expected at
224 random and given the phylogeny (see methods for details). We show that, across all
225 mimicry rings, co-mimetic species share structural features (either scale type,
226 nanostructures type or *structural syndrome*, defined as the association of scale type and
227 nanostructure type) more than expected at random and given the phylogeny (Figure 4).
228 The fact that the test remains significant when phylogenetic correction is applied means
229 that structural features are convergent between co-mimetic species. We considered
230 convergence of structural features for each individual mimicry ring (figure 4D and
231 supplementary table 3) and we showed that microstructures are convergent for 'agnosia'
232 and 'confusa' mimicry rings, where species mainly have erected scales. In other mimicry
233 rings ('hewitsoni', 'panthyale', 'theudelinda'), species all have similar piliform scales but
234 this similarity is likely due to shared ancestry and not to convergence. Regarding
235 nanostructural features, we revealed convergent evolution for 'agnosia', 'lerida',
236 'eurimedia', 'panthyale' and 'theudelinda' mimicry rings, characterized by nipples for the
237 three first ones and by pillar for the two last ones (Figure 4D, Supplementary table 3). We
238 showed convergence in structural syndromes (association between micro- and
239 nanostructures) for 'agnosia', where 71% of species harbour a combination of erected
240 scales and nipples and for 'panthyale' where 100% of species combine piliform scales and
241 pillar (Figure 4D, Supplementary table 3). For the mimicry ring 'theudelinda', 80% of
242 species harbour a combination of piliform scales and pillars, but this similarity is best
243 explained by shared ancestry.
244 The fact that both transmission properties and underlying structures show some
245 degree of convergence raises the question of whether specific structures have been
246 selected in co-mimetic species because they confer a peculiar visual aspect, typical of the
247 mimicry ring. To address this question, we investigated the link between structural
248 features and transmission properties in transparent patches.

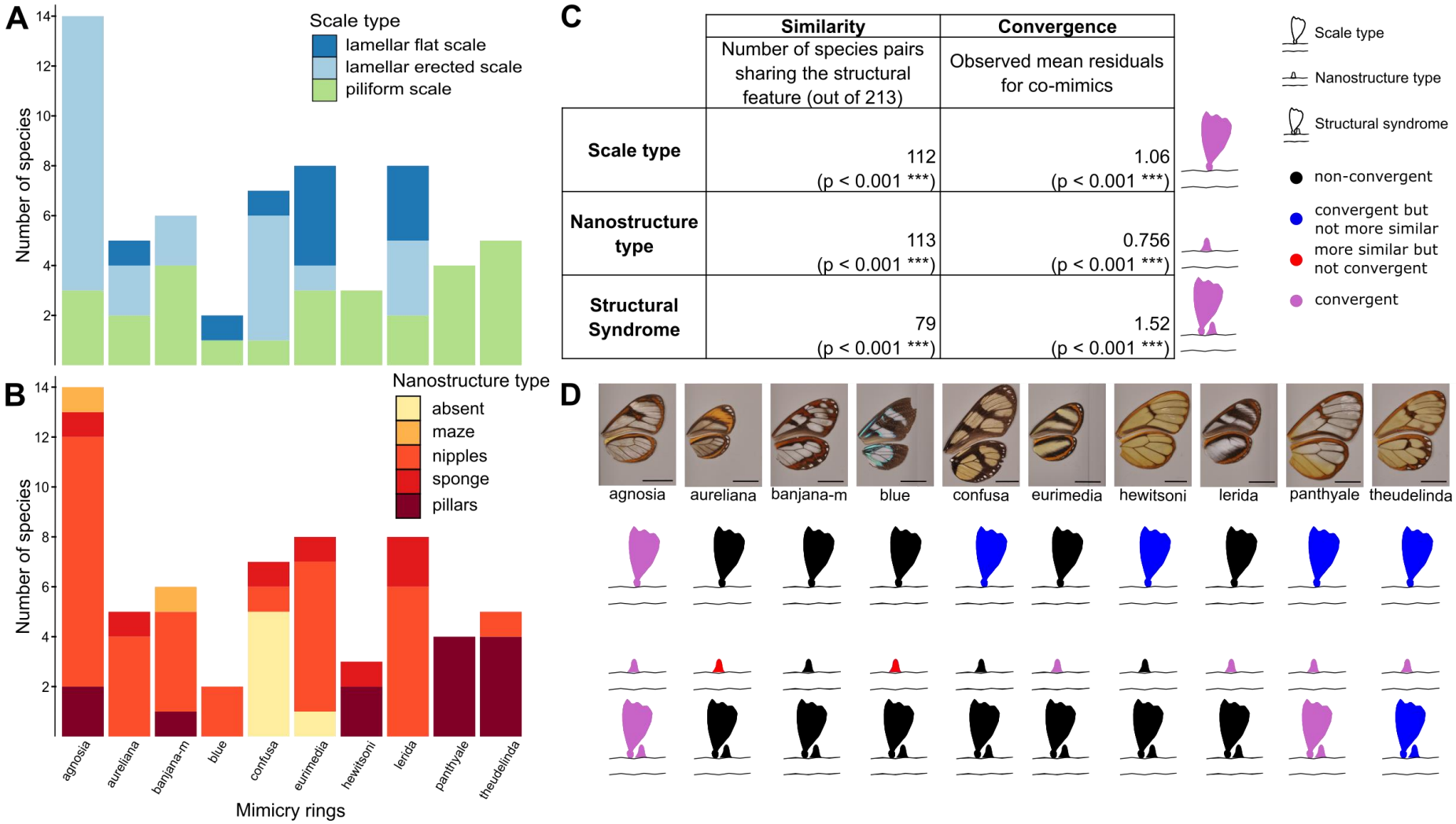


**Figure 4. Convergence of structures underlying transparency.**

**A,B. Distribution of micro- (A) and nanostructures (B) among the different mimicry rings (indicated at the bottom on panel B).**

**C. Results of the test of convergence for structural features (either scale type, nanostructure type or structural syndrome, i. e., the association of scale type and nanostructure type).** To test for similarity independently of the underlying process, we compare whether the number of co-mimetic species sharing the same structural feature (out of 213 co-mimetic species pairs) is higher than expected at random. To do so, we randomize 10000 times the sharing variable over all pairs of species and we calculate the p-value (indicated in brackets) as the proportion of randomisations where the number of co-mimetic species sharing the structural feature is higher than the observed number of co-mimetic species pairs sharing the structural feature. To test for convergence on structural features, we tested whether the observed mean residuals of the generalised linear model linking structure sharing and phylogenetic distance was higher than expected given the phylogeny and we calculated the p-value (indicated in brackets) as the proportion of randomisations of model's residuals where the mean residuals for co-mimetic species is higher than the observed mean residuals for co-mimetic species.

**D. Graphical representation of the results of the test of convergence for each mimicry ring.** For each mimicry ring, we tested whether the structural features were more similar than expected at random and given the phylogeny (with the same tests described above, see supplementary table 3 for details). We represented the results for scale type, nanostructure type and structural syndrome. Black structures indicate neither more similar structures than expected at random nor convergent structures; red structures indicate structure more similar than expected at random but not convergence; blue structures indicate structures not more similar than expected at random but convergent and purple structures indicate convergent structures.

267 **Link between structural features and transmission properties**

268 To investigate whether transmission properties depend on structural features we used
269 the above measurements of the specular transmittance of transparent patches of each
270 species and we calculated the mean transmittance over 300-700nm, hereafter called
271 mean transmittance, for each spectrum. The physical property 'mean transmittance' (a
272 proxy for the degree of transparency), is correlated to what is predicted to be perceived
273 by predators based on vision modelling, (Supplementary result 1 for details). Across the
274 62 species, the mean transmittance ranges from 0.0284% in *Eresia nauplius* to 71.7% in
275 *Godyris panthyale* (mean: 29.2%, median: 31.6%, supplementary table 5). We performed
276 Phylogenetic Generalized Least Squares (PGLS) to assess the relationship between mean
277 transmittance and micro- and nanostructural features (type, insertion, colour, length,
278 width and density of scales; type and density of nanostructures; wing membrane
279 thickness; including some interactions), while accounting for the phylogeny. We retained
280 as best models all models within 2 AICc units of the minimal AICc value. Following this
281 procedure, eight models were retained (see below).

282 Mean transmittance depends mainly on scale type, scale density and
283 nanostructure density, and to a lesser extent on membrane thickness and scale colour
284 (Figure 5A, Supplementary table 6). The effect of scale type is retained in all eight models
285 and is significant in all of them. Wings covered with piliform scales transmit more light
286 than those covered with lamellar scales (Figure 5B). Among wings covered with lamellar
287 scales, those with erected scales transmit more light than those with flat scales. The effect
288 of scale density is retained in the eight best models and is significant in five of those
289 (Supplementary table 6): mean transmittance decreases as scale density increases. The
290 effect of nanostructure density is retained in six models and is significant in four of those:
291 mean transmittance increases when nanostructure density increases (Figure 5C).

292 The interaction between scale density and nanostructure density is retained in
293 three out of eight models and it is marginally significantly different from zero in two of
294 those three models (supplementary table 6). The coefficient is always negative, meaning
295 that the increase in light transmission due to the increase in nanostructure density is not
296 as strong when scale density is high than when scale density is low. This suggests that the
297 contribution of nanostructures to transparency is stronger when scale density is low.

**A**

| Structural features | | Estimate | Std.Error | t value | p-value |
|---|---|---|---|---|---|
| Scale type | P vs. L contrast | 6.90 | 1.51 | 4.56 | < 0.001 *** |
| | LF vs. LE contrast | 6.67 | 1.99 | 3.36 | 0.00142 ** |
| Scale density | | -0.00634 | 0.00852 | -0.744 | 0.460 |
| Nanostructure density | | 1.08 | 0.383 | 2.82 | 0.00671 ** |
| Interaction between nanostructure density and scale density | | -0.00136 | 0.000783 | -1.73 | 0.0888 . |

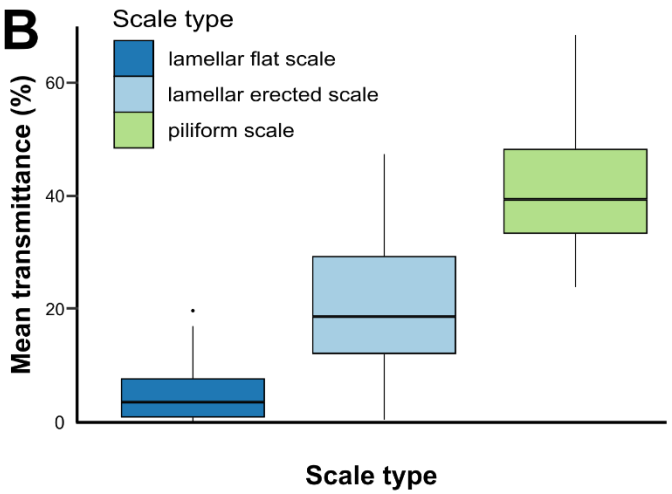


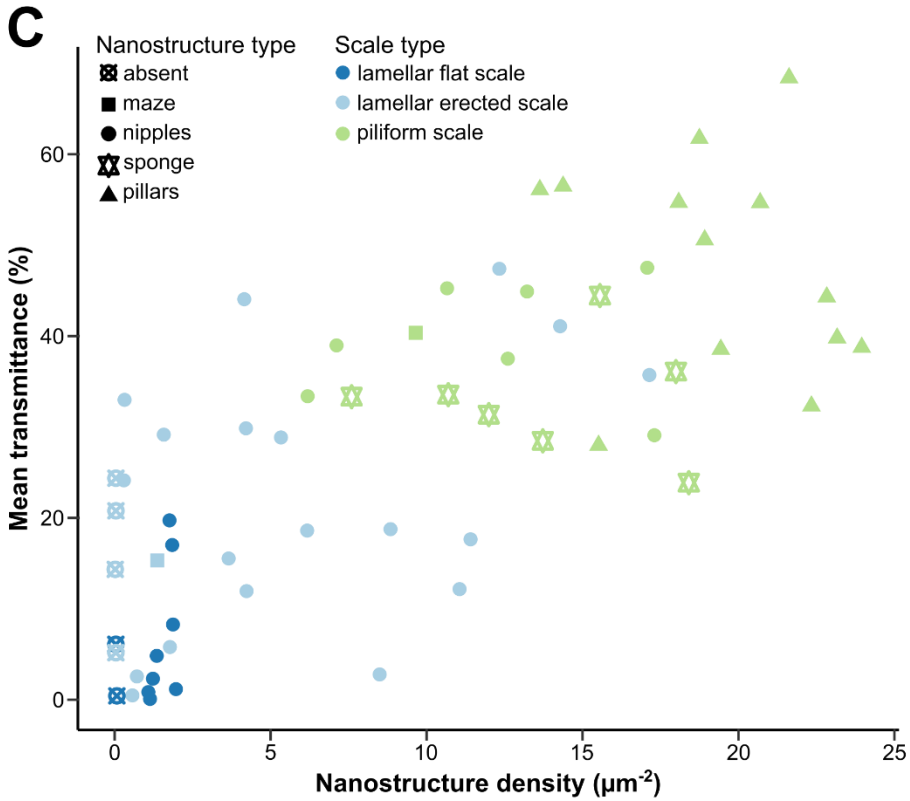


**Figure 5. Link between mean transmittance over 300-700 nm and structural features.**

**A.** Results of the best PGLS model ($F_{5,56}$ = 26.65 (p-value <0.001 ***), AICc = 469.9, $R_{adj}^2$ = 0.678, $\lambda$ = 0 (p-value < 0.001 ***)) linking mean transmittance and micro- and nanostructure features. The explicative variables haven't been scaled or centred. Nanostructure density has been measured in $\mu m^{-2}$, Scale density in $mm^{-2}$. Scale type is a categorical variable with 3 levels (either flat lamellar scale (LF), erected lamellar scale (LE) or piliform scale (P))

**B.** Link between mean transmittance measured between 300 and 700 nm and scale type.

**C.** Link between mean transmittance measured between 300 and 700 nm and nanostructure density, nanostructure type (represented by different shape) and scale type (represented by different colours).

NB. We considered the spot corresponding to the location of the SEM images for mean transmittance.

The effect of membrane thickness is retained in three out of eight models and is significantly different from zero in one of them: light transmission decreases when membrane thickness increases.

Transparent scales, which do not contain pigments, transmit more light than coloured ones, which contain pigments; a relationship which is retained in three out of eight models and is marginally significantly different from zero in one model (supplementary table 6).

Other variables that were included in the model (scale length and width, nanostructure type, the interaction between scale type and scale density and the triple interaction between scale length, width and density) are not retained in any models (Supplementary table 6). These results suggest that those variables do not have any strong effect on transparency.

## Discussion

We conducted the first comparative study on transparent aposematic mimetic Lepidoptera to assess whether transparency is involved in the aposematic signal, to uncover the diversity in structures underlying transparency and to assess the link between transparency and structural features.

*Convergence of transmission properties*

Based on bird vision modelling applied to light transmission measurements, we showed that predators see transparent patches of species belonging to the same mimicry ring as more similar than expected at random, and given the phylogeny. This shows that transparent patches in co-mimetic species are under selection for convergence, mirroring what has been shown for coloured patches in opaque species (Bybee et al., 2012; Llaurens et al., 2014; Su et al., 2015; Thurman & Seymoure, 2016). This convergent resemblance, which regards mainly the degree of transparency (a general term to refer to what extent a patch appears transparent), suggests that transparent patches might be part of the aposematic signal. Nevertheless, convergence in properties of transparent patches may also result from other selective processes. Transparency is also involved in crypsis (Arias, Elias, et al., 2020), even in aposematic prey (Arias et al., 2019; McClure et al., 2019), and the degree of transparency needed to achieve crypsis may depend on the ambient light

341 (Arias, Barbut, et al., 2020; Johnsen & Widder, 1998). Specifically, in bright environments
342 only highly transparent prey are cryptic, whereas in darker environments moderately
343 transparent prey can be cryptic. In our case, as co-mimetic species share their habitat
344 (Chazot et al., 2014) and microhabitat (Willmott et al., 2017), characterized by a specific
345 ambient light, we cannot rule out that the similarity in the degree of transparency
346 observed between co-mimetic species is the result of selection for crypsis rather than
347 aposematism. Moreover, habitat-specific conditions, such as temperature or humidity,
348 could also affect the evolution of transparent patches. In fact, the habitat and microhabitat
349 shared by co-mimetic species is also characterized by a set of abiotic factors. Therefore,
350 we cannot rule out that the observed convergence is driven by such abiotic factors
351 (related to thermoregulation for example) instead of predation pressure. However,
352 several studies on Ithomiini butterflies have shown that multiple mimicry rings may
353 coexist in the same localities (Chazot et al., 2014; Elias et al., 2008; Willmott et al., 2017).
354 For example, the species belonging to the mimicry rings 'banjana-m', 'panthyale',
355 'hewitsoni' and 'theudelinda' are all high-altitude species that are found in the same
356 localities, and are therefore exposed to the same environmental conditions (ambient light,
357 temperature, humidity). The fact that these species differ in transmission properties of
358 their transparent patches (supplementary figure 1) suggests that the convergence
359 observed is likely driven by Müllerian mimicry, and is not only the result of selection for
360 crypsis or local adaptation to abiotic factors.
361 This study therefore challenges our vision of transparency, which might have evolved
362 under multiple selective pressures in aposematic butterflies. Transparency has been
363 shown to be involved in camouflage and to decrease detectability by predators (Arias,
364 Elias, et al., 2020), even in aposematic species (Arias et al., 2019). Yet, our results suggest
365 that transparent patches might also participate in the aposematic signal and that selection
366 acts on the transmission properties of these patches, particularly on the degree of
367 transparency, but also on chromatic aspects. Therefore, transparent aposematic
368 Lepidoptera benefit from a double protection from predation, which can act at different
369 distances (Barnett et al., 2018; Cuthill, 2019; Tullberg et al., 2005): transparent
370 aposematic species are less detectable than opaque species (McClure et al., 2019), but
371 when detected they may be recognized as unpalatable by experienced predators, due to
372 their aposematic wing pattern, and spared by those predators.
373

374 *Structural features underlying transparency*

375 *Diversity of structures underlying transparency*

376 We revealed an unexpected diversity of structures underlying transparency. Across the
377 62 species of the study, we found different microstructures in the transparent patches:
378 transparent and coloured flat scales, transparent and coloured erected scales and piliform
379 scale. Forked piliform scales have previously been reported in the highly transparent
380 nymphalid species *Greta oto* (Binetti et al., 2009; Siddique et al., 2015), which belongs to
381 the mimetic butterfly Ithomiini tribe. Erected scales (*i. e.,* with a non-zero angle between
382 the scale basis and the wing membrane) have been previously reported in the riodinid
383 *Chorinea sylphina* (Dushkina et al., 2017) and in the nymphalid *Parantica sita* (Perez
384 Goodwyn et al., 2009). Here we describe, as Gomez et al. (2020, in review), some species
385 with coloured erected scales that are completely perpendicular to the wing membrane,
386 such as in the ithomiine *Methona curvifascia*. Transparent scales have already been
387 reported in the opaque papilionid *Graphium sarpedon* (Stavenga et al., 2010) and as
388 Gomez et al (2020, in review) we are describing them for the first time in transparent
389 Lepidoptera. Other means of achieving transparency reported in the literature are not
390 observed among our species (e. g., wing membrane devoid of scales, Yoshida et al. 1996).
391 However, our study is restricted to mimetic transparent butterflies and, as such, spans a
392 relatively small number of families. For a larger scale study that investigates thoroughly
393 the different structures that might be involved in transparency in all known families
394 comprising species with partially or totally transparent wings, see Gomez et al. (2020, in
395 review). Scales in Lepidoptera are not only involved in colour patterns but also play a role
396 in hydrophobicity. The scale modifications underlying transparency described in our
397 study may impair the waterproofing properties of wings as shown by Perez Goodwyn et
398 al. (2009): the wing of the translucent papilionid *Parnassius glacialis* are less hydrophobic
399 than most Lepidoptera wings. Transparency may therefore come at a cost, especially for
400 tropical Lepidoptera living in humid environments.

401 We also revealed an unexpected diversity of nanostructures covering the wing
402 membrane, which we classify into five categories: absence of nanostructures, maze-like,
403 nipple arrays, sponge-like and pillar-shaped nanostructures. While nipple arrays and
404 pillars have previously been described on the wing of the sphingid *Cephonodes hylas*
405 (Yoshida et al., 1997) and in the nymphalid *G. oto* (Binetti et al., 2009; Siddique et al.,
406 2015), respectively, maze-like nanostructures have only been reported on the corneal

surface of insect eyes (Blagodatski et al., 2015). Moreover, the sponge-like type of nanostructures is reported here for the first time. Those nanostructures can be related to the classification proposed by Blagodatski et al. (2015): pillars are a subcategory of nipple arrays, with higher and more densely packed nipples with an enlarged basis; sponge-like nanostructures are similar to dimples (holes embedded in a matrix), although with much bigger and more profound holes. Nipples, mazes and dimples have been found to be produced by Turing's reaction-diffusion models, a solid framework that explains pattern formation in biology (Turing, 1952). While the principle of formation can be elegantly modelled, developmental studies are needed to understand the process by which nanostructures are laid on butterfly wing membrane (Pomerantz et al., 2020).

*Link between structural features and transmission properties*

The diversity of structures underlying transparency described above raises the question of whether these different structures confer different visual aspects. We indeed showed that mean transmittance over 300-700 nm, which is a proxy of the degree of transparency, depends on several structural features: scale type, scale density, nanostructure density, wing membrane thickness and scale colour. To summarize, mean transmittance increases when membrane coverage decreases, either due to reduced scale surface and/or scale density, because there is less material interacting (reflecting, diffusing, or absorbing) with light. Mean transmittance also increases when nanostructure density increases. Light transmission is indeed negatively correlated to light reflection and nanostructures are known to have anti-reflective properties, as demonstrated in the sphingid *Cephonodes hylas* (Yoshida et al., 1997) and in the nymphalid *G. oto* (Siddique et al., 2015). Reflection increases as the difference in refractive index between air and organic materials increases. Nanostructures create a gradient of refractive index between air and wing tissue, and gradient efficiency in reducing reflection increases with a smooth increase in proportion of chitin inside the nanostructures. For instance, pillars with conical bases are more effective at cancelling reflection than cylinders because cones produce a smoother air:chitin gradient from air to wing than cylinders (Siddique et al., 2015). Nanostructure shape is thus important in creating a smooth gradient. In our case, nanostructure density is highly correlated to nanostructure type, which we have defined according to their shape (phylogenetic ANOVA on nanostructure density with nanostructure type as factor: $F = 26.26$, p-value = 0.001, see supplementary result 2 for details). Specifically, the

440 nanostructures whose shape likely creates the smoother gradient (pillar and moss) are
441 also the denser ones. When nanostructure density increases, light reflection thus
442 decreases. Light can either be transmitted, reflected or absorbed, and assuming that the
443 chitin wing membrane only absorbs a small amount of light between 300 and 700 nm
444 (Stavenga et al., 2014), when light reflection decreases because of the presence of
445 nanostructures light transmission necessarily increases, which explains the positive
446 effect of nanostructure density on mean transmittance.

447 We showed that mean transmittance decreases when membrane thickness
448 increases, because wing membrane is mainly made of chitin and even if chitin absorbs a
449 little amount of light (Stavenga et al., 2014), thicker membranes, which contain more
450 chitin, absorb more light than thinner ones, thereby reducing light transmission.

451 We finally showed that wings covered with transparent scales transmit more light
452 than wings covered with coloured scales. This is due to the presence of pigments, such as
453 melanins or ommochromes commonly found in butterfly scales, which absorb some part
454 of the light spectrum, thereby reducing light transmission.

455 Given the high structural diversity uncovered, future studies should thoroughly
456 quantify the relative contributions of micro and nanostructures on the produced optical
457 effects, notably on reflection in transparent patches which may encourage bio-inspired
458 applications for transparent materials.

459

460 *Selection on optical properties as a potential driver of the evolution of structures*

461 We showed that transmission properties are convergent among co-mimetic species and
462 that they depend on the underlying structural features, which confer peculiar visual
463 aspects, raising the question of the putative convergence of structural features among co-
464 mimetic species. We indeed showed that despite the high phylogenetic signal of
465 structures underlying transparency that points to the existence of developmental
466 constraints, both micro- and nanostructural features are convergent among co-mimetic
467 species for some mimicry rings. Convergence is also detected for structural syndromes
468 (i.e. association between micro- and nanostructures). Our data suggest that
469 nanostructures are more labile than microstructures. Nanostructures could therefore
470 evolve more readily in response to selection on the degree of transparency. We showed
471 that the presence and higher densities of nanostructures increase mean transmittance
472 when scale density is already low, thereby allowing fine-tuning of transparency. The

473 interplay between scales and nanostructures can thus modulate the degree of
474 transparency and the selective pressures on the transmission properties of transparent
475 patches may select specific associations of structural features.
476
477 To conclude, this study reveals convergence of transparency features in aposematic
478 mimetic Lepidoptera, which may be the result of selection by predators, likely through
479 aposematism, even though transparent patches may also be under other local selection
480 pressures such as selection for crypsis or adaptation to climatic conditions. Transparency
481 entails strong structural modifications of scales that might impair other functions such as
482 thermoregulation (Berthier, 2005), hydrophobicity (Perez Goodwyn et al., 2009) and
483 perhaps mate signalling. Transparency may therefore come at a cost in those large-
484 winged insects, which may explain why it is not pervasive among Lepidoptera.
485
486
487 **Materials & Methods**
488 For further details about materials and methods see the Supplementary Materials &
489 Methods section in the Supplementary Information.
490
491 *Material*
492 In this study, we focus on 62 different species represented by 1 or 2 specimens collected
493 with hand nets in understory forests in Peru and Ecuador, by ourselves and private
494 collectors (Supplementary table 5). They belong to 7 different families (Nymphalidae,
495 Riodinidae, Pieridae, Papilionidae, Erebidae, Notodontidae, Geometridae) and represent
496 10 different mimicry rings, following the classification used in Ithomiini: 'agnosia',
497 'aureliana', 'banjana-m', 'confusa', 'eurimedia', 'hewitsoni', 'lerida', 'panthyale',
498 'theudelinda' (Chazot et al., 2014; Willmott et al., 2017; Willmott & Mallet, 2004). In
499 addition, we call 'blue' a mimicry ring that does not include Ithomiini species.
500
501 *Phylogeny*
502 We used both published and *de novo* (see 'Phylogeny' section in SI for detailed protocol)
503 sequences from one mitochondrial gene and seven nuclear genes, representing a total
504 length of 7433 bp to infer a molecular phylogeny (knowing that for many taxa there are
505 missing data, see supplementary table 7). To improve the phylogeny topology, we added

35 species representing 8 additional families to the dataset (see Supplementary table 7 and SI). We performed a Bayesian inference of the phylogeny using BEAST 1.8.3. We forced the monophyly of some groups and we added eleven secondary calibration points (see Supplementary table 8) following Kawahara et al. (2019).

*Spectrophotometry*

Specular transmittance was measured over 300-700 nm, a range of wavelengths to which both birds and butterflies are sensitive (Briscoe & Chittka, 2001; Hart, 2001) using a custom-built spectrophotometer (see 'Spectrophotometry' section in SI for details). For each species, we measured five different spots in the transparent patches on the ventral side of the forewing (see figure 1 for location). We computed mean transmittance over 300-700 nm from smoothed spectra using Pavo2 (Maia et al., 2019), as a proxy for transparency: wing transparency increases as mean transmittance increases. On a subset of 16 species, we measured 2 to 3 specimens per species and given that measurements were repeatable (see 'Spectrophotometry' section in SI), we retained only 1 specimen per species for optical measurements.

*High-resolution imaging and structure characterisation*

We observed structures with a digital photonic microscope (Keyence VHX-5000) to determine scale form (lamellar scale vs. piliform scale), scale colour (coloured vs. transparent) and scale insertion (flat vs. erected) on ventral side. We defined as scale type the interaction between scale form and scale insertion (erected lamellar scale, flat lamellar scale and piliform scale). Wings were imaged using SEM (Zeiss Auriga 40) to determine nanostructure type and to measure scale density, scale length and width, membrane thickness, and nanostructure density (see SI for more details). We also determined for each species the structural syndrome, defined as the association between micro- and nanostructural features. On a subset of 3 species, we measured 10 specimens per species, each specimen being measured twice for density and five times for scale dimensions. Given that scale structural features were shown to be repeatable (see 'High-resolution imaging and structure characterization' section in SI) within species we retained one specimen per species in structure characterisation.

539 *Vision models*

540 We used bird vision modelling on the smoothed transmission spectra to test whether
541 transparent patches of co-mimetic species are perceived as similar by birds. Birds differ
542 in their sensitivity to UV wavelength: some are more sensitive to UV (UVS vision) than
543 others (VS vision). As predators of neotropical butterflies can belong to either category
544 (Dell'Aglio et al., 2018), we used wedge-tailed shearwater (*Puffinus pacificus*) as a model
545 for VS vision (Hart, 2004) and blue tit (*Cyanistes caeruleus*) as model for UVS vision (Hart
546 et al., 2000). We considered two different light environments differing in their intensity
547 and spectral distribution: forest shade and large gap as defined by Endler (Endler, 1993;
548 Doris Gomez & Théry, 2007). In our model, we considered that the butterfly was seen
549 against the sky (light is just transmitted through the wing). We used the receptor-noise
550 limited model of Vorobyev and Osorio (Vorobyev & Osorio, 1998) with neural noise and
551 with the following relative cone densities 1:1.9:2.7:2.7 (for UVS:S:M:L, Hart et al. 2000)
552 and 1:0.7:1:1.4 (for VS:S:M:L, Hart 2004) for UVS and VS vision respectively, and a Weber
553 fraction of 0.1 for chromatic vision (Lind et al., 2014; Maier & Bowmaker, 1993) and 0.2
554 for achromatic vision (average of the two species studied in Lind, Karlsson, and Kelber
555 2013) for both visual systems to compute chromatic and achromatic contrasts. In total we
556 calculated 4 different vision models, using the R package Pavo 2 (Maia et al., 2019),
557 representing all combinations of bird visual systems and light environments.

558 We extracted the chromatic and achromatic contrasts between each pair of species in the
559 dataset, comparing only analogous spots (i.e. occupying the same position) on the
560 forewing.

561

562 *Statistical analyses*

563 All statistical analyses were performed with the software R version 3.6.2 and 4.0.3 (R Core
564 Team, 2019).

565

566 *Convergence on optical properties*

567 To assess whether transparent patches, as perceived by predators, were more similar
568 than expected at random, we calculated the mean phenotypic distance (either chromatic
569 or achromatic contrast) for co-mimetic species and we compared this mean phenotypic
570 distance to a null distribution of this mean distance, where the phenotypic distance has
571 been randomised 10000 times over the 1891 possible pairs of species, irrespective of

572 their phylogenetic relationship. The p-value was calculated as the proportion of
573 randomisations when the calculated mean distance for co-mimetic species was smaller
574 than the observed mean distance. The result of this test allows us to determine whether
575 co-mimetic species are perceived as similar by their main predators, irrespectively of the
576 evolutionary underlying mechanism, which can be either shared ancestry of convergent
577 evolution. To disentangle the two possible mechanisms, we accounted for the
578 phylogenetic relationship between species by performing a linear regression between
579 phenotypic distances and phylogenetic distances for each pair of species, following Elias
580 et al. (2008). Pairs of species below the regression line (with a negative residual) are
581 phenotypically more similar than expected given the phylogeny. To test whether pairs of
582 co-mimetic species were mostly below the regression line, we calculated the observed
583 mean residuals for co-mimetic species and we compared it to a null distribution of mean
584 residuals for co-mimetic species, where residuals have been randomised 10000 times
585 over the 1891 possible pairs of species. The p-value was calculated as the proportion of
586 randomisations where the calculated mean residuals was smaller than the observed mean
587 residuals for co-mimetic species. We also tested for each mimicry ring whether co-
588 mimetic species were perceived as more similar as expected at random and given the
589 phylogeny by applying the tests described above as follows: we calculated mean
590 phenotypic distance and mean residuals, respectively, for pairs of species belonging to the
591 considered mimicry ring and compared these means to the random distribution of
592 phenotypic distance and residuals, respectively, of the model restricted to the same
593 number of observations (*i.e.* pair species) as in the mimicry ring considered.
594
595 *Phylogenetic signal*
596 To assess whether transmission properties and structural features were conserved in the
597 phylogeny, we estimated the phylogenetic signal of each variable. For quantitative
598 variable (mean transmittance, scale density, scale length, scale width, nanostructure
599 density and membrane thickness), we calculated both Pagel's λ (Pagel, 1999) and
600 Blomberg's K (Blomberg et al., 2003) implemented in the R package 'phytools' (Revell,
601 2012). For multicategorical variables (scale type and nanostructure type), we used the δ-
602 statistic (Borges et al., 2019) and we compared it to the distribution of values of δ when
603 the trait is randomised along the phylogeny to estimate whether the trait is randomly
604 distributed along the phylogeny. Finally, for binary variables (scale colour), we used Fritz

605 and Purvis' D (Fritz & Purvis, 2010) implemented in the R package 'caper' (Orme et al.,
606 2018).
607
608 *Convergence on structures*
609 We tested whether structural features (microstructures, i.e. scales and nanostructures,
610 but also structural syndrome, *i.e.* the association between microstructures and
611 nanostructures) are more similar between co-mimetic species as expected at random. To
612 do so, we considered every pair of species in our dataset and we calculated the number of
613 co-mimetic species sharing the same structural features. We compared this number to the
614 null distribution of the number of species sharing the same structural features where the
615 structural feature has been randomised 10000 times, a method similar to that used in
616 Willmott and Mallet (2004). We calculated the p-value as the proportion of
617 randomisations where the number of species sharing structures is higher than the
618 observed number. To determine whether this sharing of structures was due to convergent
619 evolution, we performed a generalized linear model with a binomial error distribution
620 linking the variable for structure sharing (1 if species shared the same structure, 0
621 otherwise) with phylogenetic distance. We then calculated the mean residuals of the
622 model for co-mimetic species and we compared it to a null distribution of mean residuals
623 for co-mimetic species, where residuals have been randomised 10000 times. The p-value
624 was given by the proportion of randomisation where the calculated mean residuals for
625 co-mimetic species was higher than the observed mean residuals for co-mimetic species.
626
627 *Link between transparency (mean transmittance) and structures*
628 To assess the link between structural features and the degree of transparency we only
629 used the spectrophotometric data of the points that correspond to the location of the SEM
630 images (between 1 and 3 points per species) and we calculated the average of mean
631 transmittance over 300-700 nm for each specimen. We tested the link between this
632 average mean transmittance and all the structural features we measured (scale type, scale
633 colour, scale density, scale length, scale width, nanostructure type, nanostructure density,
634 membrane thickness and the following interactions: interaction between scale type and
635 scale density, interaction between scale density and nanostructure density and the triple
636 interaction between scale density, scale length and scale width), while controlling for
637 phylogenetic relationships by performing Phylogenetic Generalised Least Square

regression (PGLS) implemented in the R package 'caper' (Orme et al., 2018). We compared all possible models with all the structural variables, but we prevented some variables from being in the same model because they were highly correlated, using the R package 'MuMIn' (Barton, 2019). Among the 308 models, we selected the best models (difference in AICc inferior to 2). Eight such models were retained.

## Acknowledgments/funding

We thank Jonathan Pairraire and Céline Houssin for the help with photonic imaging and Josquin Gerber and Edgar Attivissimo for helping with spectroscopic measurements. We thank Benoit Vincent for the identification of some Arctiini specimens. We are thankful to the Institut de Physique du Globe de Paris (IPGP) for giving us access to SEM and to the Peruvian and Ecuadorian governmental authorities for collection permits (021C/C-2005-INRENA-IANP, 002-2015-SERFOR-DGGSPFFS, 373-2017-SERFOR-DGGSPFFS, 005-IC-FAU-DNBAPVS/MA, 019-IC-FAU-DNBAPVS/MA). This work was funded by Clearwing ANR project (ANR-16-CE02-0012), HFSP project on transparency (RGP0014/2016) and a France-Berkeley fund grant (FBF #2015-58).

## References

Arias, M., Barbut, J., Rougerie, R., Dutry, M., Kohler, M., Laulan, B., Paillard, C., Berthier, S., Andraud, C., Elias, M., & Gomez, D. (2020). Ambient light and mimicry as drivers of wing transparency in Lepidoptera. *BioRxiv*. https://doi.org/10.1101/2020.06.26.172932

Arias, M., Elias, M., Andraud, C., Berthier, S., & Gomez, D. (2020). Transparency improves concealment in cryptically coloured moths. *Journal of Evolutionary Biology*, *33*(2), 247–252. https://doi.org/10.1111/jeb.13560

Arias, M., Mappes, J., Desbois, C., Gordon, S., McClure, M., Elias, M., Nokelainen, O., & Gomez, D. (2019). Transparency reduces predator detection in mimetic clearwing butterflies. *Functional Ecology*, *33*(6), 1110–1119. https://doi.org/10.1111/1365-2435.13315

Baele, G., Lemey, P., Rambaut, A., Suchard, M. A., & Valencia, A. (n.d.). *Adaptive MCMC in Bayesian phylogenetics: an application to analyzing partitioned data in BEAST*.

https://doi.org/10.1093/bioinformatics/btx088

Barnett, J. B., Michalis, C., Scott-Samuel, N. E., & Cuthill, I. C. (2018). Distance-dependent defensive coloration in the poison frog Dendrobates tinctorius, Dendrobatidae. *Proceedings of the National Academy of Sciences of the United States of America*, *115*(25), 6416–6421. https://doi.org/10.1073/pnas.1800826115

Barton, K. (2019). *MuMIn: Multi-Model Inference* (R package version 1.43.15). https://cran.r-project.org/package=MuMIn

Beccaloni, G. W. (1997). Ecology , Natural History and Behaviour of Ithomiine Butterflies and Their Mimics in Ecuador ( Lepidoptera : Nymphalidae : Ithomiinae ). *Tropical Lepidoptera*, *8*(2), 103–124.

Berthier, S. (2005). Thermoregulation and spectral selectivity of the tropical butterfly Prepona meander: A remarkable example of temperature auto-regulation. *Applied Physics A: Materials Science and Processing*, *80*(7), 1397–1400. https://doi.org/10.1007/s00339-004-3185-x

Binetti, V. R., Schiffman, J. D., Leaffer, O. D., Spanier, J. E., & Schauer, C. L. (2009). The natural transparency and piezoelectric response of the Greta oto butterfly wing. *Integrative Biology*, *1*(4), 324–329. https://doi.org/10.1039/b820205b

Blagodatski, A., Sergeev, A., Kryuchkov, M., Lopatina, Y., & Katanaev, V. L. (2015). Diverse set of Turing nanopatterns coat corneae across insect lineages. *Proceedings of the National Academy of Sciences*, *112*(34), 10750–10755. https://doi.org/10.1073/pnas.1505748112

Blomberg, S. P., Garland, T., & Ives, A. R. (2003). Testing for phylogenetic signal in comparative data: Behavioral traits are more labile. *Evolution*, *57*(4), 717–745. https://doi.org/10.1111/j.0014-3820.2003.tb00285.x

Borges, R., Machado, J. P., Gomes, C., Rocha, A. P., & Antunes, A. (2019). Measuring phylogenetic signal between categorical traits and phylogenies. *Bioinformatics*, *35*(11), 1862–1869. https://doi.org/10.1093/bioinformatics/bty800

Briscoe, A. D., & Chittka, L. (2001). The Evolution of Color Vision in Insects. *Annual Review of Entomology*, *46*, 471–510. www.annualreviews.org

Brower, L. P. (1984). Brower_1984_BoB.pdf. In *The biology of Butterflies* (pp. 109–134).

Bybee, S. M., Yuan, F., Ramstetter, M. D., Llorente-Bousquets, J., Reed, R. D., Osorio, D., & Briscoe, A. D. (2012). UV Photoreceptors and UV-Yellow Wing Pigments in Heliconius Butterflies Allow a Color Signal to Serve both Mimicry and Intraspecific

Communication. *The American Naturalist*, *179*(1), 38–51. https://doi.org/10.5061/dryad.8bb43

Chazot, N., Willmott, K. R., Santacruz Endara, P. G., Toporov, A., Hill, R. I., Jiggins, C. D., & Elias, M. (2014). Mutualistic Mimicry and Filtering by Altitude Shape the Structure of Andean Butterfly Communities. *The American Naturalist*, *183*(1), 26–39. https://doi.org/10.1086/674100

Cook, L. M., Grant, B. S., Saccheri, I. J., & Mallet, J. (2012). Selective bird predation on the peppered moth: The last experiment of Michael Majerus. *Biology Letters*, *8*(4), 609–612. https://doi.org/10.1098/rsbl.2011.1136

Cuthill, I. C. (2019). Camouflage. *Journal of Zoology*, *308*(2), 75–92. https://doi.org/10.1111/jzo.12682

Dell'Aglio, D. D., Troscianko, J., McMillan, W. O., Stevens, M., & Jiggins, C. D. (2018). The appearance of mimetic Heliconius butterflies to predators and conspecifics. *Evolution*, *72*(10), 2156–2166. https://doi.org/10.1111/evo.13583

Drummond, A. J., & Rambaut, A. (2007). BEAST: Bayesian evolutionary analysis by sampling trees. *BMC Evolutionary Biology*, *7*(1), 1–8. https://doi.org/10.1186/1471-2148-7-214

Dufour, P. C., Willmott, K. R., Padrón, P. S., Xing, S., Bonebrake, T. C., & Scheffers, B. R. (2018). Divergent melanism strategies in Andean butterfly communities structure diversity patterns and climate responses. *Journal of Biogeography*, *45*(11), 2471–2482. https://doi.org/10.1111/jbi.13433

Dushkina, N., Erten, S., & Lakhtakia, A. (2017). Coloration and Structure of the Wings of Chorinea sylphina Bates. *Journal of the Lepidopterists' Society*, *71*(1), 1–11. https://doi.org/10.18473/lepi.v71i1.a2

Elias, M., Gompert, Z., Jiggins, C., & Willmott, K. (2008). Mutualistic interactions drive ecological niche convergence in a diverse butterfly community. *PLoS Biology*, *6*(12), 1–8. https://doi.org/10.1371/journal.pbio.0060300

Endler, J. A. (1984). Progressive background matching in moths, and a quantitative measure of crypsis. *Biological Journal of the Linnean Sociey*, *22*, 187–231.

Endler, J. A. (1993). The Color of Light in Forests and Its Implications. *Ecological Monographs*, *63*(1), 1–27.

Fritz, S. A., & Purvis, A. (2010). Selectivity in mammalian extinction risk and threat types: A new measure of phylogenetic signal strength in binary traits. *Conservation*

*Biology*, *24*(4), 1042–1051. https://doi.org/10.1111/j.1523-1739.2010.01455.x

Gomez, D., Pinna, C., Pairraire, J., Arias, M., Barbut, J., Pomerantz, A., Noûs, C., Marcillac, W. D. de, Berthier, S., Patel, N., Andraud, C., & Elias, M. (2020). Transparency in butterflies and moths: structural diversity, optical properties and ecological relevance. *BioRxiv*, 2020.05.14.093450. https://doi.org/10.1101/2020.05.14.093450

Gomez, Doris, & Théry, M. (2007). Simultaneous Crypsis and Conspicuousness in Color Patterns: Comparative Analysis of a Neotropical Rainforest Bird Community. *The American Naturalist*, *169*, 42–61. https://doi.org/10.1086/510138

Greenwood, J. J. D., Cotton, P. A., Wilson, D., & M. (1989). Frequency-dependent selection on aposematic prey: some experiments. *Biological Journal of the Linnean Society*, *36*(1–2), 213–226. https://doi.org/10.1111/j.1095-8312.1989.tb00491.x

Hart, N. S. (2001). The visual ecology of avian photoreceptors. *Progress in Retinal and Eye Research*, *20*(5), 675–703.

Hart, N. S. (2004). Microspectrophotometry of visual pigments and oil droplets in a marine bird, the wedge-tailed shearwater Puffinus pacificus: Topographic variations in photoreceptor spectral characteristics. *Journal of Experimental Biology*, *207*(7), 1229–1240. https://doi.org/10.1242/jeb.00857

Hart, N. S., Partridge, J. C., Cuthill, I. C., & Bennett, A. T. D. (2000). Visual pigments, oil droplets, ocular media and cone photoreceptor distribution in two species of passerine bird: the blue tit (Parus caeruleus L.) and the blackbird (Turdus merula L.). *Journal of Comparative Physiology - A Sensory, Neural, and Behavioral Physiology*, *186*, 375–387. https://doi.org/10.1007/s003590050437

Heidrich, L., Friess, N., Fiedler, K., Brändle, M., Hausmann, A., Brandl, R., & Zeuss, D. (2018). The dark side of Lepidoptera: Colour lightness of geometrid moths decreases with increasing latitude. *Global Ecology and Biogeography*, *27*(4), 407–416. https://doi.org/10.1111/geb.12703

Hernández-Chavarría, F., Hernández, A., & Sittenfeld, A. (2004). The “windows”, scales, and bristles of the tropical moth Rothschildia lebeau (Lepidoptera: Saturniidae). *Revista de Biologia Tropical*, *52*(4), 919–926.

Johnsen, S., & Widder, E. A. (1998). Transparency and visibility of gelatinous zooplankton from the Northwestern Atlantic and Gulf of Mexico. *Biological Bulletin*, *195*(3), 337–348. https://doi.org/10.2307/1543145

Kawahara, A. Y., Plotkin, D., Espeland, M., Meusemann, K., Toussaint, E. F. A., Donath, A., Gimnich, F., Frandsen, P. B., Zwick, A., Reis, M. dos, Barber, J. R., Peters, R. S., Liu, S., Zhou, X., Mayer, C., Podsiadlowski, L., Storer, C., Yack, J. E., Misof, B., & Breinholt, J. W. (2019). Phylogenomics reveals the evolutionary timing and pattern of butterflies and moths. *Proceedings of the National Academy of Sciences*, *116*(45), 22657–22663. https://doi.org/10.1073/PNAS.1907847116

Kemp, D. J. (2007). Female butterflies prefer males bearing bright iridescent ornamentation. *Proceedings of the Royal Society B: Biological Sciences*, *274*(1613), 1043–1047. https://doi.org/10.1098/rspb.2006.0043

Lanfear, R., Calcott, B., Ho, S. Y. W., & Guindon, S. (2012). *PartitionFinder: Combined Selection of Partitioning Schemes and Substitution Models for Phylogenetic Analyses*. https://doi.org/10.1093/molbev/mss020

Lind, O., Chavez, J., & Kelber, A. (2014). The contribution of single and double cones to spectral sensitivity in budgerigars during changing light conditions. *Journal of Comparative Physiology - A*, *200*, 197–207. https://doi.org/10.1007/s00359-013-0878-7

Lind, O., Karlsson, S., & Kelber, A. (2013). Brightness Discrimination in Budgerigars (Melopsittacus undulatus). *PLoS ONE*, *8*(1), e54650. https://doi.org/10.1371/journal.pone.0054650

Llaurens, V., Joron, M., & Théry, M. (2014). Cryptic differences in colour among Müllerian mimics: How can the visual capacities of predators and prey shape the evolution of wing colours? *Journal of Evolutionary Biology*, *27*(3), 531–540. https://doi.org/10.1111/jeb.12317

Maia, R., Gruson, H., Endler, J. A., & White, T. E. (2019). pavo 2: New tools for the spectral and spatial analysis of colour in r. *Methods in Ecology and Evolution*, *10*(7), 1097–1107. https://doi.org/10.1111/2041-210X.13174

Maier, E. J., & Bowmaker, J. K. (1993). Colour vision in the passeriform bird, Leiothrix lutea: correlation of visual pigment absorbance and oil droplet transmission with spectral sensitivity. In *Journal of Comparative Physiology - A Sensory, Neural, and Behavioral Physiology Physiol A* (Vol. 172).

McClure, M., Clerc, C., Desbois, C., Meichanetzoglou, A., Cau, M., Bastin-Héline, L., Bacigalupo, J., Houssin, C., Pinna, C., Nay, B., Llaurens, V., Berthier, S., Andraud, C., Gomez, D., & Elias, M. (2019). Why has transparency evolved in aposematic

butterflies? Insights from the largest radiation of aposematic butterflies, the Ithomiini. *Proceedings of the Royal Society B: Biological Sciences*, *286*(1901), 1–10. https://doi.org/10.1098/rspb.2018.2769

Miller, M. A., Pfeiffer, W., & Schwartz, T. (2010). *Creating the CIPRES Science Gateway for Inference of Large Phylogenetic Trees*.

Montgomerie, R. (2006). Analyzing colors. In *Bird coloration mechanisms and measurements* (Vol. 1). Harvard University Press. http://ci.nii.ac.jp/naid/10025355850/en/

Müller, F. (1879). Ituna and Thyridia : a remarkable case of Mimicry in Butterflies. *Kosmos*.

Orme, D., Freckleton, R., Thomas, G., Petzoldt, T., Fritz, S., Isaac, N., & Pearse, W. (2018). *caper: Comparative Analyses of Phylogenetics and Evolution in R* (R package version 1.0.1). https://cran.r-project.org/package=caper

Pagel, M. (1999). Inferring the historical patterns of biological evolution. *Nature*, *401*(6756), 877–884. https://doi.org/10.1038/44766

Perez Goodwyn, P., Maezono, Y., Hosoda, N., & Fujisaki, K. (2009). Waterproof and translucent wings at the same time: Problems and solutions in butterflies. *Naturwissenschaften*, *96*(7), 781–787. https://doi.org/10.1007/s00114-009-0531-z

Pinheiro, J., Bates, D., DebRoy, S., Sarkar, D., & R Core Team. (2019). *{nlme}: Linear and Nonlinear Mixed Effects Models* (R package version 3.1-142). https://cran.r-project.org/package=nlme

Pomerantz, A. F., Siddique, R. H., Cash, E. I., Kishi, Y., Pinna, C., Hammar, K., Gomez, D., Elias, M., & Patel, N. H. (2020). Developmental, cellular, and biochemical basis of transparency in the glasswing butterfly Greta oto. *BioRxiv*. https://doi.org/10.1101/2020.07.02.183590

R Core Team. (2019). *R: A Language and Environment for Statistical Computing*. R Foundation for Statistical Computing. https://www.r-project.org/

Revell, L. J. (2012). phytools: An R package for phylogenetic comparative biology (and other things). *Methods in Ecology and Evolution*, *3*, 217–223. https://doi.org/10.1111/j.2041-210X.2011.00169.x

Schindelin, J., Arganda-Carreras, I., Frise, E., Kaynig, V., Longair, M., Pietzsch, T., Preibisch, S., Rueden, C., Saalfeld, S., Schmid, B., Tinevez, J. Y., White, D. J., Hartenstein, V., Eliceiri, K., Tomancak, P., & Cardona, A. (2012). Fiji: An open-source

platform for biological-image analysis. In *Nature Methods* (Vol. 9, Issue 7, pp. 676–682). Nature Publishing Group. https://doi.org/10.1038/nmeth.2019

Siddique, R. H., Gomard, G., & Hölscher, H. (2015). The role of random nanostructures for the omnidirectional anti-reflection properties of the glasswing butterfly. *Nature Communications*, *6*, 1–8. https://doi.org/10.1038/ncomms7909

Skelhorn, J., Rowland, H. M., Speed, M. P., & Ruxton, G. D. (2010). Masquerade: Camouflage without crypsis. In *Science* (Vol. 327, Issue 5961, p. 51). https://doi.org/10.1126/science.1181931

Smith, S. A., & Dunn, C. W. (2008). *Phyutility: a phyloinformatics tool for trees, alignments and molecular data*. *24*(5), 715–716. https://doi.org/10.1093/bioinformatics/btm619

Stavenga, D. G., Giraldo, M. A., & Leertouwer, H. L. (2010). Butterfly wing colors: Glass scales of graphium sarpedon cause polarized iridescence and enhance blue/green pigment coloration of the wing membrane. *Journal of Experimental Biology*, *213*(10), 1731–1739. https://doi.org/10.1242/jeb.041434

Stavenga, D. G., Hein, ·, Leertouwer, L., & Wilts, B. D. (2014). The colouration toolkit of the Pipevine Swallowtail butterfly, Battus philenor: thin films, papiliochromes, and melanin. *J Comp Physiol A*, *200*, 547–561. https://doi.org/10.1007/s00359-014-0901-7

Stoddard, M. C. (2012). Mimicry and masquerade from the avian visual perspec-tive. In *Current Zoology* (Vol. 58, Issue 4). https://academic.oup.com/cz/article-abstract/58/4/630/1787096

Stoffel, M. A., Nakagawa, S., & Schielzeth, H. (2017). rptR: repeatability estimation and variance decomposition by generalized linear mixed-effects models. *Methods in Ecology and Evolution*, *8*(11), 1639–1644. https://doi.org/10.1111/2041-210X.12797

Su, S., Lim, M., & Kunte, K. (2015). Prey from the eyes of predators: Color discriminability of aposematic and mimetic butterflies from an avian visual perspective. *Evolution*, *69*(11), 2985–2994. https://doi.org/10.1111/evo.12800

Thurman, T. J., & Seymoure, B. M. (2016). A bird's eye view of two mimetic tropical butterflies: Coloration matches predator's sensitivity. *Journal of Zoology*, *298*(3), 159–168. https://doi.org/10.1111/jzo.12305

Tullberg, B. S., Merilaita, S., & Wiklund, C. (2005). Aposematism and crypsis combined as

a result of distance dependence: Functional versatility of the colour pattern in the swallowtail butterfly larva. *Proceedings of the Royal Society B: Biological Sciences*, *272*, 1315–1321. https://doi.org/10.1098/rspb.2005.3079

Turing, A. M. (1952). The chemical basis of morphogenesis. *Philosophical Transactions of the Royal Society of London. Series B, Biological Sciences*, *237*(641), 37–72. https://doi.org/10.1098/rstb.1952.0012

Vallin, A., Dimitrova, M., Kodandaramaiah, U., & Merilaita, S. (2011). Deflective effect and the effect of prey detectability on anti-predator function of eyespots. *Behavioral Ecology and Sociobiology*, *65*(8), 1629–1636. https://doi.org/10.1007/s00265-011-1173-7

Vorobyev, M., & Osorio, D. (1998). Receptor noise as a determinant of colour thresholds. *Proceedings of The Royal Society of London B: Biological Sciences*, *265*(November 1997), 351–358. https://doi.org/10.1098/rspb.1998.0302

Wahlberg, N., & Wheat, C. W. (2008). Genomic outposts serve the phylogenomic pioneers: Designing novel nuclear markers for genomic DNA extractions of lepidoptera. *Systematic Biology*, *57*(2), 231–242. https://doi.org/10.1080/10635150802033006

Webster, R. J., Callahan, A., Godin, J. G. J., & Sherratt, T. N. (2009). Behaviourally mediated crypsis in two nocturnal moths with contrasting appearance. *Philosophical Transactions of the Royal Society B: Biological Sciences*, *364*(1516), 503–510. https://doi.org/10.1098/rstb.2008.0215

Willmott, K. R., & Mallet, J. (2004). Correlations between adult mimicry and larval host plants in ithomiine butterflies. *Proceedings of the Royal Society B: Biological Sciences*, *271*(SUPPL. 5), 266–269. https://doi.org/10.1098/rsbl.2004.0184

Willmott, K. R., Robinson Willmott, J. C., Elias, M., & Jiggins, C. D. (2017). Maintaining mimicry diversity: Optimal warning colour patterns differ among microhabitats in Amazonian clearwing butterflies. *Proceedings of the Royal Society B: Biological Sciences*, *284*(1855), 1–9. https://doi.org/10.1098/rspb.2017.0744

Yoshida, A., Motoyama, M., Kosaku, A., & Miyamoto, K. (1996). Nanoprotuberance Array in the Transparent Wing of a Hawkmoth, Cephonodes hylas. *Zoological Science*, *13*(4), 525–526. https://doi.org/10.2108/zsj.13.525

Yoshida, A., Motoyama, M., Kosaku, A., & Miyamoto, K. (1997). Antireflective Nanoprotuberance Array in the Transparent Wing of a Hawkmoth, Cephonodes

hylas. In *Zoological Science* (Vol. 14, Issue 4, pp. 737–741). https://doi.org/10.2108/zsj.13.525

# Supplementary information

**Supplementary table 1a. Tests of convergence of transparent patches, as perceived by predators, among co-mimetic species: achromatic contrasts.** All the visual systems (VS and UVS) and the illuminants (large gap 'lg' and forest shade 'fs') tested are presented. We compare whether mean achromatic contrast (dL) between co-mimetic species is smaller than expected at random (expected mean dL for co-mimics ± standard deviation (sd)). To do so, we randomized the value of the achromatic contrast 10000 times over each pair of species and we calculated the p-value as the proportion of randomizations where the mean achromatic contrast for co-mimics is smaller than the observed mean achromatic contrast. We also considered whether co-mimetic species were more similar than what is expected according to their phylogenetic relationship. To do so, we did a linear model between achromatic contrasts and phylogenetic distances to account for the effect of phylogeny on the achromatic contrast and we considered the mean of residuals for co-mimetic species. If co-mimetic species are more similar than expected according to their phylogenetic relationship, the mean of residuals should be negative. To test whether the mean of residuals is smaller than expected according to the phylogeny, we randomized residuals over all pair of species and we calculated the mean of residuals for co-mimetic species. We calculated 'p-value with phylogenetic correction' as the proportion of randomizations where the mean of residuals is smaller than the observed mean of residuals. If p-value is smaller than 0.05, it means that co-mimetic species are more similar than expected at random and if p-value with phylogenetic correction is smaller than 0.05, it means that the observed similarity is due to convergence.

| | | | Similarity | | | Convergence | |
|---|---|---|---|---|---|---|---|
| **Illuminant** | **Measured spot compared between 2 co-mimics** | **Avian visual model type** | **Observed mean dL for co-mimics** | **Expected mean dL for co-mimics ± sd** | **p-value** | **Observed mean residuals for co-mimics** | **p-value with phylogenetic correction** |
| fs | s1 | UVS | 6.779 | 7.412 ± 0.452 | 0.0819 (.) | -0.6670 | 0.0537 (.) |
| fs | s1 | VS | 6.768 | 7.406 ± 0.454 | 0.0792 (.) | -0.6646 | 0.0527 (.) |
| fs | s2 | UVS | 7.403 | 8.233 ± 0.540 | 0.0572 (.) | -0.8620 | **0.0365 (*)** |
| fs | s2 | VS | 7.390 | 8.211 ± 0.536 | 0.0601 (.) | -0.8593 | **0.0455 (*)** |
| fs | s3 | UVS | 5.150 | 6.310 ± 0.399 | **0.0009 (***)** | -1.178 | **0.0002 (***)** |
| fs | s3 | VS | 5.146 | 6.294 ± 0.400 | **0.001 (**)** | -1.176 | **0.0005 (***)** |
| fs | s4 | UVS | 5.148 | 6.727 ± 0.479 | **0.0002 (***)** | -1.613 | **0.0001 (***)** |
| fs | s4 | VS | 5.140 | 6.728 ± 0.491 | **0.0003 (***)** | -1.608 | **< 0.0001 (***)** |
| fs | s5 | UVS | 6.170 | 8.404 ± 0.601 | **< 0.0001 (***)** | -2.265 | **< 0.0001 (***)** |
| fs | s5 | VS | 6.163 | 8.396 ± 0.603 | **< 0.0001 (***)** | -2.259 | **0.0001 (***)** |
| lg | s1 | UVS | 6.778 | 7.408 ± 0.456 | 0.083 (.) | -0.6655 | 0.057 (.) |
| lg | s1 | VS | 6.765 | 7.396 ± 0.448 | 0.0793 (.) | -0.6625 | 0.0553 (.) |
| lg | s2 | UVS | 7.401 | 8.223 ± 0.538 | 0.0584 (.) | -0.8591 | **0.0388 (*)** |
| lg | s2 | VS | 7.384 | 8.207 ± 0.538 | 0.057 (.) | -0.8559 | **0.0417 (*)** |
| lg | s3 | UVS | 5.155 | 6.300 ± 0.404 | **0.001 (**)** | -1.1755 | **0.0004 (***)** |
| lg | s3 | VS | 5.140 | 6.293 ± 0.402 | **0.0005 (***)** | -1.174 | **0.0005 (***)** |
| lg | s4 | UVS | 5.147 | 6.740 ± 0.478 | **0.0001 (***)** | -1.610 | **< 0.0001 (***)** |
| lg | s4 | VS | 5.137 | 6.706 ± 0.478 | **0.0005 (***)** | -1.604 | **0.0001 (***)** |
| lg | s5 | UVS | 6.161 | 8.397 ± 0.595 | **< 0.0001 (***)** | -2.262 | **< 0.0001 (***)** |
| lg | s5 | VS | 6.153 | 8.364 ± 0.592 | **0.0001 (***)** | -2.255 | **0.0002 (***)** |

**Supplementary table 1b. Tests of convergence of transparent patches, as perceived by predators, among co-mimetic species: chromatic contrasts.** All the visual systems (VS and UVS) and the illuminants (large gap 'lg' and forest shade 'fs') tested are presented. We compare whether mean chromatic contrast (dS) between co-mimetic species is smaller than expected at random (expected mean dS for co-mimics ± standard deviation (sd)). To do so, we randomized the value of the chromatic contrast 10000 times over each pair of species and we calculated the p-value as the proportion of randomizations where the mean chromatic contrast for co-mimics is smaller than the observed mean chromatic contrast. We also considered whether co-mimetic species were more similar than what is expected according to their phylogenetic relationship. To do so, we did a linear model between chromatic contrasts and phylogenetic distances to account for the effect of phylogeny on the chromatic contrast and we considered the mean of residuals for co-mimetic species. If co-mimetic species are more similar than expected according to their phylogenetic relationship, the mean of residuals should be negative. To test whether the mean of residuals is smaller than expected according to the phylogeny, we randomized residuals over all pair of species and we calculated the mean of residuals for co-mimetic species. We calculated 'p-value with phylogenetic correction' as the proportion of randomizations where the mean of residuals is smaller than the observed mean of residuals. If p-value is smaller than 0.05, it means that co-mimetic species are more similar than expected at random and if p-value with phylogenetic correction is smaller than 0.05, it means that the observed similarity is due to convergence.

| | | | Similarity | | | Convergence | |
|---|---|---|---|---|---|---|---|
| **Illuminant** | **Measured spot compared between 2 co-mimics** | **Avian visual model type** | **Observed mean dS for co-mimics** | **Expected mean dS for co-mimics ± sd** | **p-value** | **Observed mean residuals for co-mimics** | **p-value with phylogenetic correction** |
| fs | s1 | UVS | 2.727 | 2.833 ± 0.160 | 0.2565 | -0.1168 | 0.2278 |
| fs | s1 | VS | 2.520 | 2.621 ± 0.152 | 0.2534 | -0.1084 | 0.2329 |
| fs | s2 | UVS | 3.008 | 3.278 ± 0.188 | 0.075 (.) | -0.2777 | **0.049 (*)** |
| fs | s2 | VS | 2.837 | 3.083 ± 0.167 | 0.0883 (.) | -0.2555 | 0.0709 (.) |
| fs | s3 | UVS | 2.861 | 3.071 ± 0.173 | 0.1124 | -0.2181 | 0.0985 (.) |
| fs | s3 | VS | 2.652 | 2.838 ± 0.167 | 0.1308 | -0.1929 | 0.1095 |
| fs | s4 | UVS | 2.703 | 2.879 ± 0.169 | 0.1509 | -0.1870 | 0.1204 |
| fs | s4 | VS | 2.497 | 2.672 ± 0.167 | 0.1519 | -0.1821 | 0.1282 |
| fs | s5 | UVS | 2.643 | 3.033 ± 0.178 | **0.0113 (*)** | -0.3996 | **0.0084 (**)** |
| fs | s5 | VS | 2.439 | 2.805 ± 0.171 | **0.0148 (*)** | -0.3736 | **0.0107 (*)** |
| lg | s1 | UVS | 2.707 | 2.816 ± 0.160 | 0.2422 | -0.1202 | 0.2137 |
| lg | s1 | VS | 2.520 | 2.624 ± 0.155 | 0.2563 | -0.1112 | 0.2263 |
| lg | s2 | UVS | 2.998 | 3.270 ± 0.184 | 0.0677 (.) | -0.2848 | 0.0503 (.) |
| lg | s2 | VS | 2.843 | 3.093± 0.182 | 0.0812 (.) | -0.2637 | 0.0652 (.) |
| lg | s3 | UVS | 2.846 | 3.057 ± 0.174 | 0.1137 | -0.2202 | 0.0944 (.) |
| lg | s3 | VS | 2.654 | 2.841 ± 0.168 | 0.1402 | -0.1938 | 0.1129 |
| lg | s4 | UVS | 2.679 | 2.867 ± 0.172 | 0.1441 | -0.1964 | 0.115 |
| lg | s4 | VS | 2.494 | 2.675 ± 0.170 | 0.1473 | -0.1898 | 0.1222 |
| lg | s5 | UVS | 2.616 | 3.015 ± 0.177 | 0.0099 (**) | -0.4084 | **0.0072 (**)** |
| lg | s5 | VS | 2.425 | 2.798 ± 0.174 | 0.0124 (*) | -0.3816 | **0.0091 (**)** |

**Supplementary table 2a. Results of the test of convergence of achromatic (dL) contrasts for each mimicry ring. All the visual systems (VS and UVS) and the illuminants (large gap 'lg' and forest shade 'fs') tested are presented.** For each spot measured on the forewing and for each mimicry ring (see figure on top of the table), the mean achromatic contrast has been compared to what is expected at random (1st column highlighted in grey for each mimicry ring, p-value in brackets) and to what is expected according to the phylogeny (2nd column for each mimicry ring, p-value in brackets). Mean achromatic contrast statistically different from what is expected at random or given the phylogeny are highlighted in bold. To test whether mean achromatic contrast between co-mimetic species of a given mimicry ring is smaller to what is expected at random, we randomized the value of the achromatic contrast 10000 times over each pair of species, we calculated the mean achromatic contrast for these co-mimetic species for each randomisation and we calculated the p-value as the proportion of randomisations where the mean achromatic contrast for co-mimics is smaller than the observed mean achromatic contrast. To test whether the mean achromatic contrast between co-mimetic species of a given mimicry ring is smaller than what might be expected given their phylogenetic relationship, we did a linear model between achromatic contrasts and phylogenetic distances to account for the effect of phylogeny on the achromatic contrast and we considered the mean of residuals for co-mimetic species of a given mimicry ring. If co-mimetic species are more similar than expected according to the phylogeny, the mean of residuals should be negative. To test whether the mean of residuals is smaller than expected according to the phylogeny, we randomised residuals over all pair of species and we calculated the mean of residuals for co-mimetic species of a given mimicry ring. We calculated 'p-value with phylogenetic correction' as the proportion of randomisations where the mean of residuals is smaller than the observed mean of residuals.

The figure above the table is a graphical representation of the results in the table (irrespective of the visual system or the illuminant as the results are similar): each spot measured is localised on the forewing and the results of the test are represented by the colour of the spot. Black spots stand for spots that are neither more similar than expected at random nor convergent (more similar when phylogenetic relationships are accounted for) between co-mimetic species. Blue spots stand for spots that are not more similar than expected at random but which are convergent because they are more similar that what might be expected according to their phylogenetic distance. Red spots stand for spots that are more similar than expected at random but not convergent. Purple spots stand for spots that are both more similar than expected at random and convergent (more similar than what might be expected based on phylogenetic distance). Tests' p-values are represented with the following symbols: '***' p < 0.001, '**' p < 0.01, '*' p < 0.05.

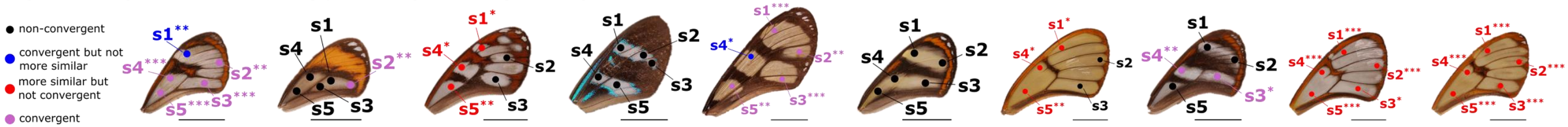


| Illuminant | Spot | Visual system | agnosia | | aureliana | | banjana-m | | blue | | confusa | | eurimedia | | hewitsoni | | lerida | | panthyale | | theudelinda | |
|---|---|---|---|---|---|---|---|---|---|---|---|---|---|---|---|---|---|---|---|---|---|---|
| | | | Observed mean dL | Observed mean residuals with phylogenetic correction | Observed mean dL | Observed mean residuals with phylogenetic correction | Observed mean dL | Observed mean residuals with phylogenetic correction | Observed mean dL | Observed mean residuals with phylogenetic correction | Observed mean dL | Observed mean residuals with phylogenetic correction | Observed mean dL | Observed mean residuals with phylogenetic correction | Observed mean dL | Observed mean residuals with phylogenetic correction | Observed mean dL | Observed mean residuals with phylogenetic correction | Observed mean dL | Observed mean residuals with phylogenetic correction | Observed mean dL | Observed mean residuals with phylogenetic correction |
| fs | s1 | UVS | 6.485 (0.111) | **-1.754 (0.006)** | 9.256 (0.819) | 2.061 (0.852) | **3.917 (0.019)** | -2.051 (0.097) | 14.923 (0.824) | 10.279 (0.882) | **4.149 (0.009)** | **-4.164 (< 0.001)** | 13.606 (1) | 5.614 (1) | **1.356 (0.025)** | -1.426 (0.401) | 7.255 (0.479) | -0.502 (0.317) | **0.443 (< 0.001)** | -2.171 (0.225) | **0.958 (< 0.001)** | -2.094 (0.153) |
| fs | s1 | VS | 6.477 (0.109) | **-1.748 (0.004)** | 9.249 (0.803) | 2.067 (0.827) | **3.908 (0.017)** | -2.05 (0.111) | 14.903 (0.837) | 10.268 (0.897) | **4.154 (0.003)** | **-4.144 (< 0.001)** | 13.581 (1) | 5.602 (1) | **1.355 (0.036)** | -1.422 (0.396) | 7.232 (0.476) | -0.511 (0.353) | **0.441 (0.001)** | -2.168 (0.258) | **0.954 (< 0.001)** | -2.092 (0.144) |
| fs | s2 | UVS | **6.818 (0.044)** | **-2.347 (0.001)** | **2.56 (0.003)** | **-5.421 (0.009)** | 6.302 (0.213) | -0.288 (0.469) | 16.451 (0.817) | 11.362 (0.889) | **4.672 (0.012)** | **-4.575 (0.001)** | 14.159 (1) | 5.274 (0.999) | 2.085 (0.075) | -0.895 (0.49) | 10.76 (0.943) | 2.143 (0.912) | **0.867 (0.001)** | -1.922 (0.293) | **1.264 (< 0.001)** | -2.021 (0.221) |
| fs | s2 | VS | **6.808 (0.044)** | **-2.338 (0.001)** | **2.56 (0.004)** | **-5.405 (0.005)** | 6.28 (0.19) | -0.297 (0.473) | 16.428 (0.829) | 11.349 (0.882) | **4.67 (0.02)** | **-4.559 (0.005)** | 14.13 (1) | 5.262 (0.999) | 2.086 (0.07) | -0.887 (0.496) | 10.73 (0.931) | 2.13 (0.916) | **0.863 (< 0.001)** | -1.92 (0.316) | **1.261 (< 0.001)** | -2.017 (0.216) |
| fs | s3 | UVS | **4.205 (< 0.001)** | **-2.821 (< 0.001)** | 4.523 (0.174) | -1.596 (0.19) | 4.755 (0.137) | -0.298 (0.449) | 11.61 (0.852) | 7.708 (0.876) | **3.404 (0.008)** | **-3.686 (< 0.001)** | 13.107 (1) | 6.296 (1) | 2.153 (0.104) | -0.132 (0.529) | **4.437 (0.048)** | **-2.169 (0.015)** | **1.624 (0.011)** | -0.515 (0.44) | **0.909 (< 0.001)** | -1.61 (0.203) |
| fs | s3 | VS | **4.198 (< 0.001)** | **-2.813 (< 0.001)** | 4.506 (0.177) | -1.599 (0.171) | 4.744 (0.154) | -0.297 (0.468) | 11.59 (0.859) | 7.698 (0.896) | **3.403 (0.003)** | **-3.672 (< 0.001)** | 13.071 (1) | 6.274 (1) | 2.151 (0.111) | -0.127 (0.551) | **4.421 (0.043)** | **-2.171 (0.012)** | **1.611 (0.014)** | -0.521 (0.462) | **0.901 (< 0.001)** | -1.61 (0.216) |
| fs | s4 | UVS | **3.584 (< 0.001)** | **-3.938 (< 0.001)** | 6.713 (0.516) | 0.193 (0.551) | **3.057 (0.015)** | -2.285 (0.089) | 12.856 (0.816) | 8.785 (0.902) | 4.46 (0.067) | **-3.132 (0.012)** | 15.149 (1) | 7.864 (1) | **1.18 (0.038)** | -1.104 (0.47) | **3.874 (0.016)** | **-3.185 (0.004)** | **0.451 (< 0.001)** | -1.671 (0.332) | **1.194 (< 0.001)** | -1.349 (0.293) |
| fs | s4 | VS | **3.581 (< 0.001)** | **-3.927 (< 0.001)** | 6.695 (0.554) | 0.188 (0.552) | **3.055 (0.007)** | -2.276 (0.103) | 12.843 (0.82) | 8.781 (0.901) | 4.459 (0.06) | **-3.119 (0.01)** | 15.121 (1) | 7.85 (1) | **1.181 (0.02)** | -1.096 (0.45) | **3.861 (0.01)** | **-3.184 (0.008)** | **0.449 (< 0.001)** | -1.668 (0.3) | **1.189 (< 0.001)** | -1.347 (0.287) |
| fs | s5 | UVS | **3.049 (< 0.001)** | **-6.181 (< 0.001)** | 7.516 (0.428) | -0.667 (0.448) | **3.549 (0.006)** | -3.402 (0.07) | 12.962 (0.795) | 7.339 (0.861) | **4.361 (0.014)** | **-4.943 (0.002)** | 15.9 (1) | 6.916 (1) | **0.481 (0.003)** | -3.273 (0.33) | 12.33 (0.982) | 3.584 (0.975) | **0.281 (< 0.001)** | -3.304 (0.19) | **1.012 (< 0.001)** | -3.012 (0.132) |
| fs | s5 | VS | **3.045 (< 0.001)** | **-6.171 (< 0.001)** | 7.503 (0.436) | -0.667 (0.423) | **3.54 (0.004)** | -3.4 (0.062) | 12.924 (0.798) | 7.311 (0.855) | **4.368 (0.014)** | **-4.922 (< 0.001)** | 15.868 (1) | 6.899 (1) | **0.482 (< 0.001)** | -3.265 (0.282) | 12.329 (0.984) | 3.597 (0.972) | **0.28 (< 0.001)** | -3.299 (0.185) | **1.01 (< 0.001)** | -3.007 (0.131) |
| lg | s1 | UVS | 6.485 (0.097) | **-1.751 (0.003)** | 9.263 (0.799) | 2.069 (0.814) | **3.923 (0.02)** | -2.044 (0.116) | 14.907 (0.861) | 10.263 (0.889) | **4.145 (0.013)** | **-4.165 (0.001)** | 13.593 (1) | 5.603 (1) | **1.352 (0.023)** | -1.431 (0.422) | 7.258 (0.437) | -0.496 (0.363) | **0.447 (< 0.001)** | -2.168 (0.214) | **0.961 (< 0.001)** | -2.091 (0.153) |
| lg | s1 | VS | 6.475 (0.096) | **-1.744 (0.004)** | 9.254 (0.796) | 2.077 (0.836) | **3.911 (0.013)** | -2.043 (0.095) | 14.882 (0.815) | 10.249 (0.896) | **4.151 (0.008)** | **-4.141 (< 0.001)** | 13.562 (1) | 5.589 (1) | **1.351 (0.033)** | -1.426 (0.402) | 7.23 (0.443) | -0.507 (0.36) | **0.444 (< 0.001)** | -2.164 (0.236) | **0.956 (< 0.001)** | -2.089 (0.161) |
| lg | s2 | UVS | **6.82 (0.042)** | **-2.339 (0.004)** | **2.558 (0.002)** | **-5.418 (0.007)** | 6.316 (0.202) | -0.27 (0.502) | 16.439 (0.837) | 11.354 (0.888) | **4.674 (0.015)** | **-4.568 (< 0.001)** | 14.154 (1) | 5.275 (0.999) | 2.078 (0.088) | -0.899 (0.474) | 10.732 (0.943) | 2.12 (0.922) | **0.871 (< 0.001)** | -1.915 (0.301) | **1.265 (< 0.001)** | -2.017 (0.197) |

| | | | | | | | | | | | | | | | | | | | | | | |
|---|---|---|---|---|---|---|---|---|---|---|---|---|---|---|---|---|---|---|---|---|---|---|
| lg | s2 | VS | 6.808<br>(0.05) | **-2.329**<br>**(0.003)** | **2.559**<br>**(0.007)** | **-5.397**<br>**(0.002)** | 6.289<br>(0.207) | -0.281<br>(0.471) | 16.411<br>(0.826) | 11.339<br>(0.886) | **4.671**<br>**(0.02)** | **-4.548**<br>**(< 0.001)** | 14.118<br>(1) | 5.26<br>(0.999) | 2.079<br>(0.075) | -0.889<br>(0.471) | 10.695<br>(0.945) | 2.105<br>(0.92) | **0.866**<br>**(< 0.001)** | -1.912<br>(0.268) | **1.263**<br>**(< 0.001)** | -2.011<br>(0.221) |
| lg | s3 | UVS | **4.205**<br>**(< 0.001)** | **-2.814**<br>**(< 0.001)** | 4.531<br>(0.207) | -1.582<br>(0.226) | 4.758<br>(0.173) | -0.292<br>(0.458) | 11.581<br>(0.841) | 7.68<br>(0.889) | **3.401**<br>**(0.012)** | **-3.682**<br>**(< 0.001)** | 13.064<br>(1) | 6.259<br>(1) | 2.149<br>(0.093) | -0.138<br>(0.523) | **4.447**<br>**(0.052)** | **-2.153**<br>**(0.023)** | **1.636**<br>**(0.003)** | -0.505<br>(0.453) | **0.918**<br>**(< 0.001)** | -1.602<br>(0.191) |
| lg | s3 | VS | **4.197**<br>**(< 0.001)** | **-2.803**<br>**(< 0.001)** | 4.51<br>(0.208) | -1.586<br>(0.212) | 4.744<br>(0.174) | -0.291<br>(0.455) | 11.556<br>(0.864) | 7.667<br>(0.902) | **3.399**<br>**(0.007)** | **-3.665**<br>**(< 0.001)** | 13.019<br>(1) | 6.233<br>(1) | 2.147<br>(0.098) | -0.131<br>(0.56) | **4.426**<br>**(0.043)** | **-2.156**<br>**(0.015)** | **1.62**<br>**(0.008)** | -0.512<br>(0.436) | **0.909**<br>**(< 0.001)** | -1.602<br>(0.203) |
| lg | s4 | UVS | **3.584**<br>**(< 0.001)** | **-3.933**<br>**(< 0.001)** | 6.723<br>(0.553) | 0.207<br>(0.58) | **3.059**<br>**(0.011)** | -2.281<br>(0.089) | 12.852<br>(0.799) | 8.782<br>(0.897) | 4.458<br>(0.067) | **-3.129**<br>**(0.011)** | 15.134<br>(1) | 7.853<br>(1) | **1.174**<br>**(0.031)** | -1.111<br>(0.446) | **3.875**<br>**(0.014)** | **-3.179**<br>**(0.003)** | **0.457**<br>**(< 0.001)** | -1.667<br>(0.301) | **1.2**<br>**(0.001)** | -1.344<br>(0.306) |
| lg | s4 | VS | **3.58**<br>**(< 0.001)** | **-3.919**<br>**(< 0.001)** | 6.7<br>(0.555) | 0.2<br>(0.563) | **3.056**<br>**(0.013)** | -2.27<br>(0.093) | 12.835<br>(0.811) | 8.777<br>(0.904) | 4.457<br>(0.065) | **-3.113**<br>**(0.013)** | 15.1<br>(1) | 7.836<br>(1) | 1.175<br>(0.051) | -1.102<br>(0.446) | **3.859**<br>**(0.012)** | **-3.178**<br>**(0.003)** | **0.453**<br>**(< 0.001)** | -1.663<br>(0.302) | **1.193**<br>**(< 0.001)** | -1.341<br>(0.312) |
| lg | s5 | UVS | **3.052**<br>**(< 0.001)** | **-6.167**<br>**(< 0.001)** | 7.518<br>(0.447) | -0.654<br>(0.423) | **3.557**<br>**(0.007)** | -3.386<br>(0.062) | 12.97<br>(0.796) | 7.354<br>(0.843) | **4.353**<br>**(0.009)** | **-4.939**<br>**(0.001)** | 15.863<br>(1) | 6.891<br>(1) | **0.473**<br>**(0.001)** | -3.278<br>(0.292) | 12.298<br>(0.985) | 3.563<br>(0.975) | **0.283**<br>**(< 0.001)** | -3.3<br>(0.183) | **1.013**<br>**(< 0.001)** | -3.008<br>(0.124) |
| lg | s5 | VS | **3.047**<br>**(< 0.001)** | **-6.154**<br>**(< 0.001)** | 7.502<br>(0.419) | -0.654<br>(0.47) | **3.545**<br>**(0.006)** | -3.384<br>(0.055) | 12.924<br>(0.801) | 7.318<br>(0.851) | **4.362**<br>**(0.014)** | **-4.913**<br>**(0.003)** | 15.824<br>(1) | 6.87<br>(1) | **0.475**<br>**(0.004)** | -3.268<br>(0.287) | 12.296<br>(0.99) | 3.578<br>(0.978) | **0.282**<br>**(< 0.001)** | -3.294<br>(0.189) | **1.011**<br>**(< 0.001)** | -3.002<br>(0.139) |

**Supplementary table 2b. Results of the test of convergence of chromatic (dS) contrasts for each mimicry ring. All the visual systems (VS and UVS) and the illuminants (large gap 'lg' and forest shade 'fs') tested are presented.** For each spot measured on the forewing and for each mimicry ring (see figure on top of the table), the mean chromatic contrast has been compared to what is expected at random (1st column highlighted in grey for each mimicry ring, p-value in brackets) and to what is expected according to the phylogeny (2nd column for each mimicry ring, p-value in brackets). Mean chromatic contrast statistically different from what is expected at random or given the phylogeny are highlighted in bold. To test whether mean chromatic contrast between co-mimetic species of a given mimicry ring is smaller to what is expected at random, we randomized the value of the chromatic contrast 10000 times over each pair of species, we calculated the mean chromatic contrast for these co-mimetic species for each randomisation and we calculated the p-value as the proportion of randomisations where the mean chromatic contrast for co-mimics is smaller than the observed mean chromatic contrast. To test whether the mean chromatic contrast between co-mimetic species of a given mimicry ring is smaller than what might be expected given their phylogenetic relationship, we did a linear model between chromatic contrasts and phylogenetic distances to account for the effect of phylogeny on the chromatic contrast and we considered the mean of residuals for co-mimetic species of a given mimicry ring. If co-mimetic species are more similar than expected according to the phylogeny, the mean of residuals should be negative. To test whether the mean of residuals is smaller than expected according to the phylogeny, we randomised residuals over all pair of species and we calculated the mean of residuals for co-mimetic species of a given mimicry ring. We calculated 'p-value with phylogenetic correction' as the proportion of randomisations where the mean of residuals is smaller than the observed mean of residuals.

The figure above the table is a graphical representation of the results in the table (irrespective of the visual system or the illuminant as the results are similar): each spot measured is localised on the forewing and the results of the test are represented by the colour of the spot. Black spots stand for spots that are neither more similar than expected at random nor convergent (more similar when phylogenetic relationships are accounted for) between co-mimetic species. Blue spots stand for spots that are not more similar than expected at random but which are convergent because they are more similar that what might be expected according to their phylogenetic distance. Red spots stand for spots that are more similar than expected at random but not convergent. Purple spots stand for spots that are both more similar than expected at random and convergent (more similar than what might be expected based on phylogenetic distance). Tests' p-values are represented with the following symbols: '***' p < 0.001, '**' p < 0.01, '*' p < 0.05.

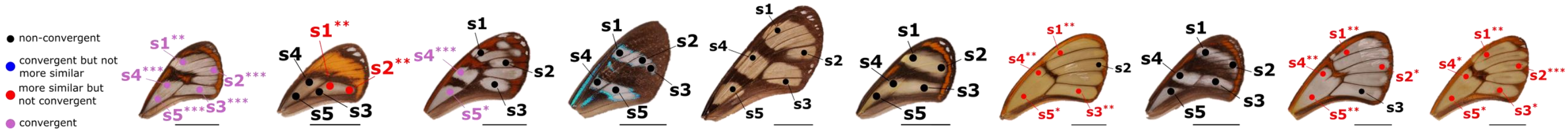


| Illuminant | Spot | Visual system | agnosia | | aureliana | | banjana-m | | blue | | confusa | | eurimedia | | hewitsoni | | lerida | | panthyale | | theudelinda | |
|---|---|---|---|---|---|---|---|---|---|---|---|---|---|---|---|---|---|---|---|---|---|---|
| | | | Observed mean dS | Observed mean residuals with phylogenetic correction | Observed mean dS | Observed mean residuals with phylogenetic correction | Observed mean dS | Observed mean residuals with phylogenetic correction | Observed mean dS | Observed mean residuals with phylogenetic correction | Observed mean dS | Observed mean residuals with phylogenetic correction | Observed mean dS | Observed mean residuals with phylogenetic correction | Observed mean dS | Observed mean residuals with phylogenetic correction | Observed mean dS | Observed mean residuals with phylogenetic correction | Observed mean dS | Observed mean residuals with phylogenetic correction | Observed mean dS | Observed mean residuals with phylogenetic correction |
| fs | s1 | UVS | 2.495 (0.068) | **-0.571 (0.008)** | **1.216 (0.012)** | **-1.557 (0.009)** | 1.825 (0.05) | -0.604 (0.173) | 2.653 (0.618) | 0.595 (0.651) | 2.51 (0.294) | -0.576 (0.116) | 4.401 (1) | 1.404 (0.998) | **0.362 (0.001)** | -1.175 (0.216) | 4.274 (0.998) | 1.343 (0.999) | **0.704 (0.002)** | -0.786 (0.209) | **1.066 (0.003)** | -0.546 (0.263) |
| fs | s1 | VS | **2.211 (0.036)** | **-0.617 (0.001)** | **1.125 (0.013)** | **-1.44 (0.007)** | 1.763 (0.068) | -0.495 (0.211) | 1.523 (0.48) | -0.402 (0.561) | 2.395 (0.35) | -0.45 (0.18) | 4.118 (1) | 1.353 (0.999) | **0.267 (0.002)** | -1.191 (0.222) | 4.149 (1) | 1.443 (0.999) | **0.59 (0.001)** | -0.826 (0.174) | **1.023 (0.005)** | -0.503 (0.255) |
| fs | s2 | UVS | **2.111 (< 0.001)** | **-1.481 (< 0.001)** | **0.775 (< 0.001)** | **-2.414 (0.001)** | 3.157 (0.455) | 0.441 (0.757) | 3.257 (0.598) | 1.052 (0.672) | 3.002 (0.347) | -0.618 (0.147) | 6.14 (1) | 2.644 (1) | 1.168 (0.105) | -0.319 (0.463) | 4.893 (0.996) | 1.488 (0.997) | **1.34 (0.036)** | -0.082 (0.51) | **0.678 (< 0.001)** | -0.914 (0.129) |
| fs | s2 | VS | **1.886 (< 0.001)** | **-1.5 (< 0.001)** | **0.573 (< 0.001)** | **-2.428 (0.002)** | 3.06 (0.491) | 0.513 (0.782) | 1.786 (0.528) | -0.273 (0.557) | 2.861 (0.339) | -0.552 (0.169) | 6.183 (1) | 2.888 (1) | 0.998 (0.096) | -0.374 (0.449) | 4.632 (0.999) | 1.424 (0.999) | **1.189 (0.038)** | -0.122 (0.464) | **0.633 (< 0.001)** | -0.839 (0.175) |
| fs | s3 | UVS | **2.19 (0.001)** | **-1.13 (< 0.001)** | 2.754 (0.393) | -0.25 (0.394) | **1.936 (0.044)** | -0.695 (0.14) | 4.74 (0.749) | 2.51 (0.822) | 3.3 (0.682) | -0.043 (0.498) | 5.586 (1) | 2.341 (1) | **0.359 (< 0.001)** | -1.306 (0.186) | 3.269 (0.68) | 0.095 (0.611) | 2.79 (0.432) | 1.176 (0.853) | **1.383 (0.016)** | -0.364 (0.355) |
| fs | s3 | VS | **1.895 (< 0.001)** | **-1.178 (< 0.001)** | 2.69 (0.472) | -0.083 (0.472) | 1.838 (0.056) | -0.582 (0.179) | 2.843 (0.608) | 0.805 (0.685) | 3.218 (0.76) | 0.123 (0.599) | 5.526 (1) | 2.523 (1) | **0.31 (< 0.001)** | -1.193 (0.242) | 3.026 (0.642) | 0.092 (0.595) | 2.43 (0.375) | 0.975 (0.814) | **1.261 (0.008)** | -0.32 (0.355) |
| fs | s4 | UVS | **2.117 (0.001)** | **-1.024 (< 0.001)** | 2.751 (0.454) | -0.059 (0.458) | **0.733 (< 0.001)** | **-1.687 (< 0.001)** | 2.295 (0.588) | 0.295 (0.655) | 3.653 (0.897) | 0.488 (0.815) | 5.644 (1) | 2.581 (1) | **0.376 (0.001)** | -1.033 (0.268) | 3.221 (0.75) | 0.233 (0.72) | **0.881 (0.008)** | -0.475 (0.335) | **1.083 (0.003)** | -0.411 (0.315) |
| fs | s4 | VS | **1.806 (< 0.001)** | **-1.105 (< 0.001)** | 2.683 (0.537) | 0.078 (0.602) | **0.6 (< 0.001)** | **-1.646 (0.001)** | 1.185 (0.374) | -0.673 (0.522) | 3.529 (0.924) | 0.596 (0.849) | 5.552 (1) | 2.713 (1) | **0.328 (0.002)** | -0.985 (0.29) | 3.047 (0.771) | 0.277 (0.703) | **0.694 (0.003)** | -0.57 (0.313) | **1.04 (0.012)** | -0.351 (0.34) |
| fs | s5 | UVS | **1.592 (< 0.001)** | **-1.694 (< 0.001)** | 2.444 (0.261) | -0.521 (0.255) | **1.39 (0.004)** | **-1.2 (0.024)** | 3.716 (0.659) | 1.532 (0.743) | 3.31 (0.702) | 0.002 (0.528) | 5.895 (1) | 2.685 (1) | **0.735 (0.021)** | -0.878 (0.288) | 4.055 (0.978) | 0.918 (0.979) | **0.714 (0.002)** | -0.847 (0.227) | **1.445 (0.025)** | -0.25 (0.418) |
| fs | s5 | VS | **1.329 (< 0.001)** | **-1.708 (< 0.001)** | 2.397 (0.327) | -0.344 (0.352) | **1.309 (0.005)** | **-1.083 (0.039)** | 4.01 (0.701) | 1.994 (0.812) | 3.208 (0.759) | 0.149 (0.629) | 5.739 (1) | 2.771 (1) | **0.664 (0.043)** | -0.824 (0.348) | 3.68 (0.946) | 0.78 (0.952) | **0.655 (0.002)** | -0.785 (0.261) | **1.384 (0.023)** | -0.18 (0.439) |
| lg | s1 | UVS | 2.455 (0.072) | **-0.594 (0.006)** | **1.2 (0.003)** | **-1.556 (0.007)** | **1.822 (0.043)** | -0.592 (0.177) | 2.553 (0.611) | 0.509 (0.68) | 2.484 (0.287) | -0.586 (0.13) | 4.443 (0.998) | 1.463 (0.998) | **0.354 (0.002)** | -1.17 (0.21) | 4.255 (0.999) | 1.341 (0.999) | **0.677 (0.002)** | -0.801 (0.202) | **1.051 (0.004)** | -0.549 (0.242) |
| lg | s1 | VS | **2.189 (0.026)** | **-0.642 (0.003)** | **1.115 (0.013)** | **-1.453 (0.009)** | 1.772 (0.072) | -0.488 (0.212) | 1.542 (0.499) | -0.385 (0.541) | 2.377 (0.302) | -0.473 (0.177) | 4.195 (1) | 1.426 (0.999) | **0.259 (0.001)** | -1.2 (0.18) | 4.166 (0.998) | 1.456 (0.999) | **0.568 (< 0.001)** | -0.849 (0.18) | **1.018 (0.005)** | -0.51 (0.224) |
| lg | s2 | UVS | **2.079 (< 0.001)** | **-1.51 (< 0.001)** | **0.745 (< 0.001)** | **-2.441 (< 0.001)** | 3.147 (0.46) | 0.436 (0.729) | 3.12 (0.574) | 0.921 (0.675) | 2.969 (0.309) | -0.649 (0.128) | 6.223 (1) | 2.729 (1) | 1.136 (0.091) | -0.343 (0.431) | 4.894 (0.996) | 1.491 (0.998) | **1.311 (0.039)** | -0.103 (0.519) | **0.665 (< 0.001)** | -0.918 (0.133) |

| | | | | | | | | | | | | | | | | | | | | | | |
|---|---|---|---|---|---|---|---|---|---|---|---|---|---|---|---|---|---|---|---|---|---|---|
| lg | s2 | VS | **1.869 (< 0.001)** | **-1.533 (< 0.001)** | **0.549 (< 0.001)** | **-2.464 (< 0.001)** | 3.074 (0.509) | 0.516 (0.777) | 1.791 (0.47) | -0.274 (0.554) | 2.84 (0.348) | -0.588 (0.16) | 6.318 (1) | 3.008 (1) | 0.973 (0.096) | -0.401 (0.44) | 4.62 (0.997) | 1.398 (0.998) | **1.166 (0.033)** | -0.145 (0.498) | **0.626 (< 0.001)** | -0.847 (0.16) |
| lg | s3 | UVS | **2.14 (< 0.001)** | **-1.168 (< 0.001)** | 2.758 (0.348) | -0.232 (0.416) | **1.938 (0.044)** | -0.679 (0.154) | 4.537 (0.746) | 2.323 (0.831) | 3.283 (0.648) | -0.047 (0.503) | 5.722 (1) | 2.489 (1) | **0.362 (0.001)** | -1.284 (0.217) | 3.221 (0.644) | 0.06 (0.574) | 2.72 (0.411) | 1.125 (0.86) | **1.363 (0.009)** | -0.366 (0.369) |
| lg | s3 | VS | **1.859 (< 0.001)** | **-1.219 (< 0.001)** | 2.709 (0.466) | -0.066 (0.496) | 1.849 (0.053) | -0.571 (0.209) | 2.654 (0.595) | 0.619 (0.672) | 3.212 (0.776) | 0.113 (0.581) | 5.699 (1) | 2.693 (1) | **0.312 (0.002)** | -1.184 (0.174) | 2.999 (0.648) | 0.06 (0.572) | 2.376 (0.348) | 0.93 (0.818) | **1.247 (0.014)** | -0.326 (0.367) |
| lg | s4 | UVS | **2.058 (< 0.001)** | **-1.07 (< 0.001)** | 2.746 (0.471) | -0.05 (0.488) | **0.712 (< 0.001)** | **-1.694 (< 0.001)** | 2.169 (0.56) | 0.184 (0.67) | 3.624 (0.899) | 0.473 (0.795) | 5.752 (1) | 2.702 (1) | **0.364 (0.001)** | -1.03 (0.274) | 3.183 (0.766) | 0.208 (0.702) | **0.842 (0.009)** | -0.498 (0.335) | **1.07 (0.003)** | -0.409 (0.313) |
| lg | s4 | VS | **1.762 (< 0.001)** | **-1.156 (< 0.001)** | 2.696 (0.561) | 0.086 (0.55) | **0.589 (< 0.001)** | **-1.659 (0.001)** | 1.147 (0.394) | -0.711 (0.503) | 3.514 (0.911) | 0.575 (0.855) | 5.708 (1) | 2.863 (1) | **0.321 (0.003)** | -0.988 (0.317) | 3.037 (0.788) | 0.262 (0.743) | **0.664 (0.007)** | -0.596 (0.327) | **1.036 (0.008)** | -0.353 (0.34) |
| lg | s5 | UVS | **1.537 (< 0.001)** | **-1.732 (< 0.001)** | 2.461 (0.273) | -0.486 (0.276) | **1.379 (0.001)** | **-1.192 (0.025)** | 3.822 (0.665) | 1.66 (0.781) | 3.294 (0.699) | 0.003 (0.528) | 6.001 (1) | 2.808 (1) | **0.721 (0.039)** | -0.869 (0.313) | 3.95 (0.95) | 0.829 (0.957) | **0.695 (0.004)** | -0.843 (0.222) | **1.421 (0.012)** | -0.252 (0.409) |
| lg | s5 | VS | **1.288 (< 0.001)** | **-1.747 (< 0.001)** | 2.427 (0.349) | -0.308 (0.381) | **1.309 (0.002)** | **-1.075 (0.032)** | 4.16 (0.708) | 2.156 (0.833) | 3.207 (0.773) | 0.151 (0.602) | 5.884 (1) | 2.92 (1) | **0.653 (0.048)** | -0.817 (0.321) | 3.563 (0.92) | 0.667 (0.908) | **0.641 (0.001)** | -0.781 (0.233) | **1.37 (0.023)** | -0.178 (0.446) |

**Supplementary table 3. Results of the test of convergence of structural features for each mimicry ring.** We consider convergence in scale type (either piliform scale, lamellar erected scale or lamellar flat scale), in nanostructures type (either absent, maze, nipple, sponge or pillar) and in structural syndrome which corresponds to the association of one type of scale with one type of nanostructures.

For each mimicry ring, we test the similarity of structures between co-mimetic species, independently of their phylogenetic relationship by comparing the sum of co-mimetic species sharing the same structure to what is expected at random (1st column, highlighted in grey for each mimicry ring; we specified the number of co-mimetic species pair in brackets for each mimicry ring), based on 10000 randomisations of the variable 'shared structures'. The p-value (in brackets) has been calculated as the proportion of randomisations where the sum of co-mimetic species sharing the same structure is higher than the observed sum of co-mimetic species sharing the same structure. We also tested the putative convergence of structures between co-mimetic species by performing a generalized linear model with binomial error linking the variable 'shared structures' (1 if the co-mimetic species share the same structures, 0 otherwise) and phylogenetic distance. We compared the mean of the model residuals for co-mimetic species to what is expected according to the phylogeny (2nd column for each mimicry ring), based on 10000 randomisations of residuals along all pairs of species. The p-value (in brackets) was calculated as the proportion of randomisations where the mean of residuals in higher than the observed mean of residuals.

The results are presented graphically in the figure above the table. Black structures indicate neither more similar than expected at random nor convergent structures; red structures indicate structure more similar than expected at random but not convergent; blue structures indicate structures not more similar than expected at random but convergent and purple structures indicate both more similar than expected at random and convergent structures.

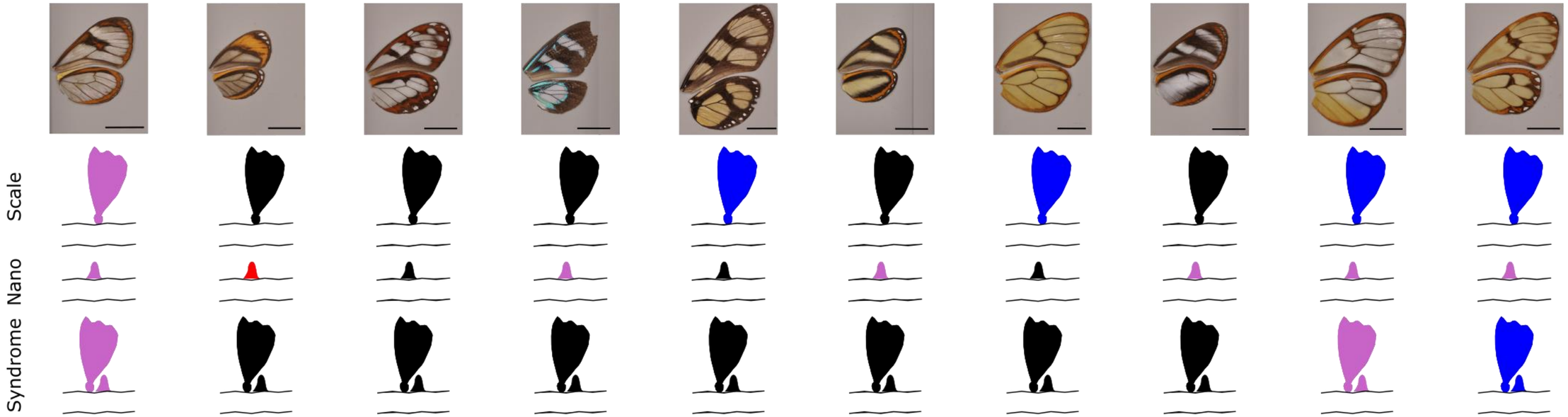


| | agnosia | | aureliana | | banjana-m | | blue | | confusa | | eurimedia | | hewitsoni | | lerida | | panthyale | | theudelinda | |
|---|---|---|---|---|---|---|---|---|---|---|---|---|---|---|---|---|---|---|---|---|
| | Sum of species sharing the same structure (out of 91) | Observed mean residuals with phylogenetic correction | Sum of species sharing the same structure (out of 10) | Observed mean residuals with phylogenetic correction | Sum of species sharing the same structure (out of 15) | Observed mean residuals with phylogenetic correction | Sum of species sharing the same structure (out of 1) | Observed mean residuals with phylogenetic correction | Sum of species sharing the same structure (out of 21) | Observed mean residuals with phylogenetic correction | Sum of species sharing the same structure (out of 28) | Observed mean residuals with phylogenetic correction | Sum of species sharing the same structure (out of 3) | Observed mean residuals with phylogenetic correction | Sum of species sharing the same structure (out of 28) | Observed mean residuals with phylogenetic correction | Sum of species sharing the same structure (out of 6) | Observed mean residuals with phylogenetic correction | Sum of species sharing the same structure (out of 10) | Observed mean residuals with phylogenetic correction |
| Scale type | **58 (< 0.001)** | **2.114 (< 0.001)** | 2 (0.783) | -0.760 (0.862) | 7 (0.151) | -0.028 (0.639) | 0 (0.388) | -2.941 (0.974) | 10 (0.121) | **1.306 (0.017)** | 9 (0.643) | 0.115 (0.527) | **3 (< 0.001)** | 1.221 (0.191) | 7 (0.862) | -0.357 (0.865) | **6 (< 0.001)** | 1.206 (0.145) | **10 (< 0.001)** | 1.253 (0.095) |
| Nanostructure type | **46 (0.001)** | **0.631 (0.004)** | **6 (0.025)** | 1.06 (0.065) | 6 (0.267) | 0.201 (0.298) | **1 (< 0.001)** | 2.884 (0.075) | 10 (0.078) | 0.496 (0.144) | **15 (0.019)** | **0.767 (0.039)** | 1 (0.332) | -0.025 (0.3) | **16 (0.005)** | **0.927 (0.013)** | **6 (< 0.001)** | **2.951 (< 0.001)** | **6 (0.037)** | **1.157 (0.029)** |

| | | | | | | | | | | | | | | | | | | | | |
|---|---|---|---|---|---|---|---|---|---|---|---|---|---|---|---|---|---|---|---|---|
| Structural syndrom | **46 (< 0.001)** | **3.032 (< 0.001)** | 1 (0.548) | -0.397 (0.638) | 2 (0.495) | -0.416 (0.701) | 0 (0.179) | -1.324 (0.851) | 6 (0.054) | 1.153 (0.052) | 4 (0.556) | -0.371 (0.778) | 1 (0.076) | 0.056 (0.461) | 7 (0.082) | 0.435 (0.191) | **6 (< 0.001)** | **3.117 (0.024)** | **6 (0.001)** | 1.373 (0.078) |

**Supplementary table 4. Phylogenetic signal for structural features and transmission properties.** Measure of the phylogenetic signal (estimated as Pagel's λ and Blomberg's K for quantitative traits; δ for multicategorial traits and Purvis and Fritz's D for binary traits) of the different features associated to micro- and nanostructures and of mean transmittance. When λ or K are equal to 0, the trait is distributed randomly across the phylogeny, whereas when λ or K are equal to 1 the trait evolves according to a Brownian motion model along the phylogeny. When D is equal to 1, the trait is randomly distributed across the phylogeny whereas when D is equal to 0, the trait evolves according to Brownian motion model along the phylogeny. The value of δ can be any positive real number and the higher this value, the higher the phylogenetic signal of the trait. For δ, to determine whether the distribution of the trait is different from a random distribution we randomized the trait 1000 times along the phylogeny, and we calculated δ for each randomisation. We then compared the value of δ to the distribution of values of δ under the random hypothesis and we calculated a p-value as the number of randomisations in which δ is higher than the value obtained for the real distribution of the trait.

| Variable | Phylogenetic signal | p-value |
|---|---|---|
| Scale length | λ = 0.672 | < 0.001 *** |
| | K = 0.419 | 0.001 *** |
| Scale width | λ = 1.00 | < 0.001 *** |
| | K = 1.17 | 0.001 *** |
| Scale density | λ = 0.574 | 0.0529 . |
| | K = 0.238 | 0.003 ** |
| Membrane width | λ = 0.996 | <0.001 *** |
| | K = 0.563 | 0.001 *** |
| Nanostructure density | λ = 0.903 | <0.001 *** |
| | K = 0.935 | 0.001 *** |
| Mean transmittance | λ = 0.973 | <0.001 *** |
| | K = 1.06 | 0.001 *** |
| Nanostructure type | δ = 4.44 | < 0.001 *** |
| Scale type | δ = 5.41 | < 0.001 *** |
| Scale colour (coloured vs. transparent) | D = -0.0945 | $p_{(D = 1)} = 0$ $p_{(D = 0)} = 0.583$ |

**Supplementary table 5. Information about specimens used for optical and structural measurements.**

| Family | Subfamily | Tribe | Genus | species | ssp | mimicry ring | Tip label in MCCtree | Specimen ID for transmission | Specimen ID for MEB | Collection location | Year of collection | Measured spots used for link between mean transmittance and structures | Scale form | Scale insertion | Scale colour | Mean scale length (µm), calculated from 3 scales | Scale length measurement standard error (µm), calculated from 3 scales | Mean scale width (µm), calculated from 3 scales | Scale width standard error (µm), calculated from 3 scales | Mean scale density (mm⁻²), calculated from 3 squares | Scale density standard error (mm⁻²), calculated from 3 squares | Mean membrane thickness (nm), calculated from 2 to 5 photos | Membrane thickness standard error (nm), calculated from 2 to 5 photos | Nanostructure type | Mean nanostructure density (µm⁻²) from 2 photos (when available) | Nanostructure density standard error (µm⁻²) from 2 photos (when available) | Mean transmittance over 300-700 nm for the chosen spots (%), calculated from on 1 to 3 | Transmittance over 300-700 nm for the chosen spots standard error (%), calculated from 1 to 3 spots | Average mean transmittance over 300-700 nm for the 5 measured spots (%) | standard error for mean transmittance over 300-700 nm for the 5 measured spots (%) |
|---|---|---|---|---|---|---|---|---|---|---|---|---|---|---|---|---|---|---|---|---|---|---|---|---|---|---|---|---|---|---|
| Erebidae | Arctiinae | Arctiini | Dyasschema | sp. | | confusa | ME15_88_DYSSSP1 | ME15-88 | ME15-88 | Peru, San Martin, Carachamera | 2015 | s2 | lamellar | erected | coloured | 111.54 | 2.37 | 31.55 | 3.65 | 301.93 | 3.43 | 1225.74 | 410.38 | nipples | 0.32 | 0.15 | 32.99 | NA | 12.59 | 11.81 |
| Erebidae | Arctiinae | Arctiini | Hyalurga | egeon | | lerida | ME16_67_HYALEGE | ME16-67 | ME16-67 | Peru, San Martin, Chazuta | 2016 | s2 | lamellar | erected | coloured | 82.09 | 4.57 | 21.87 | 1.44 | 650.30 | 77.43 | 690.48 | 224.88 | nipples | 0.71 | 0.13 | 2.56 | NA | 14.98 | 12.06 |
| Erebidae | Arctiinae | Arctiini | Hyalurga | grandis | | agnosia | TR17_17_HYALGRA | TR17-17 | TR17-17 | Peru, San Martin, Shapaja | 2015 | s3 | lamellar | erected | coloured | 107.42 | 30.68 | 11.97 | 2.63 | 725.66 | 63.44 | 583.04 | 133.18 | nipples | 1.77 | 0.01 | 5.80 | NA | 7.65 | 5.81 |
| Erebidae | Arctiinae | Arctiini | Hypocrita | strigifera | | blue | ME16_58_HYPOSTRI | ME16-58 | ME16-58 | Peru, San Martin, Chazuta | 2016 | s2, s3, s5 | lamellar | flat | transparent | 107.36 | 1.66 | 84.45 | 5.30 | 152.34 | 20.27 | 1010.80 | 148.42 | nipples | 1.23 | 0.98 | 2.31 | 1.07 | 2.34 | 0.89 |
| Erebidae | Arctiinae | Arctiini | Notophyson | tiresias | | confusa | ME16_63_NOTOTIR | ME16-63 | ME16-63 | Peru, San Martin, Urahuasha | 2016 | s2 | lamellar | flat | coloured | 85.32 | 6.12 | 108.47 | 5.00 | 144.10 | 21.36 | 1864.49 | 602.64 | absent | 0.04 | 0.04 | 6.10 | NA | 7.23 | 0.72 |
| Erebidae | Arctiinae | | | Arctiina1 | | eurimedia | TR17_7_MOTH1 | TR17-7 | TR17-7 | Peru, Loreto, Shucushyacu | 2015 | s2, s3 | lamellar | flat | coloured | 71.49 | 3.92 | 87.67 | 5.09 | 276.84 | 13.58 | 3085.06 | 454.88 | absent | 0.07 | NA | 0.43 | 0.39 | 2.91 | 4.61 |
| Erebidae | Arctiinae | | | Arctiinae2 | | lerida | 11_1065_MOTH2 | 11-1065 | 11-1065 | Peru, San Martin, Tarapoto | 2011 | s1, s2 | lamellar | erected | coloured | 111.13 | 2.05 | 7.63 | 0.39 | 463.10 | 20.26 | 1487.68 | 660.50 | nipples | 0.30 | 0.08 | 24.13 | 1.57 | 20.93 | 7.65 |
| Erebidae | Arctiinae | | | Arctiinae3 | | blue | ME16_15_METASP1 | ME16-15 | ME16-15 | Peru, San Martin, Chazuta | 2016 | s4, s5 | piliform | erected | coloured | 102.02 | 12.73 | 2.34 | 0.19 | 153.04 | 11.10 | 1777.00 | 135.72 | nipples | 7.11 | 0.16 | 38.97 | 3.84 | 31.36 | 8.10 |
| Geometridae | Ennominae | | | Geo1 | | agnosia | 11_1002_GEO1 | 11-1002 | 11-1002 | Peru, San Martin, Jepelacio | 2011 ? | s3 | lamellar | erected | coloured | 65.49 | 7.19 | 17.82 | 3.25 | 563.97 | 37.39 | 711.43 | 118.33 | nipples | 1.58 | 0.11 | 29.16 | NA | 26.79 | 15.30 |
| Geometridae | Ennominae | | | Geo2 | | agnosia | ME16_100_GEO2 | ME16-100 | ME16-100 | Peru, San Martin, Rumiyacu | 2016 | s1, s2, s3 | lamellar | erected | coloured | 94.53 | 10.88 | 15.49 | 3.33 | 190.74 | 23.20 | 708.46 | 145.41 | nipples | 6.17 | 0.39 | 18.61 | 3.52 | 21.92 | 12.49 |
| Geometridae | Larentiinae | | Hagnagora | mortipax | | agnosia | Hagnagora_mortipax | TR17-10 | TR17-10 | Ecuador, Qda del diablo | 2011 ? | s2, s3 | lamellar | erected | transparent | 68.05 | 5.96 | 32.84 | 1.43 | 1039.69 | 84.38 | 392.42 | 46.28 | nipples | 4.23 | 0.07 | 11.95 | 7.68 | 16.67 | 14.31 |
| Geometridae | Larentiinae ? | | | Geo9 | | agnosia | TR17_16_GEO9 | TR17-16 | TR17-16 | NA | 2006 | s2, s3, s4 | lamellar | erected | transparent | 67.19 | 10.87 | 41.35 | 5.13 | 569.64 | 85.67 | 677.16 | 56.26 | nipples | 12.33 | 1.21 | 47.40 | 6.88 | 48.50 | 6.03 |
| Geometridae | | | | Geo12 | | eurimedia | ME16_105_GEO1 | ME16-105 | ME16-105 | Peru, San Martin, Carachamera | 2016 | s2, s3 | lamellar | erected | transparent | 97.78 | 18.74 | 20.80 | 6.76 | 629.95 | 115.41 | 626.20 | 93.04 | nipples | 0.57 | 0.09 | 0.47 | 0.07 | 0.37 | 0.12 |
| Geometridae | | | | Geo3 | | agnosia | 11_1879_GEO3 | 11-1879 | 11-1879 | Peru, San Martin, Tarapoto | 2011 | s1, s2 | lamellar | erected | transparent | 77.41 | 10.47 | 35.18 | 8.31 | 579.88 | 61.16 | 1565.60 | 215.52 | maze | 1.37 | 0.67 | 15.32 | 3.46 | 14.94 | 5.62 |
| Notodontidae | | | | Noto1 | | agnosia | ME16_92_GEO4 | ME16-92 | ME16-92 | Peru, San Martin, Rumipata | 2016 | s2 | lamellar | erected | coloured | 59.06 | 18.48 | 13.52 | 1.49 | 382.38 | 39.48 | 634.60 | 257.91 | nipples | 4.16 | 0.37 | 44.05 | NA | 42.53 | 8.10 |
| Notodontidae | | | | Noto2 | | agnosia | TR17_1_GEO11 | TR17-1 | TR17-1 | Peru, San Martin, Tunel | 2012 | s2, s3 | lamellar | erected | transparent | 106.97 | 22.84 | 2.47 | 0.07 | 436.13 | 12.78 | 585.24 | 23.76 | nipples | 4.21 | 0.04 | 29.86 | 17.41 | 38.53 | 14.93 |
| Nymphalidae | Biblidinae | Biblidini | Vila | azeca | | lerida | LS11_2414_ERES1 | LS11-2414 | LS11-2414 | Peru, San Martin, Shapaja-Chazuta | 2012 | s1, s2 | lamellar | flat | transparent | 101.81 | 15.43 | 43.46 | 10.39 | 360.56 | 45.71 | 416.41 | 87.53 | nipples | 1.76 | 0.50 | 19.73 | 22.96 | 23.77 | 12.64 |
| Nymphalidae | Biblidinae | Biblidini | Vila | emilia | | lerida | ME16_56_ERESCLI | ME16-56 | ME16-61 | Peru, San Martin, Chazuta | 2016 | s2 | lamellar | flat | transparent | 99.13 | 3.15 | 54.19 | 1.06 | 468.07 | 20.92 | 470.67 | 176.31 | nipples | 1.35 | 0.08 | 4.83 | NA | 8.85 | 10.63 |
| Nymphalidae | Danainae | Danaini | Lycorea | ilione | | confusa | Lycorea_ilione | LS11-1860 | 11-1000 | Peru, San Martin, Puente Serranoyacu | 2011 | s2 | lamellar | erected | coloured | 123.16 | 1.93 | 16.29 | 1.74 | 119.30 | 11.85 | 2015.07 | 190.90 | absent | 0.02 | 0.01 | 14.34 | NA | 14.52 | 4.37 |
| Nymphalidae | Danainae | Ithomiini | Callithomia | lenea | zelie | confusa | Callithomia_lenea_zelie | 20623 | 20623 | Ecuador, Orellana, Anangu | 2005 | s3, s4, s5 | piliform | erected | coloured | 108.45 | 18.72 | 2.62 | 0.24 | 235.02 | 15.46 | 732.66 | 25.11 | sponge | 8.41 | 2.70 | 23.87 | 4.11 | 28.16 | 7.16 |
| Nymphalidae | Danainae | Ithomiini | Godyris | hewitsoni | | hewitsoni | Godyris_hewitsoni | 21050 | 21050 | Ecuador, Zamora-Chinchipe, Arco Iris | 2006 | s2, s3 | piliform | erected | coloured | 144.58 | 28.62 | 4.13 | 1.05 | 155.53 | 16.51 | 1171.18 | 157.67 | pillars | 18.92 | 1.49 | 50.58 | 8.01 | 54.18 | 5.31 |
| Nymphalidae | Danainae | Ithomiini | Godyris | panthyale | panthyale | panthyale | Godyris_panthyale_panthyale | 21189 | 21207 | Ecuador, Zamora-Chinchipe, Arco Iris | 2006 | s1 | piliform | erected | coloured | 176.37 | 56.36 | 6.28 | 2.26 | 98.88 | 28.52 | 905.76 | 58.67 | pillars | 21.62 | NA | 68.41 | NA | 65.14 | 8.62 |
| Nymphalidae | Danainae | Ithomiini | Heterosais | nephele | | agnosia | Heterosais_nephele_nephele | 20778 | 20688 | Ecuador, Orellana, Anangu | 2005 | s4, s5 | piliform | erected | coloured | 161.38 | 30.78 | 4.31 | 0.31 | 133.75 | 4.07 | 854.20 | 15.38 | pillars | 13.63 | 1.36 | 56.11 | 0.24 | 50.81 | 7.36 |
| Nymphalidae | Danainae | Ithomiini | Hyalenna | paradoxa | praestigiosa | panthyale | Hyalenna_paradoxa_praestigiosa | 21541 | 21641 | Ecuador, Zamora-Chinchipe, Arco Iris | 2006 | s1 | piliform | erected | coloured | 224.17 | 87.13 | 5.83 | 0.76 | 126.52 | 5.27 | 1095.41 | 78.53 | pillars | 14.38 | NA | 56.49 | NA | 51.14 | 12.11 |
| Nymphalidae | Danainae | Ithomiini | Hypomenitis | enigma | pseudortygia | panthyale | Hypomenitis_enigma | 21292 | 21270 | Ecuador, Zamora-Chinchipe, Arco Iris | 2006 | s1, s2 | piliform | erected | coloured | 121.77 | 11.57 | 3.34 | 0.50 | 261.29 | 14.06 | 684.28 | 102.66 | pillars | 20.70 | 0.83 | 54.67 | 6.87 | 53.88 | 14.92 |
| Nymphalidae | Danainae | Ithomiini | Hypomenitis | lydia | | hewitsoni | Hypomenitis_lydia | 21522 | 21272 | Ecuador, Zamora-Chinchipe, Arco Iris | 2006 | s1, s2 | piliform | erected | coloured | 162.36 | 57.79 | 4.75 | 1.06 | 294.65 | 32.01 | 851.90 | 100.09 | pillars | 23.95 | 0.89 | 38.76 | 12.01 | 48.16 | 11.78 |
| Nymphalidae | Danainae | Ithomiini | Hypomenitis | oneidodes | | theudelinda | Hypomenitis_oneidodes | 21535 | 21245 | Ecuador, Zamora-Chinchipe, Arco Iris | 2006 | s3 | piliform | erected | coloured | 157.07 | 54.40 | 4.05 | 1.14 | 151.34 | 14.98 | 814.48 | 29.10 | pillars | 22.83 | NA | 44.31 | NA | 50.44 | 7.97 |
| Nymphalidae | Danainae | Ithomiini | Hypomenitis | ortygia | ortygia | panthyale | Hypomenitis_ortygia_ortygia | 21273 | 21078 | Ecuador, Zamora-Chinchipe, Arco Iris | 2006 | s1 | piliform | erected | coloured | 144.24 | 30.11 | 3.87 | 0.87 | 275.01 | 16.99 | 646.56 | 129.70 | pillars | 18.08 | 0.59 | 54.71 | NA | 55.54 | 9.58 |
| Nymphalidae | Danainae | Ithomiini | Hypomenitis | theudelinda | zalmunna | theudelinda | Hypomenitis_theudilinda_zalmunna | 21469 | 21642 | Ecuador, Zamora-Chinchipe, Arco Iris | 2006 | s4, s5 | piliform | erected | coloured | 125.82 | 10.86 | 4.52 | 0.75 | 224.18 | 24.14 | 620.90 | 110.05 | pillars | 18.75 | 0.31 | 61.74 | 3.14 | 54.32 | 9.47 |
| Nymphalidae | Danainae | Ithomiini | Ithomia | agnosia | agnosia | agnosia | Ithomia_agnosia_agnosia | CP17-3 | CP17-3 | Peru, Moyobamba | 2016 | s2 | piliform | erected | coloured | 100.48 | 18.73 | 2.85 | 0.67 | 544.34 | 49.18 | 440.60 | 128.35 | pillars | 19.43 | 0.93 | 38.54 | NA | 46.80 | 8.66 |
| Nymphalidae | Danainae | Ithomiini | Ithomia | amarilla | | eurimedia | Ithomia_amarilla | 20569 | 20569 | Ecuador, Orellana, Anangu | 2005 | s1, s2, s3 | piliform | erected | coloured | 123.60 | 45.44 | 3.40 | 0.38 | 521.59 | 57.68 | 478.90 | 36.88 | nipples | 10.66 | 1.41 | 45.25 | 3.84 | 41.00 | 7.23 |
| Nymphalidae | Danainae | Ithomiini | Ithomia | avella | epona | theudelinda | Ithomia_avella | 21466 | ME10-160 | Ecuador, Zamora-Chinchipe, Arco Iris / Napo, Yanayacu | 2006 | s1, s2 | piliform | erected | coloured | 145.25 | 6.07 | 3.65 | 0.52 | 289.17 | 48.17 | 845.06 | 235.20 | pillars | 23.16 | 1.21 | 39.79 | 5.00 | 43.53 | 4.42 |
| Nymphalidae | Danainae | Ithomiini | Mcclungia | cymo | | eurimedia | Mcclungia_cymo | DG16-049 | DG16-049 | Peru, San Martin, Rumiyacu | 2015 | s2, s3 | piliform | erected | coloured | 132.22 | 4.81 | 3.44 | 0.22 | 684.65 | 84.39 | 591.12 | 29.69 | sponge | 18.00 | 3.12 | 36.09 | 4.78 | 45.37 | 12.70 |
| Nymphalidae | Danainae | Ithomiini | Megoleria | orestilla | orestilla | banjana-m | Megoleria_orestilla | 21296 | 21296 | Ecuador, Zamora-Chinchipe, Arco Iris | 2006 | s1, s2 | piliform | erected | coloured | 144.26 | 49.78 | 3.97 | 0.99 | 220.34 | 24.19 | 840.80 | 95.80 | maze | 9.65 | 3.38 | 40.36 | 0.29 | 42.23 | 2.72 |
| Nymphalidae | Danainae | Ithomiini | Methona | curvifascia | | confusa | Methona_curvifascia | 20731 | 20731 | Ecuador, Orellana, Anangu | 2005 | s4, s5 | lamellar | erected | coloured | 47.08 | 3.61 | 30.40 | 2.24 | 190.91 | 15.89 | 1684.80 | 28.53 | absent | 0.04 | 0.04 | 20.78 | 0.08 | 18.53 | 3.44 |
| Nymphalidae | Danainae | Ithomiini | Napeogenes | harbona | | banjana-m | Napeogenes_harbona | ME10-315 | ME10-315 | Ecuador, Napo, Yanayacu | 2010 | s1, s2 | piliform | erected | coloured | 83.08 | 5.23 | 2.93 | 0.33 | 885.97 | 152.53 | 368.96 | 67.69 | nipples | 6.19 | 0.05 | 33.38 | 3.39 | 39.77 | 8.17 |
| Nymphalidae | Danainae | Ithomiini | Napeogenes | inachia | | eurimedia | Napeogenes_inachia | 20558 | 20628 | Ecuador, Orellana, Anangu | 2005 | s1, s2, s3 | piliform | erected | coloured | 96.48 | 4.33 | 3.06 | 0.30 | 985.59 | 130.31 | 512.82 | 38.29 | nipples | 17.30 | 1.56 | 29.09 | 4.98 | 28.57 | 5.68 |
| Nymphalidae | Danainae | Ithomiini | Napeogenes | larilla | | theudelinda | Napeogenes_larilla | 21299 | 21261 | Ecuador, Zamora-Chinchipe, Arco Iris | 2006 | s1, s2, s3 | piliform | erected | coloured | 67.66 | 2.45 | 3.49 | 0.42 | 439.55 | 33.76 | 521.41 | 159.78 | nipples | 17.07 | 0.27 | 47.52 | 3.10 | 50.79 | 5.00 |
| Nymphalidae | Danainae | Ithomiini | Napeogenes | sylphis | corena | aureliana | Napeogenes_sylphis_corena | 20669 | 20669 | Ecuador, Orellana, Anangu | 2005 | s1, s2 | piliform | erected | coloured | 120.84 | 19.19 | 3.09 | 0.24 | 539.45 | 58.08 | 529.18 | 41.59 | nipples | 12.61 | 1.12 | 37.51 | 7.59 | 38.06 | 4.66 |
| Nymphalidae | Danainae | Ithomiini | Oleria | athalina | banjana | banjana-m | Oleria_athalina_banjana | 21175 | 21175 | Ecuador, Zamora-Chinchipe, Arco Iris | 2006 | s2 | piliform | erected | coloured | 96.20 | 4.04 | 3.15 | 0.19 | 616.97 | 51.88 | 436.86 | 87.36 | pillars | 15.51 | 0.05 | 27.99 | NA | 37.68 | 5.70 |
| Nymphalidae | Danainae | Ithomiini | Oleria | onega | | lerida | Oleria_onega | 20633 | 20633 | Ecuador, Orellana, Anangu | 2005 | s1, s2, s3 | piliform | erected | coloured | 117.92 | 5.50 | 3.13 | 0.44 | 466.42 | 42.62 | 441.28 | 107.26 | sponge | 7.60 | 1.87 | 33.33 | 10.52 | 34.72 | 7.84 |
| Nymphalidae | Danainae | Ithomiini | Oleria | sexmaculata | sexmaculata | lerida | Oleria_sexmaculata_sexmaculata | 20469 | 20469 | Ecuador, Orellana, Anangu | 2005 | s1, s2, s3 | piliform | erected | coloured | 101.76 | 4.32 | 3.17 | 0.64 | 662.40 | 78.71 | 274.48 | 70.38 | sponge | 10.70 | 2.51 | 33.55 | 4.26 | 36.97 | 5.57 |
| Nymphalidae | Danainae | Ithomiini | Olilantaya | olerioides | | banjana-m | Oleria_olerioides | 21309 | 21309 | Ecuador, Zamora-Chinchipe, Arco Iris | 2006 | s1, s2 | piliform | erected | coloured | 87.32 | 12.40 | 3.01 | 0.41 | 445.81 | 27.01 | 475.30 | 63.65 | nipples | 13.22 | 0.33 | 44.90 | 6.20 | 47.44 | 5.18 |
| Nymphalidae | Danainae | Ithomiini | Pseudoscada | florula | aureola | aureliana | Pseudoscada_florula_aureola | 20635 | 20635 | Ecuador, Orellana, Anangu | 2005 | s2, s3 | piliform | erected | coloured | 124.45 | 4.48 | 2.84 | 0.14 | 585.86 | 65.52 | 450.26 | 24.86 | sponge | 13.73 | 1.42 | 32.48 | NA | 46.38 | 11.08 |
| Nymphalidae | Danainae | Ithomiini | Pseudoscada | timna | utilla | agnosia | Pseudoscada_timna_utilla | 20455 | 20455 | Ecuador, Orellana, Anangu | 2005 | s2, s3 | piliform | erected | coloured | 132.33 | 38.22 | 3.26 | 0.15 | 491.09 | 40.78 | 541.36 | 14.91 | sponge | 15.56 | 1.35 | 44.45 | 11.04 | 53.75 | 13.38 |
| Nymphalidae | Danainae | Ithomiini | Pteronymia | oneida | oneida | hewitsoni | Pteronymia_oneida_oneida | 21359 | 21359 | Ecuador, Zamora-Chinchipe, Arco Iris | 2006 | s1, s2 | piliform | erected | coloured | 106.16 | 3.78 | 3.47 | 0.25 | 574.91 | 101.34 | 755.20 | 97.44 | sponge | 11.99 | 0.55 | 31.36 | 8.06 | 37.06 | 9.83 |
| Nymphalidae | Danainae | Ithomiini | Veladyris | pardalis | | theudelinda | Veladyris_pardalis | ME10-17 | ME10-17 | Ecuador, Napo, Yanayacu | 2010 | s2 | piliform | erected | coloured | 142.67 | 46.68 | 4.17 | 0.74 | 394.08 | 47.57 | 901.38 | 54.16 | pillars | 22.34 | 0.57 | 32.31 | NA | 35.24 | 3.86 |
| Nymphalidae | Nymphalinae | Melitaeini | Eresia | nauplius | plagiata | lerida | Eresia_nauplius_plagiata | ME10-292 | ME10-292 | Ecuador, Napo, Mariposa | 2010 | s2 | lamellar | flat | coloured | 134.16 | 5.68 | 46.74 | 1.27 | 431.70 | 18.32 | 393.86 | 110.27 | nipples | 1.13 | 0.10 | 0.09 | NA | 2.67 | 2.79 |
| Papilionidae | Papilioninae | Troidini | Parides | hahneli | | confusa | Parides_ephidamas | CP17-10 | CP17-10 | Brazil, Rio Arapiuns | 1978 | s1, s2 | lamellar | erected | coloured | 128.39 | 17.05 | 27.78 | 2.66 | 253.01 | 34.53 | 1563.80 | 405.99 | absent | 0.04 | 0.04 | 5.17 | 0.19 | 5.07 | 1.24 |
| Pieridae | Dismorphiinae | | Dismorphia | theucharila | leucone | lerida | TR17_14_DISMTHEU | TR17-14 | TR17-14 | Ecuador, Orellana, Anangu | | s1, s2, s3 | lamellar | erected | transparent | 47.65 | 2.52 | 35.47 | 1.03 | 600.31 | 8.68 | 632.58 | 163.70 | nipples | 11.41 | 0.32 | 17.65 | 14.15 | 23.41 | 12.78 |
| Pieridae | Dismorphiinae | | Dismorphia | theucharila | orange tip | aureliana | TR17_6_DISMTHEU | TR17-6 | TR17-22 | Ecuador, Orellana, Anangu | 2005 | s1 | lamellar | erected | coloured | 49.91 | 4.82 | 27.74 | 3.22 | 447.28 | 19.94 | 529.11 | 105.11 | nipples | 11.06 | 0.66 | 12.17 | NA | 16.50 | 5.98 |
| Pieridae | Dismorphiinae | | Dismorphia | theucharila | yolanda | banjana-m | LS11_2240_DISTH | LS11-2240 | ME10-375 | Peru, San Martin, La Antena | 2012 | s2 | lamellar | erected | transparent | 49.34 | 5.25 | 30.43 | 2.57 | 681.04 | 16.23 | 325.57 | 85.17 | nipples | 8.50 | 0.88 | 2.78 | NA | 10.88 | 5.65 |
| Pieridae | Dismorphiinae | | Moschoneura | pinthous | | eurimedia | TR17_3_MOSCPINT | LS11-2399 | TR17-3 | Peru, San Martin, Tunel | 2012 | s1, s2 | lamellar | flat | coloured | 66.67 | 1.55 | 40.98 | 3.47 | 1040.60 | 77.03 | 337.76 | 39.60 | nipples | 1.97 | 0.62 | 1.16 | 0.29 | 1.07 | 0.90 |
| Pieridae | Dismorphiinae | | Patia | orise | | confusa | Patia_orise | LS11-1414 | LS11-1414 | Peru, San Martin, Rumiyacu | 2011 | s2 | lamellar | erected | coloured | 40.52 | 1.23 | 21.60 | 2.01 | 789.66 | 28.44 | 957.06 | 169.74 | absent | 0.04 | 0.04 | 24.37 | NA | 14.02 | 11.65 |
| Pieridae | Pierinae | Pierini | Itaballia | pandosia | | eurimedia | ME16_62_ITAPAND | ME16-62 | TR17-20 | Peru, San Martin, Urahuasha | 2016 | s3 | lamellar | flat | coloured | 90.38 | 9.84 | 50.46 | 0.29 | 670.96 | 60.11 | 720.45 | 402.29 | nipples | 1.87 | 0.26 | 8.27 | NA | 2.63 | 3.20 |
| Pieridae | Pierinae | | | Perrhybris ? | Pier1 | eurimedia | MECN_140_PIER1 | MECN-140 | TR17-21 | Ecuador, Napo | | s3 | lamellar | flat | coloured | 120.73 | 2.25 | 42.68 | 4.52 | 467.12 | 34.91 | 526.06 | 85.42 | nipples | 1.08 | NA | 0.84 | NA | 0.28 | 0.32 |
| Riodinidae | Riodininae | Eurybiini | Ithomiola | floralis | orange tip | aureliana | 11-1116_ITHOFLO | 11-1116 | 11-1116 | Peru, San Martin, Tarapoto | 2011 ? | s4, s5 | lamellar | erected | transparent | 73.99 | 2.44 | 59.48 | 1.90 | 169.25 | 30.41 | 670.11 | 46.45 | nipples | 14.28 | 0.56 | 41.08 | 5.70 | 44.97 | 11.06 |
| Riodinidae | Riodininae | Eurybiini | Ithomiola | floralis | white-band | agnosia | 11_1127_ITHOFLO | 11-1127 | 11-1127 | Peru, San Martin, La Antena | 2011 | s3 | lamellar | erected | transparent | 78.45 | 6.32 | 57.57 | 1.80 | 173.63 | 16.15 | 450.56 | 102.41 | nipples | 17.14 | 0.87 | 35.72 | NA | 43.95 | 12.26 |
| Riodinidae | Riodininae | Nymphidiini | Stalachtis | euterpe | | aureliana | TR17_5_STALEUT | TR17-5 | TR17-5 | Peru, Loreto, Shucushyacu | 2015 | s1, s2 | lamellar | flat | transparent | 64.01 | 2.21 | 60.63 | 2.25 | 279.75 | 48.13 | 439.09 | 33.07 | nipples | 1.85 | 0.22 | 17.02 | 22.72 | 8.97 | 13.59 |
| Riodinidae | Riodininae | | | Riodin2 | | agnosia | TR17_12_GEO7 | TR17-12 | TR17-12 | Peru, San Martin, Tarapoto | 2015 | s3 | lamellar | erected | transparent | 64.39 | 4.63 | 40.46 | 2.73 | 667.85 | 103.57 | 437.04 | 97.73 | nipples | 5.33 | 0.36 | 28.85 | NA | 37.77 | 6.09 |
| Riodinidae | | | | Riodin3 | | banjana-m | MECN_133_BUT1 | MECN-133 | MECN-133 | Ecuador, Napo | 2011 | s4, s5 | lamellar | erected | transparent | 76.59 | 1.82 | 52.06 | 4.17 | 291.00 | 13.10 | 615.34 | 232.89 | nipples | 3.65 | 0.15 | 15.53 | 5.84 | 10.90 | 5.44 |
| Riodinidae | | | | Riodin3 | | agnosia | TR17_11_GEO8 | TR17-11 | TR17-11 | Peru, San Martin, Rumipata | 2016 | s3 | lamellar | erected | transparent | 82.14 | 1.55 | 45.09 | 2.19 | 697.70 | 41.50 | 758.11 | 153.23 | nipples | 8.84 | 0.25 | 18.76 | NA | 21.18 | 14.80 |

**Supplementary table 6. Results of the eight best PGLS (Phylogenetic Generalized Least Square) models (AICc within an interval of 2 of that of the best model).** For each model, we give: the F statistic with the degrees of freedom in indices, the p-value of the model (in brackets), the corrected Akaike criterion (AICc) of the model, the adjusted $R^2$ and the value of lambda branch length transformation which has been estimated by maximum likelihood given the statistical model linking traits. When λ equals 1, the branch length of the phylogeny is unchanged, whereas when λ equals 0 branch length is set to zero, meaning that all species are considered independent. The 'p-values' for the value of λ, given in brackets, are the probability that λ is equal to 0 or to 1. We also give for each model the value of the coefficient estimate for each variable tested and the p-value (in brackets) is represented with the follow symbols: *** : p < 0.001; ** : p < 0.01; * : p<0.05; **.** : p < 0.1; n.s. : not significantly different from 0. NA means that the variable was not retained in the model

| | **Model1** | **Model2** | **Model3** | **Model4** | **Model5** | **Model6** | **Model7** | **Model8** |
|---|---|---|---|---|---|---|---|---|
| **F-statistic (p-value)** | $F_{5,56}$ = 26.7 (< 0.001***) | $F_{6,55}$ = 23.0 (< 0.001***) | $F_{4,57}$ = 31.5 (< 0.001***) | $F_{6,55}$ = 22.5 (< 0.001***) | $F_{5,56}$ = 25.9 (< 0.001***) | $F_{4,57}$ = 31.0 (< 0.001***) | $F_{5,56}$ = 25.6 (< 0.001***) | $F_{4,57}$ = 30.6 (< 0.001***) |
| **AICc** | 469.94 | 470.18 | 470.72 | 471.13 | 471.26 | 471.42 | 471.62 | 471.88 |
| **$R^2_{adj}$** | 0.6777 | 0.6838 | 0.6664 | 0.6789 | 0.6708 | 0.6626 | 0.6689 | 0.6601 |
| **λ ($p_{(\lambda=0)}$, $p_{(\lambda=1)}$)** | λ = 0 ($p_{(\lambda=0)}$ = 1, $p_{(\lambda=1)}$< 0.001) | λ = 0 ($p_{(\lambda=0)}$ = 1, $p_{(\lambda=1)}$< 0.001) | λ = 0 ($p_{(\lambda=0)}$ = 1, $p_{(\lambda=1)}$< 0.001) | λ = 0 ($p_{(\lambda=0)}$ = 1, $p_{(\lambda=1)}$< 0.001) | λ = 0 ($p_{(\lambda=0)}$ = 1, $p_{(\lambda=1)}$< 0.001) | λ = 0 ($p_{(\lambda=0)}$ = 1, $p_{(\lambda=1)}$< 0.001) | λ = 0 ($p_{(\lambda=0)}$ = 1, $p_{(\lambda=1)}$< 0.001) | λ = 0 ($p_{(\lambda=0)}$ = 1, $p_{(\lambda=1)}$< 0.001) |
| | | | | | | | | |
| **Variable** | | | | | | | | |
| Intercept | **21.89 (***)** | **24.20 (***)** | **26.01 (***)** | **27.99 (***)** | **32.91 (***)** | **39.63 (***)** | **28.30 (***)** | **33.25 (***)** |
| Scale type Piliform vs. Lamellar | **6.898 (***)** | **8.414 (***)** | **6.497 (***)** | **7.101 (***)** | **6.787 (***)** | **8.650 (***)** | **7.737 (***)** | **10.13 (***)** |
| Scale type Lamellar Flat scale vs. Lamellar Erected scale | **6.670 (**)** | 6.838(**) | **6.707 (**)** | **6.897 (**)** | **6.976 (**)** | **7.903 (***)** | **6.851 (**)** | **7.750 (***)** |
| Scale density | -0.006339 (n.s.) | -0.005992 (n.s.) | **-0.0175 (**)** | -0.01147 (n.s.) | **-0.02242 (**)** | **-0.02612 (***)** | **-0.01814 (**)** | **-0.0201 (***)** |
| Nanostructure density | **1.078 (**)** | **0.9557 (*)** | **0.6342 (*)** | **0.9098 (*)** | 0.4813 (n.s.) | NA | 0.4936 (n.s.) | NA |
| Interaction between nanostructure density and scale density | -0.001357 (.) | -0.001493 (.) | NA | -0.001229 (n.s.) | NA | NA | NA | NA |
| Scale colour Transparent vs. Coloured | NA | 2.719 (n.s.) | NA | NA | NA | NA | 2.285 (n.s.) | 3.431 (.) |
| Membrane thickness | NA | NA | NA | -0.03611 (n.s.) | -0.004358 (n.s.) | **-0.006253 (*)** | NA | NA |

972 **Supplementary table 7. Information on specimens used to infer a phylogeny**

| Family | Subfamily | Tribe | Genus | species | ssp | mimicry ring | Tip label in MCCtree | Specimen ID for DNA | Collection location | Year of collection | CAD | COI | MDH | EF-1a | GAPDH | IDH | RpSR5 | TKT |
|---|---|---|---|---|---|---|---|---|---|---|---|---|---|---|---|---|---|---|
| Bombycidae | Bombycinae | | Bombyx | mori | | | Bombyx_mori | additional species | NA | NA | EU141315 | AB649195 | EU141617 | EU136667 | EU141495 | EU141552 | EU141393 | NA |
| Cyclotornidae | | | Cyclotorna | sp. | | | Cyclotorna_sp | additional species | NA | NA | GU828262 | GU929758 | GU830488 | GU829094 | GU829868 | GU830169 | GU830747 | NA |
| Drepanidae | Drepaninae | | Drepana | curvatula | | | Drepana_curvulata | additional species | NA | NA | GU828107 | KX050080 | GU830317 | AY948512 | GU829758 | GU829994 | GU830616 | NA |
| Epicopeiidae | | | Epicopeia | hainesii | | | Epicopeia_hainesii | additional species | NA | NA | GU828052 | GU828343 | GU830264 | FJ768755 | NA | GU829932 | GU830574 | NA |
| Erebidae | Arctiinae | Arctiini | Calodesma | albiapex | | | Calodesma_albiapex | additional species | NA | NA | KX300479 | KX300241 | KX300715 | KX300361 | KX300554 | KX300636 | KX300820 | NA |
| Erebidae | Arctiinae | Arctiini | Dysschema | leucophaea | | | Dysschema_leucophaea | additional species | NA | NA | NA | HQ006240 | HQ006658 | HQ006427 | HQ006493 | HQ006571 | HQ006751 | NA |
| Erebidae | Arctiinae | Arctiini | Dysschema | sp. | | confusa | ME15_88_DYSSSP1 | ME15-88 | Peru, San Martin, Carachamera | 2015 | to be added | to be added | to be added | NA | NA | NA | NA | NA |
| Erebidae | Arctiinae | Arctiini | Episcea | extravagans | | | Episcea_extravagans | additional species | NA | NA | KX300482 | KX300254 | KX300717 | KX300374 | KX300555 | KX300638 | KX300823 | NA |
| Erebidae | Arctiinae | Arctiini | Euchlaenidia | transcisa | | | Euchlaenidia_transcisa | additional species | NA | NA | KX300483 | KX300258 | KX300718 | KX300378 | KX300556 | NA | KX300824 | NA |
| Erebidae | Arctiinae | Arctiini | Hyalurga | egeon | | lerida | ME16_67_HYALEGE | ME16-67 | Peru, San Martin, Chazuta | 2016 | to be added | to be added | to be added | NA | NA | NA | NA | NA |
| Erebidae | Arctiinae | Arctiini | Hyalurga | fenestrata | | | Hyalurga_fenestrata | additional species | NA | NA | KX300481 | KX300273 | KX300716 | KX300390 | NA | KX300637 | KX300822 | NA |
| Erebidae | Arctiinae | Arctiini | Hyalurga | grandis | | agnosia | TR17_17_HYALGRA | TR17-17 | Peru, San Martin, Shapaja | 2015 | to be added | to be added | NA | NA | NA | NA | NA | NA |
| Erebidae | Arctiinae | Arctiini | Hypocrita | confluens | | | Hypocrita_confluens | additional species | NA | NA | KX300478 | KX300276 | KX300713 | KX300393 | NA | KX300635 | KX300818 | NA |
| Erebidae | Arctiinae | Arctiini | Hypocrita | strigifera | | blue | ME16_58_HYPOSTRI | ME16-58 | Peru, San Martin, Chazuta | 2016 | NA | to be added | to be added | NA | NA | NA | NA | NA |
| Erebidae | Arctiinae | Arctiini | Hypocrita | strigifera | | | ME16_44_HYPOSTR | ME16-44 (additional species) | Peru, Lorerto, PB-mk7.1 | 2016 | to be added | to be added | to be added | NA | NA | NA | NA | NA |
| Erebidae | Arctiinae | Arctiini | Hypocrita | strigifera | | | ME16_64_HYPOSTR | ME16-64 (additional species) | Peru, San Martin, Urahuasha | 2016 | to be added | to be added | NA | NA | NA | NA | NA | NA |
| Erebidae | Arctiinae | Arctiini | Notophyson | tiresias | | confusa | ME16_63_NOTOTIR | ME16-63 | Peru, San Martin, Urahuasha | 2016 | to be added | to be added | to be added | NA | NA | NA | NA | NA |
| Erebidae | Arctiinae | Arctiini | Notophyson | tiresias | | | TR17_9_NOTOTIRE | TR17-9 (additional species) | | | NA | to be added | NA | NA | NA | NA | NA | NA |
| Erebidae | Arctiinae | Arctiini | Notophyson | tiresias | | | TR17_8_NOTOTIR | TR17-8 (additional species) | Peru, Loreto, Shucushyacu | | to be added | to be added | to be added | NA | NA | NA | NA | NA |
| Erebidae | Arctiinae | Arctiini | Notophyson | tiresias | | | TR17_4_NOTOTIRE | TR17-4 (additional species) | Ecuador | | NA | to be added | to be added | NA | NA | NA | NA | NA |
| Erebidae | Arctiinae | Arctiini | Pseudophaloe | troetschi | | | Pseudophaloe_troetschi | additional species | NA | NA | GU828046 | GU828336 | GU830258 | GU828880 | NA | GU829925 | GU830569 | NA |
| Erebidae | Arctiinae | Arctiini | Sthenognatha | gentilis | | | Sthenognatha_gentilis | additional species | NA | NA | KX300480 | KX300329 | NA | KX300446 | NA | NA | KX300821 | NA |
| Erebidae | Arctiinae | Ctenuchini | Metastatia | pyrrhorhoea | | | Metastatia_pyrrhorhoea | additional species | NA | NA | NA | JQ524029 | NA | NA | NA | NA | NA | NA |
| Erebidae | Arctiinae | Ctenuchini ? | | | | | ME16_16_METASP2 | ME16-16 (additional species) | Peru, San Martin, Chazuta | 2016 | to be added | to be added | NA | NA | NA | NA | NA | NA |
| Erebidae | Arctiinae | Ctenuchini ? | | | | | TR17_13_CHTEN2 | TR17-13 (additional species) | Peru, San Martin, Chazuta | 2015 | NA | to be added | NA | NA | NA | NA | NA | NA |
| Erebidae | Arctiinae | Ctenuchini ? | | | | | 11_996_CHTEN1 | 11-996 (additional species) | Peru, San Martin, Jepelacio | 2011 ? | to be added | to be added | to be added | NA | NA | NA | NA | NA |
| Erebidae | Arctiinae | | | Arctiinae1 | | eurimedia | TR17_7_MOTH1 | TR17-7 | Peru, Loreto, Shucushyacu | 2015 | to be added | to be added | to be added | NA | NA | NA | NA | NA |
| Erebidae | Arctiinae | | | Arctiinae2 | | lerida | 11_1065_MOTH2 | 11-1065 | Peru, San Martin, Tarapoto | 2011 ? | NA | to be added | to be added | NA | NA | NA | NA | NA |
| Erebidae | Arctiinae | | | Arctiinae3 | | blue | ME16_15_METASP1 | ME16-15 | Peru, San Martin, Chazuta | 2016 | NA | to be added | to be added | NA | NA | NA | NA | NA |
| Erebidae | | | | | | | ME16_91_MOTH3 | ME16-91 (additional species) | Peru, San Martin, Rumiyacu | 2016 | to be added | to be added | NA | NA | NA | NA | NA | NA |
| Geometridae | Alsophilinae | | Inurois | fumosa | | | Inurois_fumosa | additional species | NA | NA | NA | AB980825 | NA | AB553238 | NA | NA | NA | AB553145 |
| Geometridae | Ennominae | | Biston | panterinaria | | | Biston_panterinaria | additional species | NA | NA | KX950066 | KP239036 | NA | KP239754 | KU355232 | NA | KX950339 | NA |
| Geometridae | Ennominae | | Plutodes | costatus | | | Plutodes_costatus | additional species | NA | NA | JF785267 | JF784784 | JF784906 | JF785402 | JF785458 | JF785538 | JF785016 | NA |
| Geometridae | Ennominae | | | Geo1 | | agnosia | 11_1002_GEO1 | 11-1002 | Peru, San Martin, Jepelacio | 2011 ? | to be added | to be added | to be added | NA | NA | NA | NA | NA |
| Geometridae | Ennominae | | | Geo2 | | agnosia | ME16_100_GE02 | ME16-100 | Peru, San Martin, Rumiyacu | 2016 | NA | to be added | to be added | NA | NA | NA | NA | NA |
| Geometridae | Larentiinae | | Hagnagora | mortipax | | agnosia | Hagnagora_mortipax | TR17-10 | Ecuador, Qda del diablo | 2011 ? | JF785169 | JF784682 | JF784825 | JF785307 | NA | NA | NA | NA |
| Geometridae | Larentiinae | | Operophtera | brumata | | | Operophtera_brumata | additional species | NA | NA | KX343869 | JQ616454 | KX343791 | JF785366 | KX343449 | KX343384 | KX343322 | NA |
| Geometridae | Larentiinae ? | | | Geo9 | | agnosia | TR17_16_GEO9 | TR17-16 | NA | 2006 | NA | to be added | to be added | NA | NA | NA | NA | NA |
| Geometridae | | | | Geo12 | | eurimedia | ME16_105_GEO1 | ME16-105 | Peru, San Martin, Carachamera | 2016 | to be added | to be added | to be added | NA | NA | NA | NA | NA |
| Geometridae | | | | Geo3 | | agnosia | 11_1879_GEO3 | 11-1879 | Peru, San Martin, Tarapoto | 2011 | NA | to be added | to be added | NA | NA | NA | NA | NA |
| Geometridae | | | | | | | ME16_87_GEO1 | ME16-87 (additional species) | Peru, San Martin, Rumiyacu | 2016 | NA | to be added | to be added | NA | NA | NA | NA | NA |
| Geometridae | | | | | | | 11_1001_GEO2 | 11-1001 (additional species) | Peru, San Martin, Jepelacio | 2011 ? | NA | to be added | to be added | NA | NA | NA | NA | NA |
| Lasiocampidae | Macromphaliinae | | Tolype | velleda | | | Tolype_velleda | additional species | NA | NA | GU828060 | GU828351 | NA | GU828894 | GU829729 | GU829940 | GU830580 | NA |
| Notodontidae | Phalerinae | | Phalera | bucephala | | | Phalera_bucephala | additional species | NA | NA | GU828108 | JF415410 | GU830358 | GU829235 | NA | GU829995 | GU830651 | NA |
| Notodontidae | | | | Noto1 | | agnosia | ME16_92_GEO4 | ME16-92 | Peru, San Martin, Rumipata | 2016 | NA | to be added | to be added | NA | NA | NA | NA | NA |
| Notodontidae | | | | Noto2 | | agnosia | TR17_1_GEO11 | TR17-1 | Peru, San Martin, Tunel | 2012 | NA | to be added | to be added | NA | NA | NA | NA | NA |
| Notodontidae | | | | | | | 11_994_GEO5 | 11-994 (additional species) | Peru, San Martin, Jepelacio | 2011 ? | to be added | to be added | to be added | NA | NA | NA | NA | NA |
| Notodontidae | | | | | | | 11_1064_GEO6 | 11-1064 (additional species) | Peru | 2011 | NA | to be added | NA | NA | NA | NA | NA | NA |
| Notodontidae | | | | | | | TR17_15_GEO4 | TR17-15 (additional species) | Peru, San Martin, Tarapoto | 2015 | NA | to be added | to be added | NA | NA | NA | NA | NA |
| Nymphalidae | Biblidinae | Biblidini | Vila | azeca | | lerida | LS11_2414_ERES1 | LS11-2414 | Peru, San Martin, Shapaja-Chazuta | 2011 | to be added | to be added | to be added | NA | NA | NA | NA | NA |
| Nymphalidae | Biblidinae | Biblidini | Vila | emilia | | lerida | ME16_56_ERESCLI | ME16-56 | Peru, San Martin, Chazuta | 2016 | to be added | to be added | to be added | NA | NA | NA | NA | NA |
| Nymphalidae | Danainae | Danaini | Lycorea | ilione | | confusa | Lycorea_ilione | LS11-1860 | Peru, San Martin, Puente Serranoyacu | 2011 | to be added | GQ864780 | to be added | GQ864874 | NA | NA | NA | NA |
| Nymphalidae | Danainae | Ithomiini | Callithomia | lenea | zelie | confusa | Callithomia_lenea_zelie | NA | NA | NA | MG210038 | EU068959 | MG209883 | EU069127 | MG210246 | NA | NA | KY749989 |
| Nymphalidae | Danainae | Ithomiini | Godyris | hewitsoni | | hewitsoni | Godyris_hewitsoni | NA | NA | NA | NA | JX573764 | NA | JX573693 | NA | NA | NA | KX362244 |
| Nymphalidae | Danainae | Ithomiini | Godyris | panthyale | panthyale | panthyale | Godyris_panthyale_panthyale | NA | NA | NA | NA | JX573765 | NA | JX573694 | NA | NA | NA | KX362248 |
| Nymphalidae | Danainae | Ithomiini | Heterosais | nephele | | agnosia | Heterosais_nephele_nephele | NA | NA | NA | NA | EU068984 | NA | EU069149 | NA | NA | NA | KX362212 |
| Nymphalidae | Danainae | Ithomiini | Hyalenna | paradoxa | praestigiosa | panthyale | Hyalenna_paradoxa_praestigiosa | NA | NA | NA | MG210029 | JX573781 | MG209896 | JX573710 | MG210228 | NA | NA | MG209923 |
| Nymphalidae | Danainae | Ithomiini | Hypomenitis | enigma | pseudortygia | panthyale | Hypomenitis_enigma | NA | NA | NA | MH892965 | JX573770 | MH893225 | JX573699 | MH893140 | NA | NA | KX362153 |
| Nymphalidae | Danainae | Ithomiini | Hypomenitis | lydia | | hewitsoni | Hypomenitis_lydia | NA | NA | NA | NA | JX573776 | NA | KX361962 | NA | NA | NA | KX362167 |
| Nymphalidae | Danainae | Ithomiini | Hypomenitis | oneidodes | | theudelinda | Hypomenitis_oneidodes | NA | NA | NA | NA | JX573777 | NA | JX573706 | NA | NA | NA | KX362169 |
| Nymphalidae | Danainae | Ithomiini | Hypomenitis | ortygia | ortygia | panthyale | Hypomenitis_ortygia_ortygia | NA | NA | NA | MH892962 | JX573778 | MH893220 | JX573707 | MH893142 | NA | NA | KX362172 |
| Nymphalidae | Danainae | Ithomiini | Hypomenitis | theudelinda | zalmunna | theudelinda | Hypomenitis_theudilinda_zalmunna | NA | NA | NA | NA | JX573779 | NA | JX573708 | NA | NA | NA | KX362175 |
| Nymphalidae | Danainae | Ithomiini | Ithomia | agnosia | agnosia | agnosia | Ithomia_agnosia_agnosia | NA | NA | NA | MH892916 | EU068990 | MH893193 | EU069182 | NA | NA | NA | FJ468996 |
| Nymphalidae | Danainae | Ithomiini | Ithomia | amarilla | | eurimedia | Ithomia_amarilla | NA | NA | NA | MH892917 | EU069067 | MH893194 | EU069184 | MH893149 | NA | NA | AY704063 |
| Nymphalidae | Danainae | Ithomiini | Ithomia | avella | epona | theudelinda | Ithomia_avella | NA | NA | NA | MH892918 | JX573790 | MH893195 | AY704019 | MH893150 | NA | NA | NA |
| Nymphalidae | Danainae | Ithomiini | Mcclungia | cymo | | eurimedia | Mcclungia_cymo | NA | NA | NA | MH892923 | DQ157512 | MH893197 | DQ177957 | MH893153 | NA | NA | KX362176 |
| Nymphalidae | Danainae | Ithomiini | Megoleria | orestilla | orestilla | banjana-m | Megoleria_orestilla | NA | NA | NA | MH892947 | JX573793 | MH893219 | FN551046 | NA | NA | NA | FN568148 |
| Nymphalidae | Danainae | Ithomiini | Methona | curvifascia | | confusa | Methona_curvifascia | NA | NA | NA | MH892926 | EU069005 | MH893231 | EU069212 | NA | NA | NA | MH893466 |
| Nymphalidae | Danainae | Ithomiini | Napeogenes | harbona | | banjana-m | Napeogenes_harbona | NA | NA | NA | NA | FJ468750 | NA | FJ468888 | NA | NA | NA | FJ469034 |
| Nymphalidae | Danainae | Ithomiini | Napeogenes | inachia | | eurimedia | Napeogenes_inachia | NA | NA | NA | MH892931 | EU069007 | MH893202 | EU069221 | NA | NA | NA | FJ469057 |
| Nymphalidae | Danainae | Ithomiini | Napeogenes | larilla | | theudelinda | Napeogenes_larilla | NA | NA | NA | NA | DQ069241 | NA | DQ073033 | NA | NA | NA | AY848727 |
| Nymphalidae | Danainae | Ithomiini | Napeogenes | sylphis | corena | aureliana | Napeogenes_sylphis_corena | NA | NA | NA | NA | EU069091 | NA | EU069230 | NA | NA | NA | HM052215 |
| Nymphalidae | Danainae | Ithomiini | Oleria | athalina | banjana | banjana-m | Oleria_athalina_banjana | NA | NA | NA | MH892948 | FN651613 | MH893227 | FN551072 | NA | NA | NA | FN568169 |
| Nymphalidae | Danainae | Ithomiini | Oleria | onega | | lerida | Oleria_onega | NA | NA | NA | MH892968 | EU068970 | MH893233 | EU069243 | MH893173 | NA | NA | HM052264 |
| Nymphalidae | Danainae | Ithomiini | Oleria | sexmaculata | sexmaculata | lerida | Oleria_sexmaculata_sexmaculata | NA | NA | NA | MH892954 | EU069100 | MH893206 | FN551161 | NA | NA | NA | FN568247 |
| Nymphalidae | Danainae | Ithomiini | Ollantaya | olerioides | | banjana-m | Oleria_olerioides | NA | NA | NA | MG210022 | JX573805 | NA | FN551054 | NA | NA | NA | FN568156 |
| Nymphalidae | Danainae | Ithomiini | Pseudoscada | florula | aureola | aureliana | Pseudoscada_florula_aureola | NA | NA | NA | NA | EU068971 | NA | EU069247 | NA | NA | NA | HM052164 |
| Nymphalidae | Danainae | Ithomiini | Pseudoscada | timna | utilla | agnosia | Pseudoscada_timna_utilla | NA | NA | NA | NA | EU069015 | NA | EU069249 | NA | NA | NA | KX362181 |
| Nymphalidae | Danainae | Ithomiini | Pteronymia | oneida | oneida | hewitsoni | Pteronymia_oneida_oneida | NA | NA | NA | NA | KY750077 | NA | KY750158 | NA | NA | NA | KY749925 |
| Nymphalidae | Danainae | Ithomiini | Veladyris | pardalis | | theudelinda | Veladyris_pardalis | NA | NA | NA | MG209995 | JX573827 | MG209855 | DQ177993 | MG210197 | NA | NA | KX362141 |
| Nymphalidae | Nymphalinae | Melitaeini | Eresia | nauplius | plagiata | lerida | Eresia_nauplius_plagiata | ME10-292 | Ecuador, Napo, Mariposa | 2010 | NA | EF493944 | to be added | EF493994 | NA | NA | NA | NA |
| Nymphalidae | | | | Nymp1 | | | ME16_46_NYMP1 | ME16-46 (additional species) | Peru, Loreto, PB-mk7.1 | 2016 | NA | to be added | to be added | NA | NA | NA | NA | NA |
| Papilionidae | Papilioninae | Papilionini | Papilio | glaucus | | | Papilio_glaucus | additional species | NA | NA | EU141334 | EU141368 | EU141635 | EU136675 | EU141512 | EU141571 | NA | NA |
| Papilionidae | Papilioninae | Troidini | Parides | hahneli | | confusa | Parides_iphidamas | Parides iphidamas | NA | NA | JN204942 | JQ602236 | NA | JN204982 | JN204990 | JN205007 | JN205035 | JN204926 |
| Pieridae | Dismorphiinae | | Dismorphia | teresa | | | TR17_18_DISMSP1 | TR17-18 (additional species) | Ecuador | 2006 | to be added | to be added | to be added | NA | NA | NA | NA | NA |
| Pieridae | Dismorphiinae | | Dismorphia | theucharila | leucone | lerida | TR17_14_DISMTHEU | TR17-14 | Ecuador, Orellana, Anangu | 2011 ? | to be added | to be added | to be added | NA | NA | NA | NA | NA |
| Pieridae | Dismorphiinae | | Dismorphia | theucharila | orange tip | aureliana | TR17_6_DISMTHEU | TR17-6 | Ecuador, Orellana, Anangu | 2005 | NA | to be added | to be added | NA | NA | NA | NA | NA |
| Pieridae | Dismorphiinae | | Dismorphia | theucharila | yolanda | banjana-m | LS11_2240_DISTH | LS11-2240 | Peru, San Martin, La Antena | 2011 | to be added | to be added | to be added | NA | NA | NA | NA | NA |
| Pieridae | Dismorphiinae | | Dismorphia | zathoe | | | Dismorphia_zathoe | additional species | NA | NA | KM046512 | AY954566 | NA | AY870578 | KM046859 | NA | KM046618 | NA |
| Pieridae | Dismorphiinae | | Moschoneura | pinthous | | eurimedia | TR17_3_MOSCPINT | TR17-3 | Peru, San Martin, tunel | NA | to be added | to be added | to be added | NA | NA | NA | NA | NA |
| Pieridae | Dismorphiinae | | Moschoneura | pinthous | | | Moschoneura_pinthous_GB | additional species | NA | NA | KM046539 | KM046823 | KM046711 | AY870575 | KM046887 | KM046773 | NA | NA |
| Pieridae | Dismorphiinae | | Patia | orise | | confusa | Patia_orise | NA | NA | NA | KM046544 | KM046826 | NA | AY870577 | KM046893 | KM046778 | NA | NA |
| Pieridae | Pierinae | Pierini | Itaballia | demophile | | | Itaballia_demophile | additional species | NA | NA | KM046528 | KM046816 | KM046702 | AY870584 | KM046875 | KM046764 | NA | NA |
| Pieridae | Pierinae | Pierini | Itaballia | pandosia | | eurimedia | ME16_62_ITAPAND | ME16-62 | Peru, San Martin, Urahuasha | 2016 | NA | to be added | to be added | NA | NA | NA | NA | NA |
| Pieridae | Pierinae | Pierini | Itaballia | pandosia | | | Itaballia_pandosia | additional species | NA | NA | NA | KP849016 | NA | NA | NA | NA | NA | NA |
| Pieridae | Pierinae | | Perrhybris ? | Pier1 | | eurimedia | MECN_140_PIER1 | MECN-140 | Ecuador, Napo | 2011 ? | to be added | to be added | to be added | NA | NA | NA | NA | NA |
| Pyralidae | Pyralinae | | Pyralis | farinalis | | | Pyralis_farinalis | additional species | NA | NA | NA | KX043023 | GU830302 | GU828925 | GU829747 | GU829979 | GU830604 | NA |
| Riodinidae | Riodininae | Eurybiini | Ithomiola | callixena | | | Ithomiola_callixena | additional species | NA | NA | KT286319 | KT286488 | NA | KT286188 | NA | NA | NA | NA |
| Riodinidae | Riodininae | Eurybiini | Ithomiola | floralis | orange tip | aureliana | 11-1116_ITHOFLO | 11-1116 | Peru, San Martin, Tarapoto | 2011 ? | NA | to be added | to be added | NA | NA | NA | NA | NA |
| Riodinidae | Riodininae | Eurybiini | Ithomiola | floralis | white-band | agnosia | 11_1127_ITHOFLO | 11-1127 | Peru, San Martin, La Antena | 2011 ? | to be added | to be added | to be added | NA | NA | NA | NA | NA |
| Riodinidae | Riodininae | Nymphidiini | Stalachtis | euterpe | | aureliana | TR17_5_STALEUT | TR17-5 | Peru, Loreto, Shucushyacu | 2015 | to be added | to be added | to be added | NA | NA | NA | NA | NA |
| Riodinidae | Riodininae | Nymphidiini | Stalachtis | euterpe | | | Stalachtis_euterpe_GB | additional species | NA | NA | NA | KT286550 | NA | KT286243 | MG607738 | NA | MG608163 | NA |
| Riodinidae | Riodininae | | | Riodin2 | | agnosia | TR17_12_GEO7 | TR17-12 | Peru, San Martin, Tarapoto | 2015 | NA | to be added | NA | NA | NA | NA | NA | NA |
| Riodinidae | | | | Riodin1 | | banjana-m | MECN_133_BUT1 | MECN-133 | Ecuador, Napo | 2011 | NA | to be added | NA | NA | NA | NA | NA | NA |
| Riodinidae | | | | Riodin3 | | agnosia | TR17_11_GEO8 | TR17-11 | Peru, San Martin, Rumipata | 2016 | NA | to be added | to be added | NA | NA | NA | NA | NA |
| Saturniidae | Agliinae | | Aglia | tau | | | Aglia_tau | additional species | NA | NA | GU828131 | GU828430 | GU830340 | EF654540 | GU829770 | GU830019 | GU830636 | NA |

973 **Supplementary table 8. Node constraints used to calibrate the phylogeny** For all constraints, we used uniform distribution priors whose
974 bound were determined according to 95% HSPD inferred by Kawahara et al. 2019 on their phylogeny of Lepidoptera.

| Nodes constrained (crown age) | Mean node age (in million year) | Upper bound | Lower bound |
|---|---|---|---|
| Bombicoidae + Lasiocampoidae | 84.05 | 74.15 | 94.4 |
| (Bombicoidae + Lasiocampoidae) + Geometroidae | 88.66 | 78.61 | 99.27 |
| ((Bombicoidae + Lasiocampoidae) + Geometroidae) + Noctuoidae | 91.15 | 80.92 | 101.97 |
| (((Bombicoidae + Lasiocampoidae) + Geometroidae) + Noctuoidae) + Drepanoidae | 93.73 | 83.27 | 104.79 |
| ((((Bombicoidae + Lasiocampoidae) + Geometroidae) + Noctuoidae) + Drepanoidae) + Pyraloidae = InMoth | 101.33 | 90.18 | 113.05 |
| InMoth_Papilionoidae = Ingroup | 107.64 | 95.97 | 119.94 |
| ingroup_Zygaenoidae | 111 | 98.99 | 123.66 |
| Erebidae + Notodontidae = Noctuoidae | 77.6 | 66.97 | 88.57 |
| Riodinidae + Nymphalidae | 78.64 | 68.19 | 89.59 |
| (Riodinidae + Nymphalidae) + Pieridae | 84.91 | 74.18 | 96.29 |
| ((Riodinidae + Nymphalidae) + Pieridae) + Papilionidae = Papilionoidae | 98.34 | 86.85 | 110.33 |

975

976 **Supplementary table 9. Results of the best partition (based on BIC) for the 8 different genes obtained with Partition Finder**
977 **v1.0.1, with linked branch length and greedy algorithm.** For each gene, pos1, pos2 and pos3 refer to codon positions. Only the substitution
978 models available in BEAST were tested. GTR : general time reversible (base frequencies are variable, substitution matrix is symmetrical), HKY :
979 Hasegawa-Kishino-Yano (base frequencies are variable, there are one transition rate and one tranversion rate), TrN : Tamura-Nei (base frequencies
980 are variable, transversion rates are equal, transition rates are variable), I : proportion of invariable sites, G : gamma distribution (rate variation
981 among sites is gamma distributed).

| Gene fragment and codon position | Best substitution model |
|---|---|
| CAD_pos1, IDH_pos1, MDH_pos1, TKT_pos1 | GTR+I+G |
| CAD_pos2, MDH_pos2, TKT_pos2 | GTR+I+G |
| CAD_pos3, MDH_pos3 | HKY+I+G |
| COI_pos1 | GTR+I+G |
| COI_pos2 | HKY+I+G |
| COI_pos3 | HKY+G |
| EF-1a_pos1, GAPDH_pos1, RpS5_pos1 | TrN+I+G |
| EF-1a_pos2, GAPDH_pos2, IDH_pos2, RpS5_pos2 | HKY+I+G |
| EF-1a_pos3 | GTR+I+G |
| GAPDH_pos3, IDH_pos3, RpS5_pos3 | GTR+I+G |
| TKT_pos3 | HKY+G |

982

**Supplementary table 10a. Repeatability of transmission measurements and structural features.** For each grouping factor (either the number of species or the number of individuals or the total number of different spots measured; indicated in the 'number of groups' column), we calculated the value of repeatability R based on several measurements of the same element of a grouping factor. The calculation of repeatability is based on mixed linear models. Confidence intervals are calculated with parametric bootstraping and p-values (associated to the test R > 0) are calculated with two methods : with likelihood ratio test comparing the likelihood of the model with and without the tested random effect and with permutation tests. We also calculated the coefficient of variation (CV, as the mean of the group devided by the standard error) for each group and we give here the median value of the CV distribution.

| Dependent Variable | Fixed effect | Random effect | Total number of observations | Number of groups | R | 95% confidence interval | p-value (obtained by LRT) | p-value (obtained by permutation) | Median CV (%) |
|---|---|---|---|---|---|---|---|---|---|
| Mean transmittance over 400-700 nm | | Species, Individual, spot | 476 obs | 11 groups | $\mathbf{R_{species} = 0.586}$ | [0.285 ; 0.752] | < 0.001 *** | 0.836 | |
| | | | | 32 groups | $R_{individual} = 0.0535$ | [~0 ; 0.155] | 0.033 * | 0.407 | |
| | | | | 160 groups | $\mathbf{R_{spot} = 0.34}$ | [0.201 ; 0.601] | < 0.001 *** | 0.001 *** | 2.23 |
| Chroma over 400-700 nm | | Species, Individual, spot | 476 obs | 11 groups | $\mathbf{R_{species} = 0.583}$ | [0.271 ; 0.745] | < 0.001 *** | 0.79 | |
| | | | | 32 groups | $R_{individual} = 0.0476$ | [0 ; 0.161] | 0.053 **.** | 0.412 | |
| | | | | 160 groups | $\mathbf{R_{spot} = 0.355}$ | [0.210 ; 0.635] | < 0.001 *** | 0.001 *** | 3.41 |
| Scale density | Species, sex | Individual, spot | 120 obs | 30 groups | $R_{individual} = 0$ | [0 ; 0.18] | 1 | 1 | |
| | | | | 60 groups | $\mathbf{R_{spot} = 0.327}$ | [0.144 ; 0.455] | < 0.001 *** | 0.001 *** | 13.1 |
| Scale length | | | | | | | | | |
| Bifid piliform scale | Species, sex | Individual, spot | 246 obs | 30 groups | $R_{individual} = 0.0779$ | [0 ; 0.259] | 0.196 | 0.318 | |
| | | | | 50 group | $\mathbf{R_{spot} = 0.245}$ | [0.0717 ; 0.406] | < 0.001 *** | 0.001 *** | 7.69 |
| Monofid piliform scale | Species, sex | Individual, spot | 354 obs | 30 groups | $R_{individual} = 0$ | [0 ; 0.0864] | 1 | 1 | |
| | | | | 60 groups | $\mathbf{R_{spot} = 0.113}$ | [0.00917 ; 0.193] | <0.001 *** | 0.001 *** | 16.5 |
| Scale width | | | | | | | | | |
| Bifid piliform scale | Species, sex | Individual, spot | 246 obs | 30 groups | $R_{individual} = 0.149$ | [$2.31*10^{-12}$ ; 0.315] | 0.026 | 0.166 | |
| | | | | 50 groups | $\mathbf{R_{spot} = 0.149}$ | [0.0322 ; 0.292] | < 0.001 *** | 0.001 *** | 8.65 |
| Monofid piliform scale | Species, sex | Individual, spot | 354 obs | 30 groups | $R_{individual} = 0$ | [0 ; 0.0599] | 1 | 1 | |
| | | | | 60 groups | $\mathbf{R_{spot} = 0.0816}$ | [0.0105 ; 0.131] | < 0.001 *** | 0.001 *** | 9.33 |

**Supplementary table 10b. Repeatability of transmission measurements and structural features.** For each grouping factor (either the number of species, or the number of different spots measured per species; indicated in the 'number of groups' column), we calculated the value of repeatability R based on several measurements of the same element of a grouping factor. The calculation of repeatability is based on mixed linear model. Confidence intervals are calculated with parametric bootstraping and p-values (associated to the test R > 0) are calculated with two methods : with likelihood ratio test comparing the likelihood of the model with and without the tested random effect and with permutation tests. We also calculated the coefficient of variation (CV, as the mean of the group devided by the standard error) for each group and we give here the median value of the CV distribution.

| Dependent Variable | Random effect | Number of observations | Number of groups | R | 95% confidence interval | p-value (obtained by LRT) | p-value (obtained by permutation) | Median CV (%) |
|---|---|---|---|---|---|---|---|---|
| Mean transmittance over 400-700 nm | Species, spot$ | 272 obs. | 19 groups<br>95 groups | $\mathbf{R_{species} = 0.671}$<br>$\mathbf{R_{spot} = 0.145}$ | [0.466 ; 0.796]<br>[0.0702 ; 0.253] | < 0.001 ***<br>< 0.001 *** | 0.247<br>< 0.001 *** | 23.4 |
| Chroma over 400-700 nm | Species, spot$ | 272 obs | 19 groups<br>95 groups | $\mathbf{R_{species} = 0.671}$<br>$\mathbf{R_{spot} = 0.0441}$ | [0.466 ; 0.796]<br>[~0 ; 0.155] | < 0.001 ***<br>0.022 * | 0.049*<br>0.026 * | 19 |
| Scale density | spot$ | 120 obs | 6 groups | $\mathbf{R_{spot} = 0.644}$ | [0.204 ; 0.838] | < 0.001 *** | 0.001 *** | 30.1 |
| Scale length | | | | | | | | |
| Bifid piliform scale | spot$ | 246 obs | 5 groups | $\mathbf{R_{spot} = 0.213}$ | [0.0152 ; 0.444] | <0.001 *** | 0.001 *** | 12.1 |
| Monofid piliform scale | spot$ | 354 obs | 6 groups | $\mathbf{R_{spot} = 0.248}$ | [0.0342 ; 0.463] | <0.001 *** | 0.001 *** | 20 |
| Scale width | | | | | | | | |
| Bifid piliform scale | spot$ | 246 obs | 5 groups | $\mathbf{R_{spot} = 0.346}$ | [0.0328 ; 0.607] | < 0.001 *** | 0.001 *** | 10.3 |
| Monofid piliform scale | spot$ | 354 obs | 6 groups | $\mathbf{R_{spot} = 0.537}$ | [0.146 ; 0.747] | < 0.001 *** | 0.001 *** | 12.2 |

**Supplementary table 11. Similarity between conspecific individuals for chromatic and achromatic contrasts.**

To test whether conspecific individuals were perceived as more similar than expected at random for each spot on the forewing, we randomized the contrasts over all pair of species and we calculated the mean distance for conspecific individuals. We compared the mean phenotypic distance (either chromatic or achromatic contrast) for the observed data to the distribution of mean phenotypic distance calculated for 10000 randomizations and we calculated the p-value as the number of randomizations where mean phenotypic distance was smaller than the observed phenotypic distance. We conclude that conspecific individuals are perceived as more similar than expected at random, implying that any individual is representative of its species.

| Dependant variable | Spot considered | factor | Observed mean contrast | p-value |
|---|---|---|---|---|
| chromatic contrast dS | s1 | conspecific | 2.337709 | < 0.001 *** |
| | s2 | conspecific | 2.700542 | < 0.001 *** |
| | s3 | conspecific | 1.750813 | < 0.001 *** |
| | s4 | conspecific | 1.831995 | < 0.001 *** |
| | s5 | conspecific | 1.761623 | < 0.001 *** |
| achromatic contrast dL | s1 | conspecific | 3.236455 | < 0.001 *** |
| | s2 | conspecific | 3.509987 | < 0.001 *** |
| | s3 | conspecific | 1.838903 | < 0.001 *** |
| | s4 | conspecific | 1.807439 | < 0.001 *** |
| | s5 | conspecific | 1.651972 | < 0.001 *** |

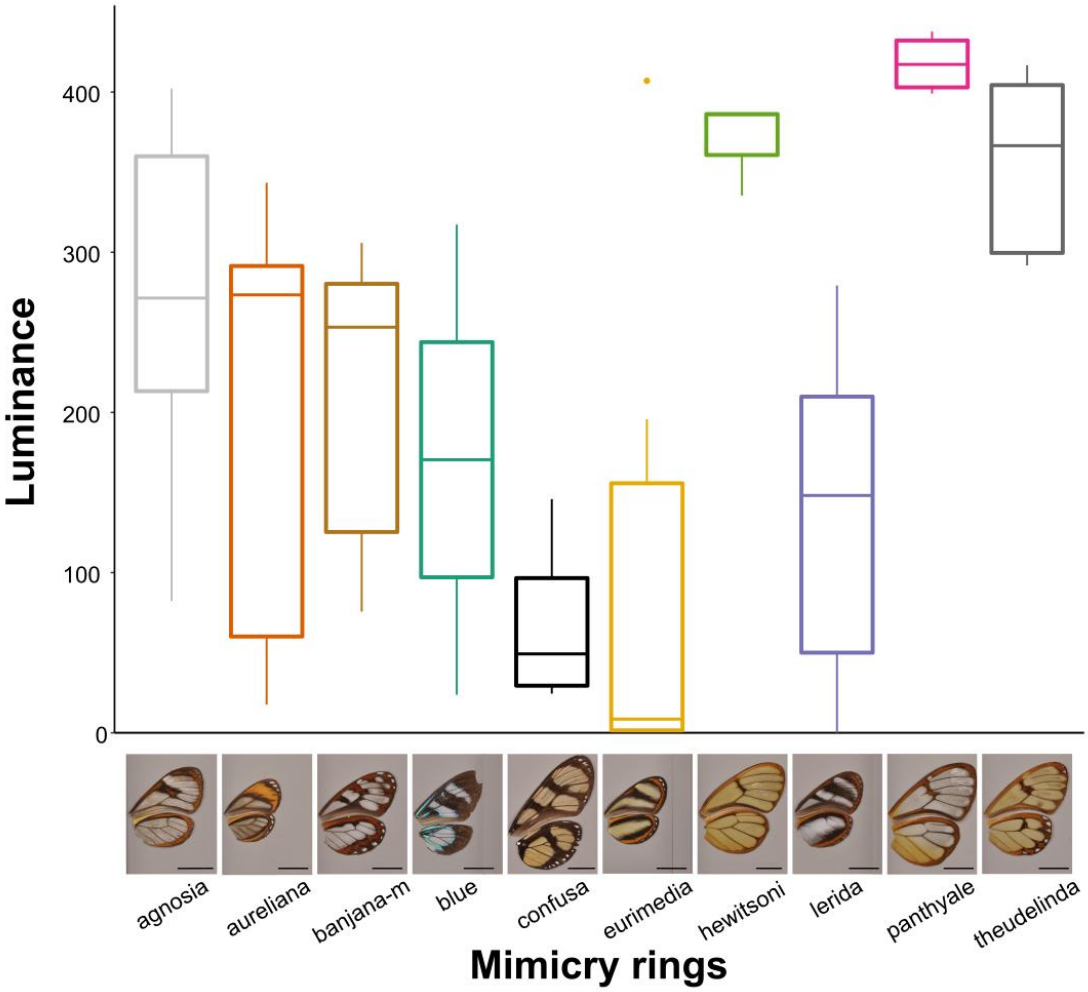


**Supplementary figure 1. Differences in an avian analogue of luminance (quantum catch for brightness channel) between mimicry rings.** The values presented here correspond to a vision model for large gap illuminants and UVS visual system, for the most proximal spot on the forewing. Results for other spots, other visual systems and illuminants are similar.

**Supplementary figure 2. Maximum clade credibility tree of all the specimens obtained with BEAST 1.8.3.** Each tip label represents one individual and the species name, when known, is given in the supplementary table 7. Median node age is given at each node and the 95% interval of the node age post distribution is represented by a horizontal blue bar.

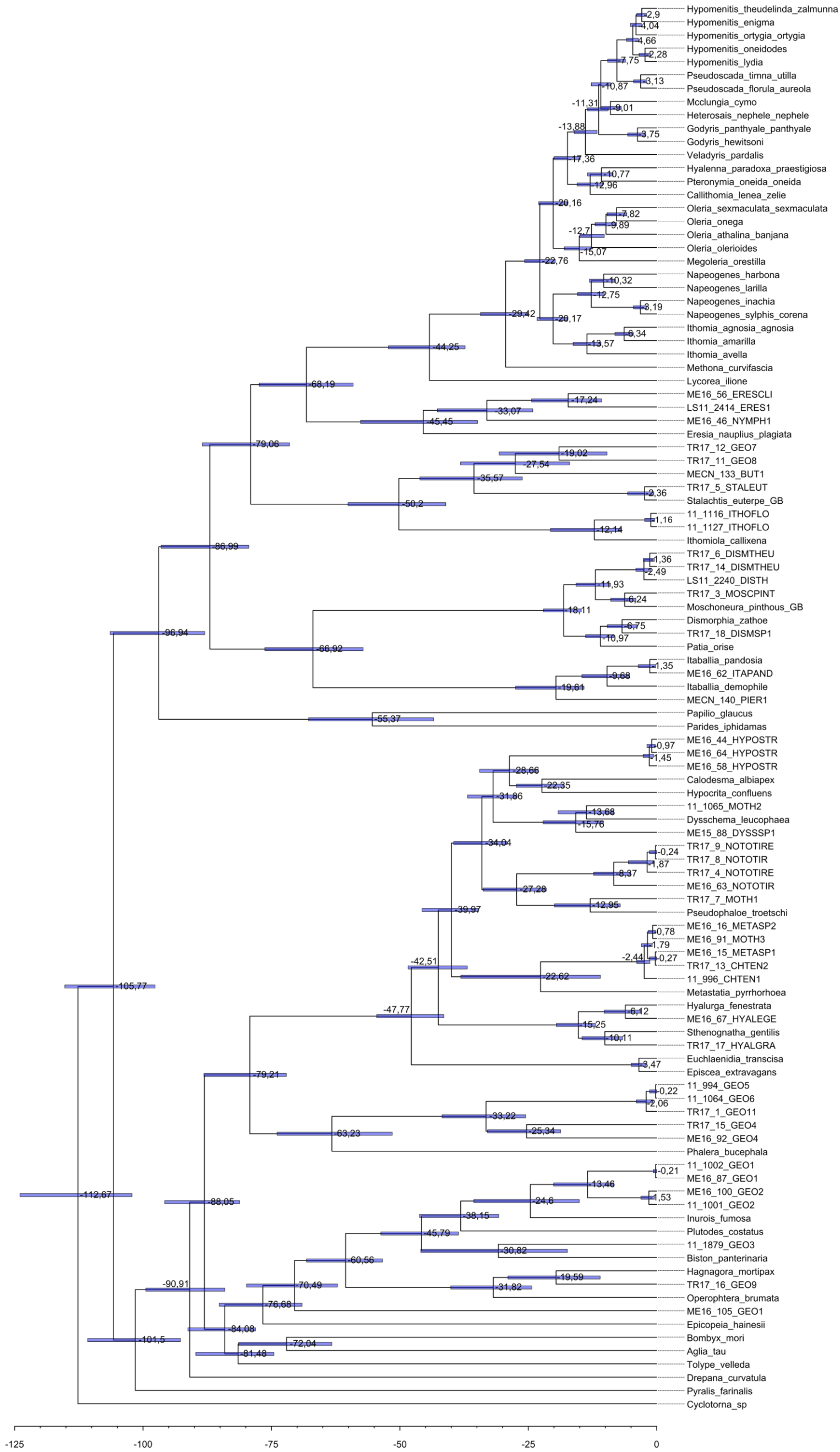

**Supplementary result 1. Link between physical and biologically relevant descriptors of transparency.**

| | Value | Standard error | Degree of freedom | t-value | p-value |
|---|---|---|---|---|---|
| (Intercept) | 0.000 | 0.0263 | 244 | 0 | 1 |
| x | -1.07 | 0.166 | 244 | -6.46 | < 0.001 *** |
| y | -0.701 | 0.137 | 244 | -5.10 | < 0.001 *** |
| z | -0.273 | 0.0475 | 244 | -5.74 | < 0.001 *** |
| Luminance | 0.792 | 0.0173 | 244 | 45.7 | < 0.001 *** |

**Table 1a.** Results of the linear mixed model linking mean transmittance over 300-700 nm (physical descriptor of transparency) and coordinates in tetrahedral colour space (x, y, z) and luminance extracted from vision models (biologically relevant descriptors of transparency). For each species, the 5 measurements were used, and the specimen was taken as random effect.

| | $\chi^2$ | Degree of freedom | Pr ( > $\chi^2$) |
|---|---|---|---|
| x | 42.4 | 1 | < 0.001 *** |
| y | 26.5 | 1 | < 0.001 *** |
| z | 33.5 | 1 | < 0.001 *** |
| Luminance | 2122 | 1 | < 0.001 *** |

**Table 1b.** Analysis of deviance table to check the importance of the effect of each variable on mean transmittance over 300-700 nm.

| | Value | Standard error | t-value | Pr(>\|t\|) |
|---|---|---|---|---|
| (Intercept) | -0.142 | 0.114 | -1.25 | 0.218 |
| x | -1.16 | 0.408 | -2.85 | 0.00605 ** |
| y | -0.765 | 0.333 | -2.39 | 0.0202 * |
| z | -0.297 | 0.122 | -2.43 | 0.0181 * |
| Luminance | 0.789 | 0.0367 | 21.5 | < 0.001 *** |

**Table 1c.** Results of the PGLS model ($F_{4,57}$ = 163.4 (p-value <0.001 ***), AICc = -29.73, $R_{adj}^2$ = 0.914, $\lambda$ = 0.905 (probability$_{(\lambda=0)}$ < 0.001)) linking average mean transmittance over 300-700 nm (physical descriptor of transparency) with average coordinates in tetrahedral space (x, y and z) and luminance extracted from vision models (biologically relevant descriptors of transparency).

We confirmed that mean transmittance is correlated to the x, y and z coordinates and luminance by performing a mixed linear model linking mean transmittance to the x, y and z coordinates and the luminance for each spectrum with specimen as random factor (table 1a), using the lme function from the nlme R package (Pinheiro et al. 2019). The deviance analysis (table 1b) on this linear model showed that each variable had a significant effect on mean transmittance. We also confirmed with a phylogenetic least square analysis (PGLS), which accounts for species relatedness, that average mean transmittance is correlated to average coordinates in tetrahedral space and luminance (table 1c). Taken together, these results mean that what is perceived by predators is correlated to the physical property, in this case mean transmittance.

1043 **Supplementary result 2. Link between nanostructure density and nanostructure**
1044 **type.**

| | Sum of square | Mean square | F value | Pr (> F) |
|---|---|---|---|---|
| Nanostructure type | 2341 | 585.3 | 26.26 | 0.001 |
| Residual | 1271 | 22.29 | | |

1045 Results of the phylogenetic ANOVA on nanostructure density with nanostructure type as factor.
1046 The p-value is based on simulations.

| | **Absence of nanostructures** | **Maze** | **Nipples** | **Sponge** | **pillar** |
|---|---|---|---|---|---|
| **Absence of nanostructures** | 0 (p =1) | | | | |
| **Maze** | 1.418 (p = 1) | 0 (p =1) | | | |
| **Nipples** | 2.976 (p = 0.16) | 0.220 (p = 1) | 0 (p =1) | | |
| **Sponge** | **5.204 (p = 0.01)** | 2.167 (p = 0.62) | 3.800 (p = 0.89) | 0 (p =1) | |
| **pillar** | **8.344 (p =0.01)** | **3.897 (p = 0.02)** | **8.588 (p = 0.01)** | **2.609 (p = 0.01)** | 0 (p =1) |

1047 Results of the post-hoc tests (t values) to determine which type of nanostructure is different in
1048 density to others. P-value were corrected with Bonferroni correction and are indicated in brackets
1049 after t-values. Significant differences between nanostructure types are highlighted in bold.
1050

1051 **Supplementary Materials & Methods**

1052 *Phylogeny*

1053 We used published sequences from eight gene regions to infer a molecular phylogeny: the
1054 mitochondrial cytochrome oxidase c subunit 1 (COI) gene and the nuclear genes
1055 carbamyl-phosphate synthase II (CAD), malate dehydrogenase (MDH), elongation factor
1056 1 alpha (EF-1α), tektin (TKT), ribosomal protein S5 (RpS5), isocitrate dehydrogenase
1057 (IDH) and Glyceraldehyde 3-phosphate dehydrogenase (GAPDH), which represent a total
1058 length of 7433 bp (Supplementary table 7). To improve phylogeny topology, we added 35
1059 species representing 8 additional families to the dataset. When no sequence was available
1060 for a particular species on Genbank, we sequenced *de novo* the COI, CAD and MDH genes
1061 of that species (Supplementary table 7). We have missing data for some species, but we
1062 had at least the COI sequence for each species considered.

1063 For *de novo* sequencing, DNA was extracted from butterfly legs with a DNeasy®
1064 Blood & Tissue Kit (QIAGEN laboratory) and targeted genes were amplified with PCR
1065 conditions adapted from Wahlberg and Wheat (2008). COI, CAD and MDH were amplified
1066 in two pieces with the primers described in Wahlberg and Wheat (2008). PCR were
1067 performed in a volume of 25 µL with 2 to 4 µL of genomic DNA, 1 µL of each primer at a
1068 concentration of 100 pmol/µL, 1 µL of nucleotides at a concentration of 2 mM, 2.5 µL of
1069 DreamTaq buffer, 0.125 µL of DreamTaq polymerase. The elongation phase was reduced
1070 to 70 seconds. For CAD and MDH, the annealing temperature was reduced to 50°C for
1071 most specimens. Eurofins Genomics sequenced the PCR products with Sanger method.
1072 Sequences were aligned with CodonCodeAligner (version 3.7.1.1, CodonCode
1073 Corporation, http://www.codoncode.com/) and concatenated with PhyUtility (version
1074 2.2, Smith and Dunn 2008). The dataset was then partitioned by gene and codon positions
1075 and the best models of substitution were selected over all models implemented in BEAST,
1076 using the 'greedy' algorithm and linked rates implemented in Partition Finder 1.0.1
1077 (Lanfear et al. 2012, see supplementary table 9 for best scheme). We performed a
1078 Bayesian inference of the phylogeny using BEAST 1.8.3 (Baele et al., n.d.) on the Cipres
1079 server (Miller et al., 2010). We constrained some clades to be monophyletic (notably
1080 Ithomiini, Danainae, Nymphalidae, Riodinidae, Pieridae, Papilionidae, Erebidae,
1081 Notodontidae, Geometridae, Noctuoidae, Papilionoidae) and we calibrated the crown age
1082 and divergence time of some groups (see supplementary table 8), following Kawahara et
1083 al. (2019). Four independent analyses were run for 50 million generations, with one

Monte Carlo Markov chain each and a sampling frequency of one out of 50 000 generations (resulting in 1000 posterior trees). After checking for convergence of the two best analyses, the posterior distributions of these two runs were combined (using logCombiner 1.8.2, Drummond and Rambaut 2007), with a burnin of 10%. The maximum clade credibility (MCC) tree with median node ages was computed using TreeAnnotator 1.8.2 (supplementary figure 5). Species not represented in our dataset were then pruned from the tree. The MCC tree was used for subsequent phylogenetic analyses.

*Spectrophotometry*

Specular transmission was measured over 300-700 nm, a range of wavelength to which both butterflies and birds, which are supposed to be their main predators, are sensitive (Briscoe & Chittka, 2001; Hart, 2001) with a custom-built set-up composed of a 300W Xenon lamp emitting light over 200-1160 nm, a collimated emitting optic fibre (UV to NIR multimod fibre with a core diameter of 50 µm) illuminating the wing sample with a 1mm diameter spot and a collimated collecting optic fibre (Avantes UV to IR multimod fibre with a core diameter of 200 µm, FC-UVIR 200-1) connected to the spectrometer (SensLine AvaSpec-ULS2048XL-EVO, Avantes). Fibres are aligned and 14 cm apart. The wing is placed perpendicular to the fibres at equal distance with the ventral side facing the illuminating fibre. The spectrometer has a resolution of 0.5 nm and transmittance is calculated relative to a dark (light patch blocked at the end of the illuminating fibre) and to a white reference (no sample between the fibres):

$$Transmittance\ (\lambda) = \frac{S_{sample}\ (\lambda) - S_{dark}\ (\lambda)}{S_{reference}\ (\lambda) - S_{dark}\ (\lambda)},$$

where λ represent the wavelength, S the number of photons counted by the spectrometer for this wavelength for sample, dark and reference measurements.

Each spectrum was smoothened with the loess function using R software (version 3.6.2.) (0.2 span on 500-700nm, and 0.05 on 300-700nm). We computed mean transmittance over 300-700 nm (B2) using Pavo2 (Maia et al., 2019), as a proxy for transparency: wing transparency increases as mean transmittance increases.

We assessed measurement repeatability on 11 species, representing part of six mimicry rings and belonging to 6 different families. We measured 3 times each of the five spots on the forewing (see supplementary figure 2 for location) for 2 to 3 individuals per species. We assessed measurement repeatability of mean transmittance (B2,

1116 Montgomerie 2006) and of chroma (S8, Montgomerie 2006) over 400-700 nm by
1117 calculating repeatability with species (11 groups for the 11 species considered),
1118 individual (32 groups for the 2 to 3 specimens per species) and spot (160 groups for the
1119 5 spots measured for each of the 32 specimens) as random effect with rpt function from
1120 rptR package (Stoffel et al., 2017): $R_{species, B2} = 0.586$, p-value < 0.001; $R_{individual, B2} = 0.0535$,
1121 p-value = 0.033; $R_{spot, B2} = 0.34$, p-value < 0.001; $R_{species, S8} = 0.583$, p-value < 0.001;
1122 $R_{individual, S8} = 0.0476$, p-value = 0.053; $R_{spot, S8} = 0.355$, p-value < 0.001 (supplementary
1123 table 10a).

1124 We assessed intraspecific variation on 19 species, for which we had more than one
1125 individual, that represented six mimicry rings and belonged to 6 different families. We
1126 measured each of the five spots on the forewing once (see supplementary figure 2 for
1127 location) for 2 to 3 individuals per species. We assessed intraspecific variation of mean
1128 transmittance (B2, Montgomerie 2006) and of chroma (S8, Montgomerie 2006) over 400-
1129 700 nm by calculating repeatability with species (19 different groups) and spot (95
1130 different groups corresponding to the 5 spot for each species) as random effect with rpt
1131 function from rptR package (Stoffel et al., 2017): $R_{species, B2} = 0.671$, p-value < 0.001; $R_{spot,}$
1132 $_{B2} = 0.145$, p-value < 0.001; $R_{species, s8} = 0.671$, p-value < 0.001; $R_{spot, S8} = 0.0441$, p-
1133 value = 0.022 (supplementary table 10b). As all measurements were repeatable, we
1134 considered that any individual is representative of its species. One specimen per species
1135 was therefore used in all analyses.

1136 Due to technical issues, measurements for repeatability could only be performed
1137 for wavelengths ranging from 400 to 700 nm. However, both mean transmittance and
1138 chroma over 400-700 nm were highly correlated to mean transmittance and chroma over
1139 300-700 nm, respectively (correlation coefficient equals 0.9979 [0.9974 ; 0.9983] (p-
1140 value < 0.001) for mean transmittance and 0.9765 [0.9707 ; 0.9812] (p-value < 0.001) for
1141 chroma). Repeatability in measurements over 400-700 nm can therefore be extrapolated
1142 to the full 300-700 nm range.

1143

1144 *High-resolution imaging and structure characterisation*

1145 Dry wings were cut from specimens before being gold-coated (10 nm thick layer) and
1146 observed in SEM (Zeiss Auriga 40). Top-view and cross section SEM images were analysed
1147 with ImageJ 1.52 (Schindelin et al., 2012) to measure scale density, scale length and width,
1148 membrane thickness, and nanostructure density. To measure scale density, we counted

the number of scales in 3 different rectangular areas on a SEM photo and we calculated the mean scale density for each specimen. We measured scale length and width on 3 different scales, and we calculated the mean length and width for each specimen. We measured membrane thickness on 5 different photos per specimen and we calculated the mean membrane thickness. For nanostructure density, we coded macros (one for each type of nanostructure) in ImageJ (Schindelin et al., 2012) to count the number of structures on the image. For each specimen, we had two types of images with different magnifications. As the densities were congruent between the two types of images (measure of repeatability with rptR package: R = 0.368, p-value < 0.001), we calculated the mean nanostructure density between them.

We assessed intraspecific variation for scale characteristics (density, length and width) on three species, belonging to the mimicry ring agnosia: *Ithomia agnosia*, *Pseudoscada timna* and *Heterosais nephele.* We used 5 males and 5 females per species. We measured scale density for proximal and distal zone on forewing twice and we measured scale length and width for 10 different scales per specimen. We assessed repeatability with rptR with species as random effect (see supplementary table 10): for density, $R_{species}$ = 0.545 (p-value < 0.001); for scale length, $R_{species}$ = 0.241 (p-value < 0.001); for scale width, $R_{species}$ = 0.579 (p-value < 0.001). As scale structural features were repeatable within species, we used one specimen per species.

## References


Baele, G., Lemey, P., Rambaut, A., Suchard, M. A., & Valencia, A. (n.d.). *Adaptive MCMC in Bayesian phylogenetics: an application to analyzing partitioned data in BEAST*. https://doi.org/10.1093/bioinformatics/btx088

Briscoe, A. D., & Chittka, L. (2001). The Evolution of Color Vision in Insects. *Annual Review of Entomology*, *46*, 471–510. www.annualreviews.org

Drummond, A. J., & Rambaut, A. (2007). BEAST: Bayesian evolutionary analysis by sampling trees. *BMC Evolutionary Biology*, *7*(1), 1–8. https://doi.org/10.1186/1471-2148-7-214

Hart, N. S. (2001). The visual ecology of avian photoreceptors. *Progress in Retinal and Eye Research*, *20*(5), 675–703.

Kawahara, A. Y., Plotkin, D., Espeland, M., Meusemann, K., Toussaint, E. F. A., Donath, A.,

1182 Gimnich, F., Frandsen, P. B., Zwick, A., Reis, M. dos, Barber, J. R., Peters, R. S., Liu, S.,
1183 Zhou, X., Mayer, C., Podsiadlowski, L., Storer, C., Yack, J. E., Misof, B., & Breinholt, J.
1184 W. (2019). Phylogenomics reveals the evolutionary timing and pattern of butterflies
1185 and moths. *Proceedings of the National Academy of Sciences*, *116*(45), 22657–22663.
1186 https://doi.org/10.1073/PNAS.1907847116
1187 Lanfear, R., Calcott, B., Ho, S. Y. W., & Guindon, S. (2012). *PartitionFinder: Combined*
1188 *Selection of Partitioning Schemes and Substitution Models for Phylogenetic Analyses*.
1189 https://doi.org/10.1093/molbev/mss020
1190 Maia, R., Gruson, H., Endler, J. A., & White, T. E. (2019). pavo 2: New tools for the spectral
1191 and spatial analysis of colour in r. *Methods in Ecology and Evolution*, *10*(7), 1097–
1192 1107. https://doi.org/10.1111/2041-210X.13174
1193 Miller, M. A., Pfeiffer, W., & Schwartz, T. (2010). *Creating the CIPRES Science Gateway for*
1194 *Inference of Large Phylogenetic Trees*.
1195 Montgomerie, R. (2006). Analyzing colors. In *Bird coloration mechanisms and*
1196 *measurements* (Vol. 1). Harvard University Press.
1197 http://ci.nii.ac.jp/naid/10025355850/en/
1198 Pinheiro, J., Bates, D., DebRoy, S., Sarkar, D., & R Core Team. (2019). *{nlme}: Linear and*
1199 *Nonlinear Mixed Effects Models* (R package version 3.1-142). https://cran.r-
1200 project.org/package=nlme
1201 Schindelin, J., Arganda-Carreras, I., Frise, E., Kaynig, V., Longair, M., Pietzsch, T.,
1202 Preibisch, S., Rueden, C., Saalfeld, S., Schmid, B., Tinevez, J. Y., White, D. J.,
1203 Hartenstein, V., Eliceiri, K., Tomancak, P., & Cardona, A. (2012). Fiji: An open-source
1204 platform for biological-image analysis. In *Nature Methods* (Vol. 9, Issue 7, pp. 676–
1205 682). Nature Publishing Group. https://doi.org/10.1038/nmeth.2019
1206 Smith, S. A., & Dunn, C. W. (2008). *Phyutility: a phyloinformatics tool for trees, alignments*
1207 *and molecular data*. *24*(5), 715–716.
1208 https://doi.org/10.1093/bioinformatics/btm619
1209 Stoffel, M. A., Nakagawa, S., & Schielzeth, H. (2017). rptR: repeatability estimation and
1210 variance decomposition by generalized linear mixed-effects models. *Methods in*
1211 *Ecology and Evolution*, *8*(11), 1639–1644. https://doi.org/10.1111/2041-
1212 210X.12797
1213 Wahlberg, N., & Wheat, C. W. (2008). Genomic outposts serve the phylogenomic
1214 pioneers: Designing novel nuclear markers for genomic DNA extractions of

lepidoptera. *Systematic Biology*, *57*(2), 231–242. https://doi.org/10.1080/10635150802033006